博士論文

Thermodynamic Analysis and Optimization of HVAC System

(空調システムにおける熱力学的解析とその最適化に関する研究)

尹　航

Abstract

Thermodynamic Analysis and Optimization of HVAC System

Under the background of global energy saving, the reduction of building energy consumption and the improvement in the system performance of HVAC (Heating Ventilation Air Conditioning) system have attracted more and more attention in recent years. In HAVC system, heat transfer equipments are the important components since any thermodynamic process is closely related to the heat transfer process. The optimization of the heat transfer equipment helps to improve the heat transfer performance and the COP of chiller or any other air conditioning equipment. On the other hand, for some large and complex HVAC system, the pumping power accounts for a considerable proportion of system total energy consumption, which has an important effect on the system performance of HVAC system. The use of some suitable system renovations and modification and the development of assessment method of system are significant for the improvement of system performance. Therefore, the above-mentioned two points are focused on in this study, aiming at supplying some good optimization and evaluation methods and some useful conclusions.

At first, the modified number of entropy production units, *Ns*, represented by Xu is adopted as the objective function of heat exchanger optimization. According to the two types of losses in heat exchanger, namely heat transfer through a finite temperature difference and a pressure drop in the heat transfer fluids, *Ns* can be divided into *Ns* due to heat transfer ($Ns_{\Delta T}$) and *Ns* due to friction ($Ns_{\Delta P}$), respectively. In order to clarify the proportion of irreversible loss due to heat transfer and pressure loss, respectively, to make sense of the main inducement of irreversible process in the heat exchanger for different working mediums, the values of $Ns_{\Delta T}$ and $Ns_{\Delta P}$ of three kinds of heat exchangers (air-to-air, water-to-water, air-to-water) are compared under three kinds of inlet temperature differences, three kinds of length-to-diameter ratios, and nine kinds of inlet Reynolds numbers. It can be found that for water-to-water heat exchanger, the irreversible loss is caused by heat transfer at any Reynolds number; for air-to-water and air-to-air heat exchangers, the irreversible loss is mainly caused by heat transfer at lower Reynolds number and by pressure loss at higher Reynolds number.

Then, the optimization of a water-to-water plate-fin heat exchanger is carried out. The convective heat transfer coefficients of the plate and fin are defined as independent parameters in the optimization, and their values are calculated by applying the multiple regression analysis equation to numerical simulation results of 45 cases. $Ns_{\Delta T}$, $Ns_{\Delta P}$, and Ns are considered as three single objective functions. Finally, according to the single objective optimization and multi-objective optimization, the optimal structural parameters of the heat exchanger are obtained using GA. Meanwhile, the optimizations based on fixed overall dimension of an assumed heat exchanger are also carried out. After the thermodynamic optimization, the efficiency of heat exchanger increases from 30.8% to 33.0%; the heat transfer amount also increases 7.1% from 49.3 kW to 52.8 kW.

Next, in order to clarify the effects of different variable-flow control methods and supply water temperatures on the exergy budget of chilled water circuit, the exergy analysis on an assumed chilled-water circuit system under four variable-flow control modes (throttle-valve control, constant-pressure control, constant-differential-pressure control, and predictive-system-curve control) and two supply water temperatures are carried out. The pumping head, pumping power, and the input exergy rate of each case are compared and analysis. it can be found that the rates of exergy input and exergy consumption under any partial-load condition are significantly smaller than those under full-load condition; the rates of exergy input and exergy consumption under any variable-frequency control mode are smaller than those under throttle-valve control mode; in variable-frequency control mode, the rate of exergy inputs decrease in the following order: constant-pressure control, constant-differential-pressure control, and predictive-system-curve control. Moreover, regarding the effect of the supply water temperature, the rate of exergy inputs are smaller at 12°C than at 7°C. Therefore, the use of the variable-frequency control mode and a higher chilled water temperature will effectively reduce the exergy input to the system.

Finally, performance of an actual heat pump system at each step of the system renovation and modification are compared and analysed. Meanwhile, in order to clarify the effect of chilled water temperature, operation mode of compressor and pumps, and the type of heat exchanger on the system performance, the exergy analysis based on three sets of representative operating data of heat pump system are carried out. It can be seen that, for the three sets of representative operating data, after the variable-frequency transformation of compressor and water pumps, the temperature adjustment of child water, and the replacement of heat exchanger from stainless steel plate heat exchanger to aluminium plate-fin heat exchanger, a good system performance is obtained. The COP of heat pump chiller increases from 4.2, 5.0, to 6.4; the system COP increases from 2.2, 2.9 to 3.2; the exergy efficiency of the system increases from 26.4%, 33.8% to 38.7%.

This study provides a useful optimization method of heat exchanger and a more reasonable and clear analysis method (exergy analysis) for system evaluation and renovations. By adopting these methods, more research can be carried out in future focused on different heat transfer equipments and different HVAC systems.

Table of Contents

Table of Contents 1

List of Figures 4

Chapter 1 Introduction 9

§ 1.1 Research background and purpose 11

§ 1.2 Previous research 11

1.2.1 Method of thermodynamic optimization 11

1.2.2 Optimization of plate-fin heat exchanger 12

1.2.3 Exergy analysis of HVAC system 13

§ 1.3 Research content 14

§ 1.4 Research flow chart 16

Chapter 2 Thermodynamic analysis of heat exchanger 17

§ 2.1 Development of thermodynamic optimization of heat exchanger 19

§ 2.2 Design methods of heat exchanger 20

2.2.1 LMTD method 20

2.2.2 Ɛ-NTU method 21

2.2.3 Applicable scope of the two methods 23

§ 2.3 Derivation of objective function 23

2.3.1 Choice of objective function 23

2.3.2 Expression of objective function for different working mediums 24

2.3.3 Calculation of heat transfer coefficient U and pressure loss ΔP 29

§ 2.4 Conclusions 31

Chapter 3 Sensitivity analysis of $Ns_{\Delta T}$ and $Ns_{\Delta P}$ 33

§ 3.1 Calculation conditions of case study 35

§ 3.2 Analysis of air-to-air heat exchanger 36

3.2.1 Analysis of $Ns_{\Delta T}$ and $Ns_{\Delta P}$ in different length-to-diameter ratios 36

3.2.2 Analysis of $Ns_{\Delta T}$ and $Ns_{\Delta P}$ at different inlet temperature differences 38

3.2.3 Conclusion 40

§ 3.3 Analysis of water-to-water heat exchanger 41
3.3.1 Analysis of $Ns_{\Delta T}$ and $Ns_{\Delta P}$ in different length-to-diameter ratios 41
3.3.2 Analysis of $Ns_{\Delta T}$ and $Ns_{\Delta P}$ at different inlet temperature differences 43
3.3.3 Conclusion... 44
§ 3.4 Analysis of air-to-water heat exchanger 45
3.4.1 Analysis of $Ns_{\Delta T}$ and $Ns_{\Delta P}$ in different length-to-diameter ratios 45
3.4.2 Analysis of $Ns_{\Delta T}$ and $Ns_{\Delta P}$ at different inlet temperature differences 46
3.4.3 Conclusion... 48
§ 3.5 Comparison of three kinds of heat exchangers 48
§ 3.6 Conclusions 51

Chapter 4 Fin-shape optimization of plate-fin heat exchanger 53

§ 4.1 Introduction 55
§ 4.2 Thermal modelling of plate-fin heat exchanger.. 56
4.2.1 Basic components of plate-fin heat exchanger.. 56
4.2.2 Thermal modelling 58
§ 4.3 Numerical simulation.. 62
4.3.1 Reliability of CFD software 62
4.3.2 Simulation object and conditions 64
4.3.3 Grid independence test 65
4.3.4 Results and discussion.. 66
§ 4.4 Case study... 70
4.4.1 Thermodynamic optimization with unfixed overall dimension.. 70
4.4.2 Thermodynamic optimization with fixed overall dimension.. 73
§ 4.5 Conclusions 75

Chapter 5 Exergy analysis on an assumed chilled-water circuit........................... 77

§ 5.1 Introduction 79
§ 5.2 Basic theory 80
5.2.1 Exergy of heat transfer 81
5.2.2 Exergy of flow processes... 82
§ 5.3 Assumed system and its corresponding exergy budget 83
§ 5.4 Pump power and heat-transfer characteristics of FCU 86

5.4.1 Four variable-flow control modes 86
5.4.2 Calculation of pump power 88
5.4.3 Heat-transfer characteristics of FCU 89
§ 5.5 Calculation parameters 90
5.5.1 Settings of supply water temperature 90
5.5.2 Settings of pumping head 91
5.5.3 Settings of power and flow rate of pump and fan 92
5.6.1 Pumping head and pumping power 93
5.6.2 Exergy budget of the system 94

Chapter 6 Performance analysis on a heat pump system of an actual building ... 99
§ 6.1 Introduction 101
§ 6.2 System summary 101
§ 6.3 Investigation on COP improvement of the modified system 102
§ 6.4 Exergy analysis on the heat pump system 107
6.4.1 Exergy budget of the system 108
6.4.2 Calculation results and discussion 113
§ 6.5 Conclusions 116

Chapter 7 Conclusions and recommendations 119
§ 7.1 Conclusions 121
§ 7.2 Recommendations for future studies 123

Reference 125

Appendix 133
Publication list 134
Acknowledgments 137

List of Figures

Figure 1.1 Research flow 16

Figure 2.1 Temperature distribution of working mediums in heat exchanger.......................... 21
Figure 2.2 Entropy budget of an indirect-contact-type heat exchanger.................................... 25

Figure 3.1 Analysis object 35
Figure 3.2 Variation trends of ε and Ns at three different length-to-diameter ratios 36
Figure 3.3 Variation trends of $Ns_{\Delta T}$ at three different length-to-diameter ratios 37
Figure 3.4 Variation trends of $Ns_{\Delta P}$ at three different length-to-diameter ratios 37
Figure 3.5 Variation trends of $Ns_{\Delta P}$-to-Ns ratio at different length-to-diameter ratios 38
Figure 3.6 Variation trends of ε and Ns at three different inlet temperature differences 39
Figure 3.7 Variation trends of $Ns_{\Delta T}$ at three different inlet temperature differences 39
Figure 3.8 Variation trends of $Ns_{\Delta P}$ at three different inlet temperature differences 39
Figure 3.9 Variation trends of $Ns_{\Delta P}$-to-Ns ratio at different inlet temperature differences........ 40
Figure 3.10 Variation trends of ε and Ns at three different length-to-diameter ratios 41
Figure 3.11 Variation trends of $Ns_{\Delta T}$ at three different length-to-diameter ratios 42
Figure 3.12 Variation trends of $Ns_{\Delta P}$ at three different length-to-diameter ratios 42
Figure 3.13 Variation trends of $Ns_{\Delta P}$-to-Ns ratio at different length-to-diameter ratios 42
Figure 3.14 Variation trends of ε and Ns at three different inlet temperature differences......... 43
Figure 3.15 Variation trends of $Ns_{\Delta T}$ at three different inlet temperature differences 43
Figure 3. 16 Variation trends of $Ns_{\Delta P}$ at three different inlet temperature differences 43
Figure 3.17 Variation trends of $Ns_{\Delta P}$-to-Ns ratio at different inlet temperature differences...... 44
Figure 3.18 Variation trends of ε and Ns at three different length-to-diameter ratios 45
Figure 3.19 Variation trends of $Ns_{\Delta T}$ at three different length-to-diameter ratios 45
Figure 3.20 Variation trends of $Ns_{\Delta P}$ at three different length-to-diameter ratios 46
Figure 3.21 Variation trends of $Ns_{\Delta P}$-to-Ns ratio at different length-to-diameter ratios 46
Figure 3.22 Variation trends of ε and Ns at three different inlet temperature differences......... 47
Figure 3.23 Variation trends of $Ns_{\Delta T}$ at three different inlet temperature differences 47

Figure 3.24 Variation trends of $Ns_{\Delta P}$ at three different inlet temperature differences 47
Figure 3.25 Variation trends of $Ns_{\Delta P}$-to-Ns ratio at different inlet temperature differences...... 48
Figure 3 26 Variation trends of ε for three kinds of heat exchangers 49
Figure 3.27 Variation trends of Ns for three kinds of heat exchangers 49
Figure 3.28 Variation trends of $Ns_{\Delta T}$ for three kinds of heat exchangers 50
Figure 3.29 Variation trends of $Ns_{\Delta P}$ for three kinds of heat exchangers 50
Figure 3.30 Variation trends of $Ns_{\Delta P}$ -to-Ns ratio for three kinds of heat exchangers 50

Figure 4.1 Counterflow plate-fin heat exchanger 57
Figure 4.2 Types of plate fin surfaces: (a) Plain rectangular (b) Plain trapezoidal (c)............. 57
Figure 4.3 Basic components of a plate-fin heat exchanger 57
Figure 4.4 Calculation region 62
Figure 4.5 Comparison of numerical simulation results and experimental results.................... 63
Figure 4.6 Simulation object.. 64
Figure 4.7 Grid independence test 66
Figure 4.8 Convective heat transfer coefficient (Case 1) 66
Figure 4.9 Convective heat transfer coefficient (Case 9) 67
Figure 4.10 Relation between j_{mh} and Re Figure 4.11 Relation between j_{mc} and Re 68
Figure 4.12 Relation between j_{wh} and Re Figure 4.13 Relation between j_{wc} and Re 68
Figure 4.14 Relation between j_{wh} and Re Figure 4. 15 Relation between j_{wc} and Re........ 68
Figure 4.16 Comparison of results between CFD and empirical equations 69
Figure 4.17 Iteration process for the minimisation of $Ns_{\Delta P}$ 71
Figure 4.18 Iteration process for the minimisation of $Ns_{\Delta T}$ 72
Figure 4.19 Iteration process for the minimisation of Ns 72
Figure 4.20 Values and proportions of $Ns_{\Delta P}$ and $Ns_{\Delta T}$ for each objective function 72
Figure 4.21 Ratio of $Ns_{\Delta P}$, $Ns_{\Delta T}$, and Ns between the minimizations of $Ns_{\Delta P}$ and $Ns_{\Delta T}$ (Ns)..... 73
Figure 4.22 Pareto front of multi-objective optimization 73
Figure 4.23 Optimization object before optimization.. 74
Figure 4.24 Value of Ns, ε, and heat exchange amount before and after the optimization........ 75

Figure 5.1 Classification of exergy 81
Figure 5.2 Carnot cycle and reverse Carnot cycle between two thermal reservoirs 82
Figure 5.3 Assumed chilled water circuit 84
Figure 5.4 The flow of exergy through the system 84
Figure 5.5 Throttle-valve (TV) control 87
Figure 5.6 Constant-pressure (CP) control 87
Figure 5.7 Constant-differential-pressure (CDP) control 88
Figure 5.8 Predictive-system-curve (PSC) control 88
Figure 5.9 Temperature setting under full-load condition 91
Figure 5.10 Temperature setting under partial-load condition 91
Figure 5.11 Pumping head settings 92
Figure 5.12 Relative heat-transfer rate versus relative water flow rate 92
Figure 5.13 Comparison of pumping head 93
Figure 5.14 Comparison of pumping power 94
Figure 5.15 The rates of exergy input and output (Case 1) 95
Figure 5.16 The rates of exergy input and output (Case 2) 95
Figure 5.17 The rates of exergy consumption of two Cases 96
Figure 5.18 Exergy consumption patterns of two Cases 97

Figure 6.1 The appearance 21KOMCEE 102
Figure 6.2 Heat pump systems 102
Figure 6.3 Operating data during the night of 2013/07/23 104
Figure 6.4 Operating data during the night of 2013/10/11 104
Figure 6.5 Operating data during the night of 2014/06/04 105
Figure 6.6 Operating data during the night of 2014/08/26 106
Figure 6.7 Operating data during the night of 2014/10/03 106
Figure 6.8 Operating data during the daytime of 2014/11/11 107
Figure 6.9 Analysis object in the heat pump system 108
Figure 6.10 Direction of exergy flow 108
Figure 6.11 Subsystem 1 109

Figure 6.12 Subsystem 2 110
Figure 6.13 Subsystem 3 111
Figure 6.14 Subsystem 4 112
Figure 6.15 Operating date before and after the system renovation and modification 114
Figure 6.16 Exergy budget before and after the system renovation and modification 114
Figure 6.17 Exergy efficiency and dimensionless exergy consumption rates 115

List of Tables

Table 3.1 Properties of heat exchangers 35

Table 4.1 Calculation conditions 63
Table 4.2 Simulation conditions 65
Table 4.3 Range of variables and optimal solutions 71
Table 4.4 Range of variables and optimal solutions 74

Table 6.1 Properties of heat pumps before and after the system renovation and modification 103

Chapter 1 Introduction

§ 1.1 Research background and purpose

Under the background of global energy saving, the reduction of building energy consumption and the improvement in the system performance of HVAC (Heating Ventilation Air Conditioning) system have attracted more and more attention in recent years. In HAVC system, heat transfer equipments are the important components since any thermodynamic process is closely related to the heat transfer process. The optimization of the heat transfer equipment helps to improve the heat transfer performance and the COP of chiller or any other air conditioning equipment. On the other hand, for some large and complex HVAC system, the pumping power accounts for a considerable proportion of system total energy consumption, which has an important effect on the system performance of HVAC system. The use of some suitable system renovations and modification and the development of assessment method of system are significant for the improvement of system performance. Therefore, the above-mentioned two points are focused on in this study, aiming at supplying some good optimization and evaluation methods and some useful conclusions.

§ 1.2 Previous research

1.2.1 Method of thermodynamic optimization

As for the thermodynamic optimization of heat exchanger, the design and analysis of thermal processes based on the second law of thermodynamics has received considerable attention in recent decades. McClintock (1951) first employed the irreversibility concept for estimating and minimizing the usable energy wasted in heat exchanger design. He described irreversibility analysis of heat exchangers and gave clear equations for the local optimum design of fluid passages for either side of a heat exchanger. Then Bejan (1977) presented a heat exchanger design method for fixed or for minimum irreversibility and established a direct relationship between the heat exchanger design parameters and the useful power wasted due to heat exchanger noideality. His method and related follow-up research work was elaborated in his book (Bejan, 1996). Bejan’s research has a huge impact on the thermodynamic optimization of heat exchanger. Until now, much research has been done based on this technique. Mishra (2009) did the optimization of crossflow plate-fin heat exchanger design by minimizing the number of entropy generation units for a specified heat duty under given space restriction. In Ahmadi’s (2011) research work, a thermal modeling was conducted for optimal design of compact heat exchangers in order to minimize cost and entropy generation. Asadi (2013) and Zarea (2014) also conducted the entropy-generation minimization and entropy-generation-units minimization by using Cuckoo Algorithm and Bees Algorithm, respectively. Therefore, in this study, the shape of the heat exchanger was also optimized based on the theory of Bejan's research in the part of thermodynamic optimization.

Among them, the number of entropy production units, *Ns* [-], which has been widely used by many researchers to evaluate the irreversibility loss in heat exchanger, was defined by Bejan (1982). The smaller *Ns* is, the better heat transfer performance will be obtained. But it is found that using this parameter as the objective function of heat exchanger optimization might lead to some ambiguities, such as the increase of *Ns* varying with the increase of effectiveness ε (Xu, 1996). Therefore, the chosen of objective function of heat exchanger optimization should be considered before the optimization.

1.2.2 Optimization of plate-fin heat exchanger

Any heat transfer process is characterized by two types of losses, heat transfer through a finite temperature difference and a pressure drop in the heat transfer fluids (Singh, 2008). But there are not so many researches focused on making sense of the main inducement of irreversible process in the heat exchanger for different working mediums.

As a kind of compact heat exchanger, plate-fin heat exchangers are widely used in cryogenics and the aerospace industry because of their compactness and high thermal efficiency. As the secondary heat transfer surface, the fin is regarded as the most important heat transfer component in plate-fin heat exchangers, and its size is closely related to the heat transfer characteristics and pressure losses of the heat exchanger. Thus, optimizing the shape of plate-fin heat exchangers is important for their effectiveness and economy. In previous studies, the working media of plate-fin heat exchangers were often gas-to-gas or gas-to-liquid (Wen, 2007; Peng, 2008; Rao, 2013; Zhao, 2013). There are not many applications and studies of plate-fin heat exchangers in water systems for air-conditioning applications.

On the other hand, in design calculation of plate-fin heat exchangers, the comprehensive surface efficiency of the primary (plate) and secondary (fin) heat transfer surfaces is deduced assuming that the convective heat transfer coefficients of the plate and fin are the same (Kuppan, 2002; Kays, 1984; Wang, 1984). Actually, their values differ more or less according to the fin size (Wang, 2009).

Further, in the calculation of the convective heat transfer coefficients, the Colburn heat transfer factor *j* (Colburn factor for short) and Fanning friction factor *f* (Fanning factor for short) are generally adopted.

In previous research, the Colburn and Fanning factors were often calculated using empirical equations (Mishra, 2009; Zarea, 2013; Pater, 2014; Sanaye, 2010). However, their values are generally greatly affected by the type of working media, the heat exchanger material, the fin size, and so on. According to the research of Hu and Herold (1995), for a liquid working medium, the value of the Colburn factor calculated using an empirical equation for air is approximately twice that calculated using experimental data for liquid at the same Reynolds number. Therefore, using empirical equations blindly might produce large errors in the calculation of the Colburn and Fanning factors. On the other hand, an experimental study might require time and money to obtain more precise results. Computational fluid dynamics (CFD), which has been used extensively in many fields of industry, can offer a simple high-precision method.

1.2.3 Exergy analysis of HVAC system

The energy use of an HVAC system accounts for a large proportion of a building's total energy use (Westphalen 2001). Improving the efficiency of an HVAC system would therefore make a major contribution to energy saving within a building. In an HVAC system, in which the pumping system is one of the primary components, energy-use reduction by the pumping system is important. Maximum-load operation of an HVAC system accounts for only a small percentage of the overall operating time. Most water pumps are operated only under partial load (Matsushita 2011). Therefore, reducing the energy use of the pumping system when under only partial load will significantly improve the efficiency of the HVAC system.

In any investigation involving partial load, it is necessary to determine the degree of impact of the water temperature on the heat-transfer characteristics of the terminal units, such as the fan coil units (FCU). These are another primary component of an HVAC system, which transfer heat from the air to water through a coil in proportion to the log mean temperature difference (LMTD) (Crowther 2002). This is because the water temperature affects the LMTD and then the heat-transfer characteristics of the terminal unit, and thereby ultimately affects the indoor thermal environment, the cost of the terminal units, and the power of the pumps used in the chilled water circuit (TRANE 2002; Herbert 2011).

Previous studies regarding variable-flow control have mainly focused on comparing measured energy use before and after the adjustment of the control parameters or control methods (Izumiyama 2012) or the development and verification of new control methods (Matsushita et al. 2011). Regarding those previous studies into the effect of water temperature on heat transfer, the main research efforts have involved the analysis of the relationship between the water flow rate and the temperature difference between the supply and return water, based on data derived from the manufacturer's specifications (Kido et al. 2013).

All of the above-mentioned studies were carried out from the viewpoint of the amount of energy being consumed, but not the quality of that energy. In thermodynamics, energy can be divided into available and unavailable energy. Exergy is that energy that is available for use (Perrot 1998). Unlike a conventional energy analysis, an exergy analysis enables the direction of the exergy flow, as well as the value and location of the exergy consumption, to be clearly and easily determined (Shukuya 2013).

Therefore, a greater number of exergy analyses have been applied to the field of HVAC engineering in recent years. Wang et al. (2008) investigated the impact of the air-conditioning parameters on the exergy of the chilled water supplied to radiant panels and a cooling coil. Harrell and Mathias (2009) evaluated the central chilled-water system in a campus building using exergy-based cost accounting to quantify the magnitude and cost impact of internal losses with the goal of maximizing the chiller capacity utilization while minimizing the unit cost of the delivered chilled water. Taniguchi et al. (2014) developed an energy-saving air-separation unit based on an exergy analysis. However, as far as we know, there have been no exergy analyses of a chilled water circuit from the aspects of both the variable-flow control methods and the chilled water temperature. For the performance analysis on actual HAVC system, exergy analysis is rarely taken as the evaluation methods.

§ 1.3 Research content

Based on the corresponding problems as above-mentioned, in this study, the following research contents are carried out.

At first, a modified Ns represented by Xu (1996) is adopted as the objective function of heat exchanger optimization. According to the two types of losses in heat exchanger, namely heat transfer through a finite temperature difference and a pressure drop in the heat transfer fluids (Singh, 2008), Ns can be divided into Ns due to heat transfer ($Ns_{\Delta T}$) and Ns due to friction ($Ns_{\Delta P}$), respectively. In order to clarify the proportion of irreversible loss due to heat transfer and pressure loss, respectively, to make sense of the main inducement of irreversible process in the heat exchanger for different working mediums, the values of $Ns_{\Delta T}$ and $Ns_{\Delta P}$ of three kinds of heat exchangers (air-to-air, water-to-water, air-to-water) are compared under three kinds of inlet temperature differences, three kinds of length-to-diameter ratios, and nine kinds of inlet Reynolds numbers.

Then, the optimization of a water-to-water plate-fin heat exchanger is carried out. The convective heat transfer coefficients of the plate and fin are defined as independent parameters in the optimization, and their values are calculated by applying the multiple regression analysis equation to numerical simulation results of 45 cases. $Ns_{\Delta T}$, $Ns_{\Delta P}$, and Ns are considered as three single objective functions. Finally, according to the single objective optimization and multi-objective optimization, the optimal structural parameters of the heat exchanger are obtained using GA. Meanwhile, the optimizations based on fixed overall dimension of heat exchanger are also carried out. The performance before and after the optimization are compared.

Next, in order to clarify the effects of different variable-flow control methods and supply water temperatures on the exergy budget of chilled water circuit, the exergy analysis on an assumed chilled-water circuit system under four variable-flow control modes (throttle-valve control, constant-pressure control, constant-differential-pressure control, and predictive-system-curve control) and two supply water temperatures are carried out. The pumping head, pumping power, and the input exergy rate of each case are compared and analysis.

Finally, performance of an actual heat pump system at each step of the system renovation and modification are compared and analysed. Meanwhile, in order to clarify the effect of chilled water temperature, operation mode of compressor and pumps, and the type of heat exchanger on the system performance, the exergy analysis based on the actual operating date of heat pump system are carried out.

§ 1.4 Research flow chart

Chapter 1 Introduction

- Research background and purpose
- Previous research
- Research content
- Research flow chart

Chapter 2 Thermodynamic analysis of heat exchanger

- Development of thermodynamic optimization of heat exchanger
- Design methods of heat exchanger
- Derivation of objective function
- Conclusions

Chapter 3 Sensitivity analysis of $Ns_{\Delta T}$ and $Ns_{\Delta P}$

- Calculation conditions of case study
- Analysis of air-to-air heat exchanger
- Analysis of water-to-water heat exchanger
- Analysis of air-to-water heat exchanger
- Comparison of three kinds of heat exchangers
- Conclusions

Chapter 4 Fin-shape optimization of plate-fin heat exchanger

- Introduction
- Thermal modelling of plate-fin heat exchanger
- Numerical simulation
- Case study
- Conclusion

Chapter 5 Exergy analysis on an assumed chilled-water circuit

- Introduction
- Basic theory
- Assumed system and its corresponding exergy budget
- Pump power and heat-transfer characteristics of FCU
- Calculation parameters
- Calculation Results
- Conclusion

Chapter 6 Performance analysis on a heat pump system of an actual building

- Introduction
- System summary
- Investigation on COP improvement of the modified system
- Exergy analysis on the heat pump system
- Conclusions

Chapter 7 Conclusion

- Conclusions
- Recommendations for future studies

Figure 1.1 Research flow

Chapter 2 Thermodynamic analysis of heat exchanger

The shape optimization of plate-fin heat changer is carried out from the viewpoint of thermodynamic optimization and cost optimization in this study. To clarify the process of thermodynamic optimization of heat changer, the development of related research work on thermodynamic optimization of heat exchanger and the common design methods of heat exchanger are introduced. In addition, the conception and the corresponding derivation process of the thermodynamic objective function used in this study are also described in detail in this chapter.

§ 2.1 Development of thermodynamic optimization of heat exchanger

Any thermodynamic process must obey not only the first law but also the second law of thermodynamics as well. Since the optimization based on the first law of thermodynamics only take into account the amount of energy, but not the quality of energy, in recent decades, the design and analysis of thermal processes based on the second law of thermodynamics has received considerable attention.

McClintock (1951) first employed the irreversibility concept for estimating and minimizing the usable energy wasted in heat exchanger design. He described irreversibility analysis of heat exchangers and gave clear equations for the local optimum design of fluid passages for either side of a heat exchanger.

Then Bejan (1977) presented a heat exchanger design method for fixed or for minimum irreversibility and established a direct relationship between the heat exchanger design parameters and the useful power wasted due to heat exchanger noideality. His method and related follow-up research work was elaborated in his book (Bejan, 1996).

Bejan’s research has a huge impact on the thermodynamic optimization of heat exchanger. Until now, much research has been done based on this technique. Mishra (2009) did the optimization of crossflow plate-fin heat exchanger design by minimizing the number of entropy generation units for a specified heat duty under given space restriction. In Ahmadi’s (2011) research work, a thermal modeling was conducted for optimal design of compact heat exchangers in order to minimize cost and entropy generation. Asadi (2013) and Zarea (2014) also conducted the entropy-generation minimization and entropy-generation-units minimization by using Cuckoo Algorithm and Bees Algorithm, respectively. Therefore, in this study, the shape of the heat exchanger was also optimized based on the theory of Bejan’s research in the part of thermodynamic optimization.

§ 2.2 Design methods of heat exchanger

In the process of thermodynamic optimization of heat exchanger, it is necessary to use the design methods of heat exchanger when the objective function of optimization is established. Generally, there are two types of problems in the heat exchanger design (Sukhatme, 2005). In the first type, for two given working mediums, the flow rates, and inlet and outlet temperatures are specified, the heat transfer area required for the heat exchanger is to be calculated. The log-mean temperature difference (*LMTD*) method is usually adopted for this problem. In the second type, for a given heat exchanger and two given working mediums, only the inlet temperature and flow rates are specified and the outlet temperature of the two working mediums are to be calculated. For this problem, the effectiveness-*NTU* ($\mathcal{E}$-*NTU*) method is generally used.

2.2.1 LMTD method

The rate of heat transfer $\dot{Q}$ [W] in the heat exchanger can be expressed as (Shah, 2002)

$$\dot{Q} = UA\Delta T_m \tag{2.1}$$

where U [W/(m^2·K)] and A [m^2] are the heat transfer coefficient and entire heat transfer area of the heat exchanger, respectively. ΔT_m [K] is the true mean temperature difference, which is different for different exchanger flow arrangements at the same inlet and outlet temperatures of the working mediums.

For a counter-flow or parallel-flow heat exchanger, the true mean temperature difference ΔT_m can be expressed as (Shah, 2002)

$$\Delta T_m = \Delta T_{lm} \tag{2.2}$$

where ΔT_{lm} [K] is the log-mean temperature difference given as (Shah, 2002)

$$\Delta T_{lm} = \frac{\Delta T_A - \Delta T_B}{\ln\left(\Delta T_A / \Delta T_B\right)} \tag{2.3}$$

where ΔT_A [K] and ΔT_B [K] are the temperature differences between two working mediums at each end of the heat exchanger. The corresponding temperature differences for a counter-flow ($\Delta T_{A,cf}$, $\Delta T_{B,cf}$) or parallel-flow ($\Delta T_{A,pf}$, $\Delta T_{B,pf}$) heat exchanger is represented in Equation (2.4) – (2.7) from Figure 2.1.

$$\Delta T_{A,cf} = T_{h,in} - T_{c,out} \tag{2.4}$$

$$\Delta T_{B,cf} = T_{h,out} - T_{c,in} \tag{2.5}$$

$$\Delta T_{A,pf} = T_{h,in} - T_{c,in} \tag{2.6}$$

$$\Delta T_{B,pf} = T_{h,out} - T_{c,out} \tag{2.7}$$

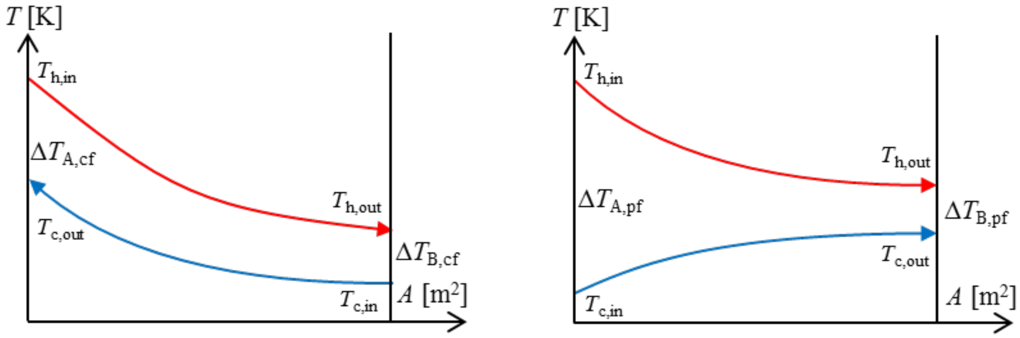
T [K]
$T_{\mathrm{h,in}}$
$\Delta T_{\mathrm{A,cf}}$
$T_{\mathrm{c,out}}$
$T_{\mathrm{h,out}}$
$\Delta T_{\mathrm{B,cf}}$
$T_{\mathrm{c,in}}$
A [m^2]
T [K]
$T_{\mathrm{h,in}}$
$T_{\mathrm{h,out}}$
$\Delta T_{\mathrm{A,pf}}$
$\Delta T_{\mathrm{B,pf}}$
$T_{\mathrm{c,out}}$
$T_{\mathrm{c,in}}$
A [m^2]

(a) Counter-flow heat exchanger (b) Parallel-flow heat exchanger

Figure 2.1 Temperature distribution of working mediums in heat exchanger

For all other flow arrangements such as cross flow, the true mean temperature difference ΔT_m can be expressed by Equation (2.8), based on the log-mean temperature difference for a counter-flow heat exchanger (Shah, 2002). That is because the maximum true mean temperature difference only obtained by the counter-flow heat exchanger under certain given inlet and outlet temperature of working mediums.

$$\Delta T_m = \phi \Delta T_{lm,cf} \tag{2.8}$$

where ϕ [-] is the correction factor of log-mean temperature difference. $\Delta T_{lm,cf}$ [K] is the log-mean temperature difference for a counter-flow heat exchanger.

2.2.2 *$\mathcal{E}$-NTU method*

The effectiveness of heat exchanger is defined as (Klein, 2011)

$$\varepsilon = \frac{\dot{Q}}{\dot{Q}_{\max}} \tag{2.9}$$

where $\dot{Q}$ [W] is the actual rate of heat transfer, which can be expressed as (Klein, 2011)

$$\dot{Q} = c_{p,h}\dot{m}_h\left(T_{h,in} - T_{h,out}\right) = c_{p,c}\dot{m}_c\left(T_{c,out} - T_{c,in}\right) \tag{2.10}$$

where c_p [J/(kg·K)], $\dot{m}$ [kg/s], and T [K] are the specific heat capacity at constant pressure, mass flow rate, and temperature of working mediums, respectively. The subscripts *h*, *c*, *in*, and *out* indicate high/low temperature and inlet/outlet, respectively.

$\dot{Q}_{max}$ [W] is the maximum possible rate of heat transfer between the working mediums. Due to the maximum true mean temperature difference of counter-flow heat exchanger, $\dot{Q}_{max}$ can only occur at a counter-flow heat exchanger with infinite length. On the other hand, in a counter-flow heat exchanger, the temperature of high-temperature working medium cannot be cooled below the inlet temperature of low-temperature working medium. Similarly, the temperature of low-temperature working medium also cannot be heated above the inlet temperature of high-temperature working medium. Therefore, the maximum possible temperature difference of inlet and outlet for a certain working medium is the inlet temperature difference of the two working mediums. In addition, Equation (2.10) indicates that the working medium with the smaller heat capacity rate will experience the larger change in temperature. Therefore, the maximum possible rate of heat transfer $\dot{Q}_{max}$ is represented as (Klein, 2011)

$$\dot{Q}_{\max} = \left(c_p\dot{m}\right)_{\min}\left(T_{h,in} - T_{c,in}\right) \tag{2.11}$$

Where $\left(c_p\dot{m}\right)_{\min}$ [W/K] is the smaller value of the two heat capacity rates.

The effectiveness of heat exchanger, ε, defined in Equation (2.9), is dependent on the number of transfer units, *NTU* [-], the heat capacity rate ratio, C_R [-], and the flow arrangement. *NTU* is the dimensionless size of the heat exchanger, defined as (Klein, 2011)

$$NTU = \frac{UA}{\left(c_p\dot{m}\right)_{\min}} \tag{2.12}$$

C_R is the ratio of the smaller to larger heat capacity rate for the two working mediums, defined as (Klein, 2011)

$$C_R = \frac{\left(c_p \dot{m}\right)_{\min}}{\left(c_p \dot{m}\right)_{\max}} \tag{2.13}$$

For the most basic counter-flow and parallel-flow heat exchanger, the effectiveness of heat exchanger, ε, can be expressed by Equation (2.14) and (2.15) (Klein, 2011), respectively.

$$\varepsilon = \begin{cases} \dfrac{1-\exp\left[-NTU\left(1-C_R\right)\right]}{1-C_R\exp\left[-NTU\left(1-C_R\right)\right]} & for \;\; C_R < 1 \\ \dfrac{NTU}{1+NTU} & for \;\; C_R = 1 \end{cases} \tag{2.14}$$

$$\varepsilon = \frac{1-\exp\left[-NTU\left(1+C_R\right)\right]}{1+C_R} \tag{2.15}$$

2.2.3 Applicable scope of the two methods

As mentioned above, for the first type of problem in the heat exchanger design, due to the specified inlet and outlet temperatures, both *LMTD* method and *ε-NTU* method can be applied, but the *LMTD* method is relatively convenient. For the second type of problem, since the outlet temperatures are unknown, the rate of heat transfer $\dot{Q}$ and the log-mean temperature difference ΔT_{lm} cannot be calculated directly, a trial-and-error approach is needed. On this occasion, the *ε-NTU* method is preferred.

In this study, the relationship between effectiveness ε and the objective function is needed, so the *ε-NTU* method is adopted in the derivation process of the objective function.

§ 2.3 Derivation of objective function

2.3.1 Choice of objective function

As mentioned above, the number of entropy production units, *Ns* [-], which has been widely used by many researchers to evaluate the irreversibility loss in heat exchanger, was defined by Bejan (1982) as

$$Ns = \frac{\dot{S}_g}{\left(c_p \dot{m}\right)_{\min}} \tag{2.16}$$

where $\dot{S}_g$ [W/K] is the rate of entropy production generated during the irreversible process in the heat exchanger. The smaller *Ns* is, the better performance would be achieved.

If both the numerator and the denominator of Equation (2.16) are multiplied by ΔT, which is the temperature change corresponding to the working medium with smaller heat capacity rate, *Ns* can be expressed as

$$Ns = \frac{\dot{S}_g \Delta T}{\left(c_p \dot{m}\right)_{\min} \Delta T} = \frac{\dot{S}_g \Delta T}{\dot{Q}} \tag{2.17}$$

So the physical meaning of *Ns* is the rate of entropy production per unit rate of heat transfer multiplied by ΔT, the temperature change of the working medium with smaller heat capacity rate. But ΔT will become larger when the heat transfer area increases, which might lead to some ambiguities, such as the increase of *Ns* varying with the increase of effectiveness ε (Xu, 1996). In order to solve this problem, Xu (1996) represented a modified *Ns*, defined as

$$Ns = \frac{\dot{S}_g \left(T_{h,in} - T_{c,in}\right)}{\dot{Q}} \tag{2.18}$$

Compared with Equation (2.17), Equation (2.18) replaces the temperature change of the working medium with smaller heat capacity rate, ΔT, with the maximum possible temperature difference, ($T_{h,in}$-$T_{c,in}$). Since the inlet temperature of each working medium is specified at first in the design of heat exchanger, the maximum possible temperature difference is constant under the condition of given inlet temperatures, which will eliminate the ambiguity of the original *Ns*. Therefore, the modified *Ns* is adopted in this study as the objective function.

2.3.2 Expression of objective function for different working mediums

In order to convert the expression of *Ns* into the function of temperature and pressure, at first, the derivation of $\dot{S}_g$ in Equation (2.18) is necessary. For a counter-flow indirect-contact-type heat exchanger, the entropy budget is shown in Figure 2.2.

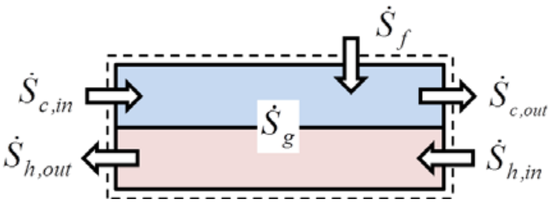

Figure 2.2 Entropy budget of an indirect-contact-type heat exchanger

The corresponding entropy budget equation is defined as Equation (2.19), where $\Delta\dot{S}_{sys}$ [W/K], $\dot{S}_{h,in}$ [W/K], $\dot{S}_{c,in}$ [W/K], $\dot{S}_f$ [W/K], $\dot{S}_{h,out}$ [W/K], and $\dot{S}_{c,in}$ [W/K] are the rate of entropy change of the system, the rate of inlet entropy of high/low temperature working medium, the rate of entropy transfer due to heat transfer between inside and outside of the heat exchanger and the rate of outlet entropy of high/low temperature working medium, respectively.

$$\Delta\dot{S}_{sys} = \dot{S}_{h,in} + \dot{S}_{c,in} + \dot{S}_f + \dot{S}_g - \dot{S}_{h,out} - \dot{S}_{c,out} \tag{2.19}$$

In usual, $\Delta\dot{S}_{sys}$ is zero for a steady-flow process. In addition, the heat exchanger is often seen as an adiabatic system; therefore, $\dot{S}_f$ is also zero. Then the entropy budget equation can be reduced as

$$\dot{S}_g = \left(\dot{S}_{h,out} - \dot{S}_{h,in}\right) + \left(\dot{S}_{c,out} - \dot{S}_{c,in}\right) \tag{2.20}$$

That is, the rate of entropy production generated during the irreversible process in the heat exchanger equals to the total rate of entropy change from inlet to outlet of high/low temperature working medium.

The entropy change of a system during a process can be determined by Equation (2.21) (Çengel, 2006) between the initial and the final states (state 1 and 2) as

$$\Delta\dot{S}_{1-2} = \dot{S}_2 - \dot{S}_1 = \int_1^2 \left(\frac{\delta\dot{Q}}{T}\right)_{\text{int } rev} \tag{2.21}$$

where the subscript "int *rev*" indicates that the process is an internally reversible process. It is important to note that the entropy depends on the state only and not the process path. Therefore, the entropy change $\Delta\dot{S}_{1-2}$ between two specified states is the same no matter what path, reversible or irreversible.

One other thing to note is that the integral of $\delta\dot{Q}/T$ gives us the value of entropy change only if the integration is carried out along an internally reversible path between the two states. Different values will be obtained when the integration is carried out along different irreversible paths (Çengel, 2006). Therefore, for convenience, the processes between inlet and outlet of the high/low temperature working mediums are assumed to be imaginary internally reversible path between the specified states in this study.

Then, by integrating Equation (2.20) and (2.21), the rate of entropy production in a counter-flow indirect-contact-type heat exchanger can be determined as

$$\dot{S}_g = \int_{h,in}^{h,out} \frac{\delta\dot{Q}}{T} + \int_{c,in}^{c,out} \frac{\delta\dot{Q}}{T} \tag{2.22}$$

where *h*, *c*, *in*, and *out* indicate high/low temperature and inlet/outlet, respectively. In addition, $\delta\dot{Q}$ can be expressed as

$$\delta\dot{Q} = \dot{m}\delta q \tag{2.23}$$

In a steady-flow system, δq can be defined as follows based on the energy balance equation (Nag, 2010)

$$\delta q = dh - vdP \tag{2.24}$$

where q [J/kg], h [J/kg], v [m^3/kg], and P [Pa] are the specific heat transfer amount, specific enthalpy, specific volume, and pressure, respectively.

In regard to the heat exchangers in the field of HAVC, if phase change is not taken into consideration, air and water are the most working mediums we contact. For air and water, the specific enthalpy change is defined as (Moran, 2010)

$$dh = c_p dT + v\left(1 - \beta T\right) dP \tag{2.25}$$

where β [1/K] is the coefficient of thermal expansion, which is defined as (Bagdade, 2002)

$$\beta = \frac{1}{v}\left(\frac{\partial v}{\partial T}\right)_p \tag{2.26}$$

Generally, air is seen as ideal gas in the analysis process for convenience. For ideal gas, based on Equation (2.26), the following conclusion can be obtained as

$$\beta T = \frac{T}{v}\left(\frac{\partial RT / P}{\partial T}\right)_p = \frac{RT}{Pv} = 1 \tag{2.27}$$

Therefore, by integrating Equation (2.23) – (2.27), when the single working medium is air or water, $\delta\dot{Q}$ can be expressed as Equations (2.28) and (2.29), respectively.

$$\delta\dot{Q} = \dot{m}c_p dT - \dot{V}dP \tag{2.28}$$

$$\delta\dot{Q} = \dot{m}c_p dT - \beta T\dot{V}dP \tag{2.29}$$

According to the type of the above-mentioned two kinds of working mediums, three kinds of typical heat exchangers can be represented, that is air-to-air, water-to-water, and air-to-water. Then, by integrating Equations (2.22), (2.28) and (2.29), the rate of entropy production $\dot{S}_g$ of the three kinds of typical heat exchangers can be expressed as follows successively. One thing to note here is that the Equation (2.32) is based on the assumption that air is high temperature working medium.

$$\dot{S}_g = c_{p,h}\dot{m}_h \ln\left(T_{h,out} / T_{h,in}\right) + c_{p,c}\dot{m}_c \ln\left(T_{c,out} / T_{c,in}\right) + \dot{V}_h \Delta P_h / T_{h,ave} + \dot{V}_c \Delta P_c / T_{c,ave} \tag{2.30}$$

$$\dot{S}_g = c_{p,h}\dot{m}_h \ln\left(T_{h,out} / T_{h,in}\right) + c_{p,c}\dot{m}_c \ln\left(T_{c,out} / T_{c,in}\right) + \beta_h \dot{V}_h \Delta P_h + \beta_c \dot{V}_c \Delta P_c \tag{2.31}$$

$$\dot{S}_g = c_{p,h}\dot{m}_h \ln\left(T_{h,out} / T_{h,in}\right) + c_{p,c}\dot{m}_c \ln\left(T_{c,out} / T_{c,in}\right) + \dot{V}_h \Delta P_h / T_{h,ave} + \beta_c \dot{V}_c \Delta P_c \tag{2.32}$$

where $\dot{V}$ [m^3/s] is the volume flow rate of working medium, ΔP [Pa] is the pressure difference between inlet and outlet for single working medium, T_{ave} [K] is the average temperature of inlet and outlet temperature. Similarly, the subscripts *h*, *c*, *in*, and *out* indicate high/low temperature and inlet/outlet, respectively.

It can be seen that the first two items in Equations (2.30) – (2.32) are the function of temperature; the other subsequent items are the function of pressure. Therefore, according to the type of irreversible loss, the rate of entropy production $\dot{S}_g$ can be defined as

$$\dot{S}_g = \dot{S}_{g,\Delta T} + \dot{S}_{g,\Delta P} \tag{2.33}$$

where $\dot{S}_{g,\Delta T}$ is the rate of entropy production due to the heat transfer through a finite temperature difference corresponding to the first two items in Equations (2.30) – (2.32); $\dot{S}_{g,\Delta T}$ is the rate of entropy production due to pressure drop corresponding to the other subsequent items in Equations (2.30) – (2.32).

Similarly, the number of entropy production units, Ns, can be defined as

$$Ns = Ns_{\Delta T} + Ns_{\Delta P} \tag{2.34}$$

By integrating Equation (2.9) – (2.11), (2.18), and (2.30) – (2.32), the number of entropy production units due to heat transfer, $Ns_{\Delta T}$, of above-mentioned three kinds of heat exchanger can be deduced as Equations (2.35); the number of entropy production units due to pressure loss, $Ns_{\Delta P}$, of above-mentioned four kinds of heat exchanger can be deduced as Equations (2.36) – (2.38), respectively, according to the order of Equations (2.30) – (2.32).

$$Ns_{\Delta T} = \frac{c_{p,h}\dot{m}_h}{\varepsilon\left(c_p\dot{m}\right)_{\min}}\ln\left[1+\frac{\varepsilon\left(c_p\dot{m}\right)_{\min}}{c_{p,h}\dot{m}_h}\left(\frac{T_{c,in}}{T_{h,in}}-1\right)\right]+\frac{c_{p,c}\dot{m}_c}{\varepsilon\left(c_p\dot{m}\right)_{\min}}\ln\left[1+\frac{\varepsilon\left(c_p\dot{m}\right)_{\min}}{c_{p,c}\dot{m}_c}\left(\frac{T_{h,in}}{T_{c,in}}-1\right)\right] \tag{2.35}$$

$$Ns_{\Delta P} = \frac{1}{\left(c_p\dot{m}\right)_{\min}\varepsilon}\left[\frac{\dot{V}_h\Delta P_h}{T_{h,in}-\dfrac{\varepsilon\left(c_p\dot{m}\right)_{\min}}{2c_{p,h}\dot{m}_h}\left(T_{h,in}-T_{c,in}\right)}+\frac{\dot{V}_c\Delta P_c}{T_{c,in}+\dfrac{\varepsilon\left(c_p\dot{m}\right)_{\min}}{2c_{p,c}\dot{m}_c}\left(T_{h,in}-T_{c,in}\right)}\right] \tag{2.36}$$

$$Ns_{\Delta P} = \frac{1}{\left(c_p\dot{m}\right)_{\min}\varepsilon}\left(\beta_h\dot{V}_h\Delta P_h+\beta_c\dot{V}_c\Delta P_c\right) \tag{2.37}$$

$$Ns_{\Delta P}=\frac{1}{\left(c_p\dot{m}\right)_{\min}\varepsilon}\left[\frac{\dot{V}_h\Delta P_h}{T_{h,in}-\dfrac{\varepsilon\left(c_p\dot{m}\right)_{\min}}{2c_{p,h}\dot{m}_h}\left(T_{h,in}-T_{c,in}\right)}+\beta_c\dot{V}_c\Delta P_c\right] \tag{2.38}$$

2.3.3 Calculation of heat transfer coefficient U and pressure loss ΔP

In order to calculate the value of $Ns_{\Delta\mathrm{T}}$ and $Ns_{\Delta\mathrm{P}}$, the heat transfer coefficient U of the heat exchanger in Equation (2.12) and the pressure loss ΔP of high/low temperature working mediums in Equations (2.36) – (2.38) should be calculated at first.

If the thermal-conduction resistance between high/low temperature working mediums is ignored, the heat transfer coefficient of the heat exchanger, U , can be expressed as

$$U=\frac{1}{\dfrac{1}{\alpha_h}+\dfrac{1}{\alpha_c}} \tag{2.39}$$

where α_h [W/(m^2·K)] and α_c [W/(m^2·K)] are the convective heat transfer coefficient of high/low temperature working mediums, respectively. The correlation of convective heat transfer coefficient is given by (Martin, 2010)

$$\alpha=Nu\frac{k}{D} \tag{2.40}$$

where Nu [-] is Nusselt number; k [W/(m·K)] is coefficient of thermal conductivity; D [m] is the hydraulic diameter of a single flow section, which is defined as (Thirumaleshwar, 2009)

$$D=4\frac{A_s}{L_s} \tag{2.41}$$

where A_s [m^2] is the area of cross-section of single flow and L_s [m] is the wetted perimeter.

For pipe flow, there are different expressions of Nusselt number corresponding to different flow states. For heat exchangers without fins, the Nusselt number can be defined as follows.

For fully developed laminar flow inside pipes, the correlation of Nusselt number is suggested by Sieder and Tate (Serth, 2014) as

$$Nu = 1.86\left(Re \cdot Pr \cdot \frac{D}{L}\right)^{1/3}\left(\frac{\mu}{\mu_s}\right)^{0.14} \quad for \;\; Re \le 2100 \tag{2.42}$$

where *Pr* [-] and *L* [m]are the Prandtl number and the length of the flow pass, respectively. μ [Pa·s] and μ_s [Pa·s] are the dynamic viscosity of the working mediums corresponding to the bulk temperature of the working medium and the wall temperature, respectively. Re [-] is Reynolds number, defined as

$$Re = \frac{uD}{v} \tag{2.43}$$

where u [m/s] and v [m^2/s] are the mean velocity and the kinematic viscosity of the working medium, respectively. For transitional flow inside pipes, Nusselt number is given by Hausen (Serth, 2014) as

$$Nu = 0.116\left(Re^{2/3} - 125\right)Pr^{1/3}\left[1 + \left(D/L\right)^{2/3}\right]\left(\frac{\mu}{\mu_s}\right)^{0.14} \quad for \;\; 2100 < Re < 10^4 \tag{2.44}$$

For turbulent flow inside pipes, the Sieder-Tate equation (Serth, 2014) is used as

$$Nu = 0.023Re^{0.8}Pr^{1/3}\left(\frac{\mu}{\mu_s}\right)^{0.14} \quad for \;\; Re \ge 10^4 \tag{2.45}$$

Then the heat transfer coefficient of the heat exchanger, U , can be calculated, according to Equations (2.40) – (2.45).

With respect to the pressure loss ΔP in heat exchanger, for convenience, the equation for calculating the pressure drop for pipe flow is adopted in this chapter as (Massoud, 2005)

$$\Delta P = \lambda \frac{L}{D} \frac{\rho u^2}{2} \tag{2.46}$$

where ρ [kg/m^3] is the density of working medium; λ [-] is the friction factor, a dimensionless empirical factor that is a function of Reynolds number. According to different flow states, friction factor λ has different expressions as follows.

For fully developed laminar flow, the friction factor λ can be defined as (Massoud, 2005)

$$\lambda = \frac{64}{Re} \quad for \quad Re \le 2000 \tag{2.47}$$

For transitional flow when 2000<Re<4000, friction factor λ is given by Зайченкоas's formula (Chen, 2012)

$$\lambda = 0.0025 \cdot \sqrt[3]{Re} \quad for \quad 2000 < Re < 4000 \tag{2.48}$$

When $Re \geq 4000$, friction factor λ is not only the function of Re, but also the function of relative roughness. Then in accordance with Альтщуль's formula (Chen, 2012), λ can be defined as

$$\lambda = 0.11 \left(\frac{\sigma}{D} + \frac{68}{Re} \right)^{0.25} \quad for \quad Re \ge 4000 \tag{2.49}$$

where σ [m] is the equivalent absolute roughness; σ/D is the relative roughness.

Then the pressure loss in heat exchanger, ΔP , can be calculated by Equations (2.46) – (2.49).

§ 2.4 Conclusions

In this Chapter, the basic design methods of heat exchanger are introduced at first. Then, based on the objective function, the number of entropy production units, *Ns*, the detailed derivation process of the objective function for three kinds of heat exchangers (air-to-air, water-to-water, and air-to-water) are carried out by us independently, which will provide the fundamental basis for the analysis and optimization of heat exchanger in the following.

Chapter 3 Sensitivity analysis of $Ns_{\Delta T}$ and $Ns_{\Delta P}$

In order to clarify the proportion of irreversible loss due to heat transfer and pressure loss, respectively, to make sense of the main inducement of irreversible process in the heat exchanger for different working mediums, the values of $Ns_{\Delta T}$ and $Ns_{\Delta P}$ of above-mentioned three kinds of heat exchangers are compared as follows by using the corresponding equations in Chapter 2.

§ 3.1 Calculation conditions of case study

As shown in Figure 3.1, for convenience, the analysis object is simplified into a simple counter-flow indirect contact type heat exchanger unit. For both high/low temperature working mediums, the cross section of flow pass is assumed as square with a constant side length, 5mm; the inlet temperature of low temperature working medium is set as a constant value, 5°C. Meanwhile, the Reynolds numbers of high/low temperature working mediums are assumed to be same for each case in calculation.

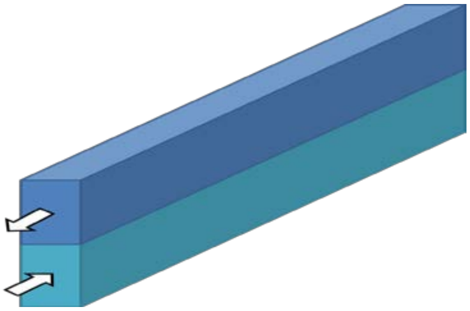

Figure 3.1 Analysis object

As for the case study, three types of heat exchanger with three kinds of inlet temperature differences, three kinds of length-to-diameter ratios, and nine kinds of inlet Reynolds numbers, namely 243 cases are calculated, as shown in Table 3.1.

Table 3.1 Properties of heat exchangers

Type of heat exchanger	Air-to-air, water-to-water, air -to-water
Inlet temperature difference	10°C, 15°C, 20°C (Inlet temp of low temp working medium: 5°C)
Length-to-diameter ratio	80, 120, 160 (Hydraulic diameter: 5mm)
Inlet Reynolds number	100, 300, 1000, 3000, 5000, 8000, 10000, 12000, 15000

With respect to the physical property parameters of the working mediums in each case, due to the uncertainty of outlet temperature in the calculation formulas as shown in Equations (2.35)-(2.38), for simplicity, the physical property parameters of high/low temperature working mediums at the average inlet temperature are adopted in each case. Meanwhile, in order to ignore the effect of temperature change on the physical property parameters of the working mediums, the dynamic viscosity ratio, $(\mu/\mu_s)^{0.14}$, in Equations (2.42), (2.44), and (2.45) are assumed to be the value of 1.

In order to clarify the effect of the type of working medium, the inlet temperature difference, the length-to-diameter ratio, and the Reynolds number on the value of ε, Ns, $Ns_{\Delta T}$, $Ns_{\Delta P}$ and the $Ns_{\Delta P}$ -to-Ns ratio, the corresponding sensitivity analysis are carried out as follows.

§ 3.2 Analysis of air-to-air heat exchanger

3.2.1 Analysis of $Ns_{\Delta T}$ and $Ns_{\Delta P}$ in different length-to-diameter ratios

When the inlet temperature difference is fixed at 10°C, the trend of ε, Ns, $Ns_{\Delta T}$, $Ns_{\Delta P}$, and $Ns_{\Delta P}$ -to-Ns ratio varying with Reynolds number at different length-to-diameter ratios are shown in Figures 3.2 – 3.5, respectively.

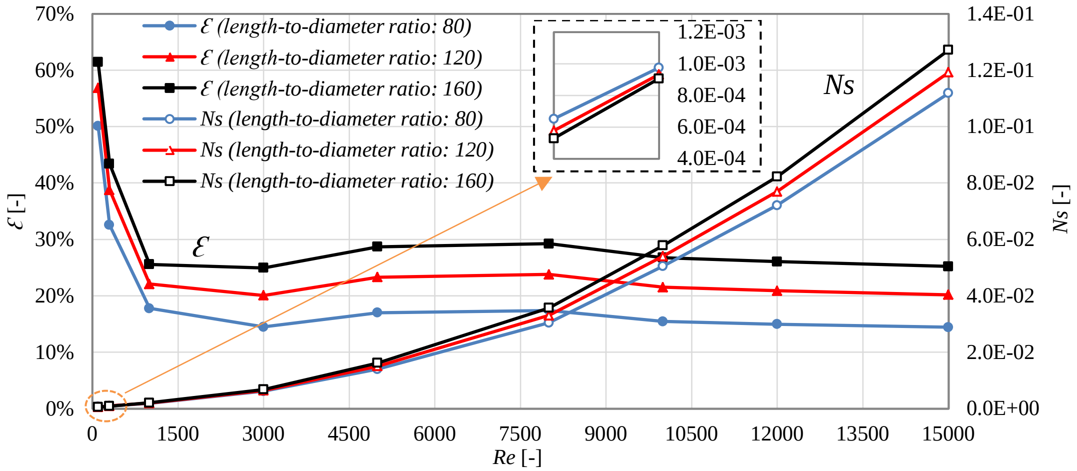

Figure 3.2 Variation trends of ε and Ns at three different length-to-diameter ratios

As shown in Figure 3.2, the variation trend of the effectiveness of heat exchanger ε and the number of entropy production units *Ns* is different. By and large, ε decreases with the increase of Reynolds number, and *Ns* is the opposite. But when the working medium is in transitional flow, ε increases slightly with the increase of Reynolds number. The reason for this is that: *NTU* has a positive correlation with ε from Equation (2.15). The heat transfer coefficient *U* and mass flow rate $\dot{m}$, as part of the numerator and denominator in the definition of *NTU* (Equation 2.12), respectively, increase with the increase of Reynolds number. But $\dot{m}$ increase faster than *U* in laminar and turbulent flow, and increase more slowly than *U* in transitional flow, so that is why ε has this trend varying with the increase of Reynolds number. Moreover, it is noted that the heat exchanger has higher effectiveness when the working medium is in laminar flow that is why lower Reynolds number of the working medium is adopted by many high-effective heat exchangers, such as plate-fin heat exchanger.

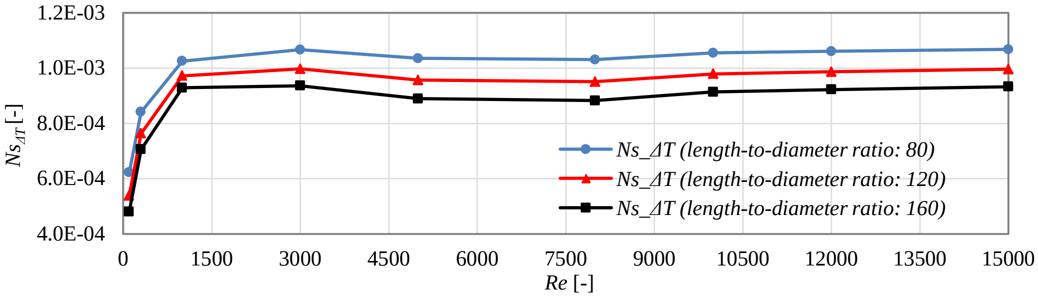

Figure 3.3 Variation trends of $Ns_{\Delta T}$ at three different length-to-diameter ratios

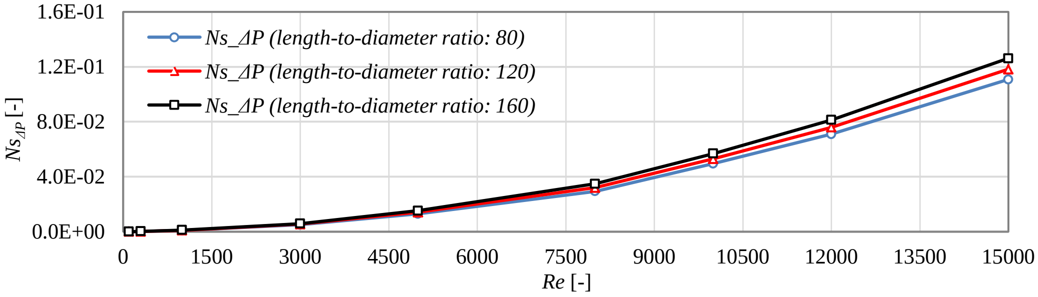

Figure 3.4 Variation trends of $Ns_{\Delta P}$ at three different length-to-diameter ratios

In addition, with respect to the effect of length-to-diameter ratios, it can be seen that both ε and *Ns* increase with the increase of length-to-diameter ratios except for the value of *Ns* at the Reynolds number of 100 and 300. The reason can be found from Figures 3.3 – 3.5. $Ns_{\Delta T}$ and $Ns_{\Delta P}$ decreases and increases, respectively, with the increase of length-to-diameter ratio, as shown in Figures 3.3 and 3.4. But the $Ns_{\Delta P}$ -to-*Ns* ratio is smaller at lower Reynolds number as shown in Figures 3.5; therefore the effect of the decrease of $Ns_{\Delta T}$ on the value of Ns varying with the increase of length-to-diameter ratio is more obvious when the Reynolds number is 100 and 300. We can learn that at low Reynolds number, higher length-to-diameter ratio helps to obtain higher heat-transfer efficiency and lower irreversible loss.

In addition, by comparing Figures 3.2 and 3.3, it can be seen that there is a strong negative correlation between the effectiveness of heat exchanger ε and the number of entropy production units Ns. It is because $Ns_{\Delta T}$ is only the function of ε but not the pressure loss of the heat exchanger, as shown in Equation 2.37.

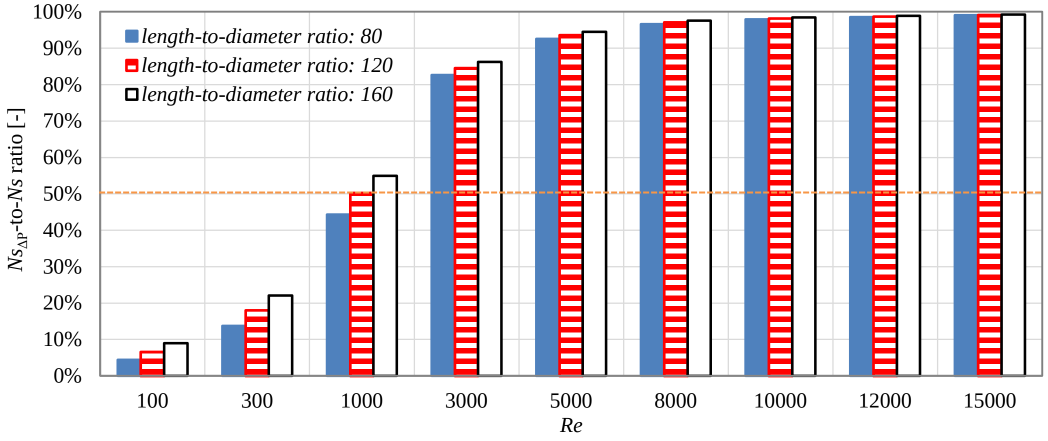

Figure 3.5 Variation trends of $Ns_{\Delta P}$-to-Ns ratio at different length-to-diameter ratios

In regard to the $Ns_{\Delta P}$ -to-Ns ratio, as shown in Figures 3.5, at any Reynolds number, $Ns_{\Delta P}$ -to-Ns ratio increases with the increase of the length-to-diameter ratio, but the rising range decreases step by step with the increase of Reynolds number. In addition, for any length-to-diameter ratio, the $Ns_{\Delta P}$ -to-Ns ratio is about 0% – 50% when the Reynolds number is 100 – 1000 and reach to high value rapidly when the Reynolds number is 3000 – 15000. Therefore, for air-to-air heat exchanger, the irreversible loss is mainly caused by heat transfer at lower Reynolds number and by pressure loss at higher Reynolds number.

3.2.2 Analysis of $Ns_{\Delta T}$ and $Ns_{\Delta P}$ at different inlet temperature differences

When the length-to-diameter ratio is fixed at 80, the trend of ε, Ns, $Ns_{\Delta T}$, $Ns_{\Delta P}$, and $Ns_{\Delta P}$ -to-Ns ratio varying with Reynolds number at different inlet temperature differences are shown in Figures 3.6 – 3.9, respectively.

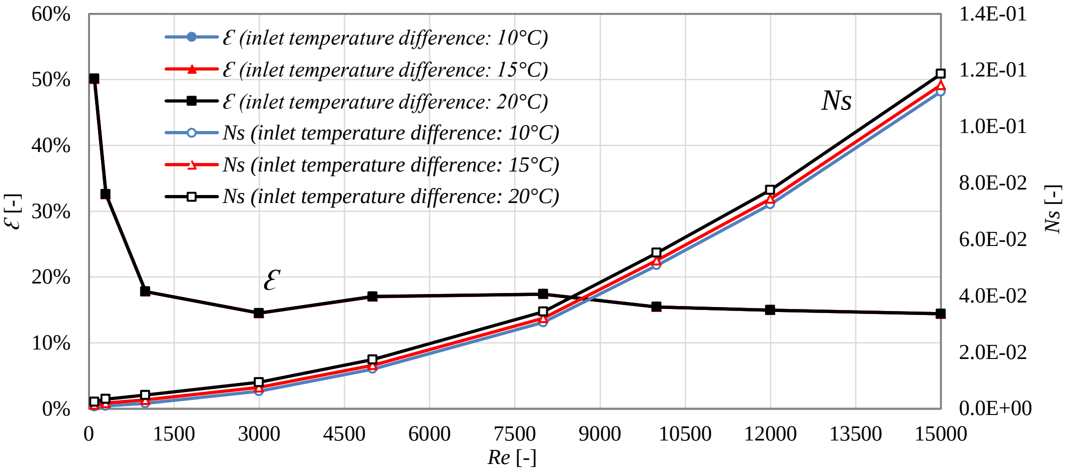

Figure 3.6 Variation trends of ε and Ns at three different inlet temperature differences

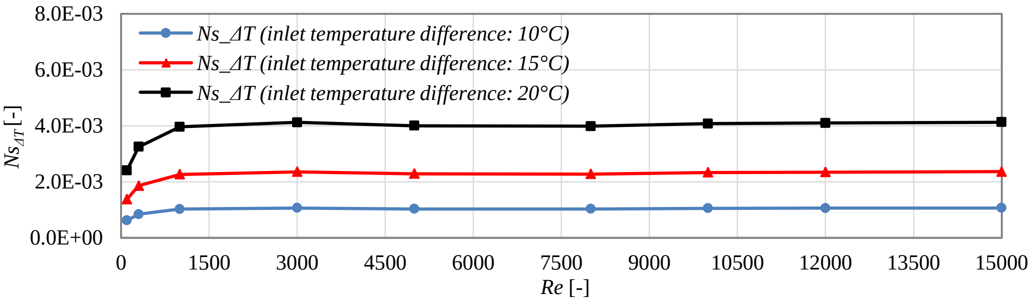

Figure 3.7 Variation trends of $Ns_{\Delta T}$ at three different inlet temperature differences

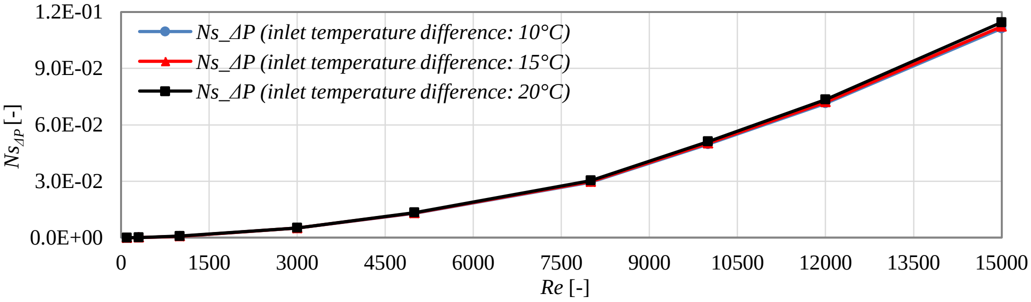

Figure 3.8 Variation trends of $Ns_{\Delta P}$ at three different inlet temperature differences

As shown in Figure 3.6, the variation trends of the effectiveness of heat exchanger ε and the number of entropy production units *Ns* at different inlet temperature differences are same with Figure 3.2. It can be also noted that higher effectiveness can be obtained when the working medium is in laminar flow. In addition, with respect to the effect of inlet temperature differences, it can be seen that ε is not sensitive to the change of inlet temperature difference; *Ns* increases slightly with the increase of inlet temperature difference. With respect to the variation trends of $Ns_{\Delta T}$ and $Ns_{\Delta P}$, $Ns_{\Delta T}$ also increases slightly with the increase of inlet temperature difference, but $Ns_{\Delta P}$ remains almost the same with increasing inlet temperature difference.

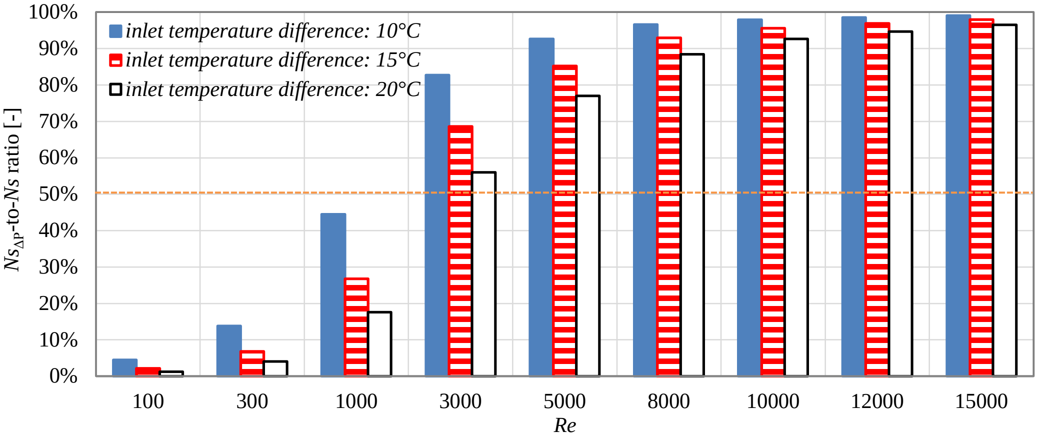

Figure 3.9 Variation trends of $Ns_{\Delta P}$-to-*Ns* ratio at different inlet temperature differences

In regard to the $Ns_{\Delta P}$-to-*Ns* ratio, as shown in Figures 3.9, at any Reynolds number, $Ns_{\Delta P}$-to-*Ns* ratio decreases with the increase of the inlet temperature difference, but the falling range decreases step by step with the increase of Reynolds number. In addition, for any inlet temperature difference, the $Ns_{\Delta P}$-to-*Ns* ratio is about 0% – 50% when the Reynolds number is 100 – 1000 and reach to high value rapidly when the Reynolds number is 3000 – 15000.

3.2.3 Conclusion

For air-to-air heat exchanger defined in section 3.1, it can be seen based on above analysis as follows:

(1) The effectiveness of heat exchanger ε increases with the increase of length-to-diameter ratio but is not sensitive to the change of inlet temperature difference.

(2) The number of entropy production units due to heat transfer, $Ns_{\Delta T}$, decreases with the increase of length-to-diameter ratio, and increases with the increase of inlet temperature difference.

(3) The number of entropy production units due to pressure loss, $Ns_{\Delta P}$, increases with the increase of length-to-diameter ratio, but is not sensitive to the change of inlet temperature difference.

(4) The $Ns_{\Delta P}$-to-*Ns* ratio increases with the increase of the length-to-diameter ratio, and decreases with

the increase of the inlet temperature difference.

(5) The irreversible loss is mainly caused by heat transfer at lower Reynolds number and by pressure loss at higher Reynolds number.

§ 3.3 Analysis of water-to-water heat exchanger

3.3.1 Analysis of $Ns_{\Delta T}$ and $Ns_{\Delta P}$ in different length-to-diameter ratios

When the inlet temperature difference is fixed at 10°C, the trend of ε, Ns, $Ns_{\Delta T}$, $Ns_{\Delta P}$, and $Ns_{\Delta P}$ -to-Ns ratio varying with Reynolds number at different length-to-diameter ratios are shown in Figures 3.10 – 3.13, respectively.

Unlike the variation trends of ε and Ns for air-to-air heat exchanger in Figure 3.2, it can be seen from Figure 3.10 that for water-to-water heat exchanger, at any Reynolds number, ε increases with the increase of length-to-diameter ratio, and Ns decreases with the increase of length-to-diameter ratio. The reason can be found from Figures 3.11 – 3.13. $Ns_{\Delta T}$ decreases with the increase of length-to-diameter ratio, but $Ns_{\Delta P}$ is not sensitive to the increase of length-to-diameter ratio, as shown in Figures 3.11 and 3.12. In addition, the $Ns_{\Delta P}$ -to-Ns ratio is only less than 2.5% at any Reynolds number as shown in Figures 3.13; therefore the variation trend of Ns is exactly the same with that of $Ns_{\Delta T}$ at any Reynolds number.

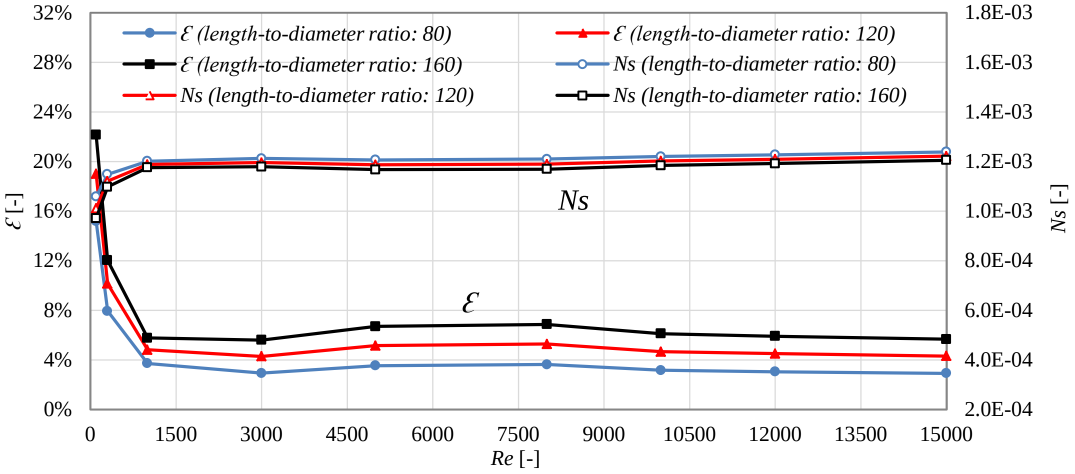

Figure 3.10 Variation trends of ε and Ns at three different length-to-diameter ratios

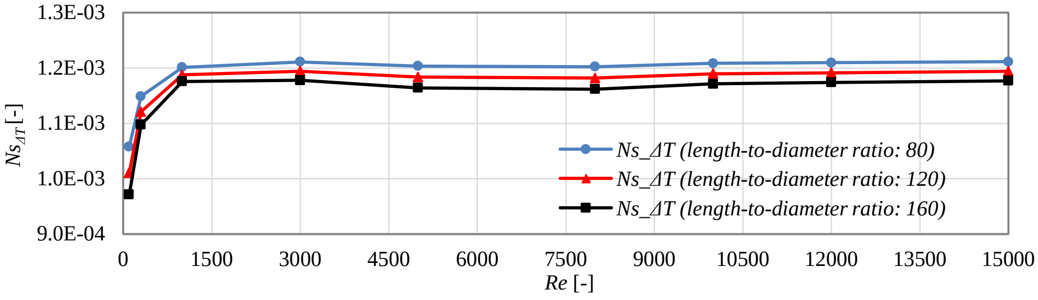

Figure 3.11 Variation trends of $Ns_{\Delta T}$ at three different length-to-diameter ratios

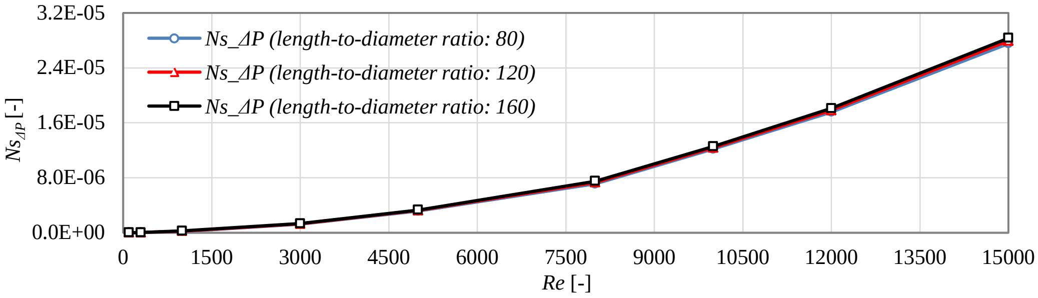

Figure 3.12 Variation trends of $Ns_{\Delta P}$ at three different length-to-diameter ratios

Moreover, as shown in Figure 3.13, the $Ns_{\Delta P}$ -to-Ns ratio also increases with the increase of length-to-diameter ratios, like Figure 3.5, but the difference is that the rising range increases step by step with the increase of Reynolds number in Figure 3.13.

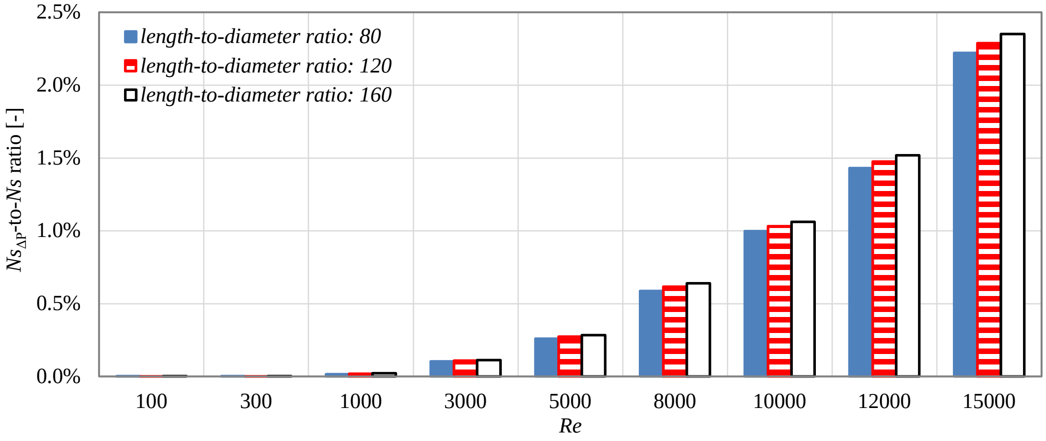

Figure 3.13 Variation trends of $Ns_{\Delta P}$-to-Ns ratio at different length-to-diameter ratios

3.3.2 Analysis of $Ns_{\Delta T}$ and $Ns_{\Delta P}$ at different inlet temperature differences

When the length-to-diameter ratio is fixed at 80, the trend of ε, *Ns*, $Ns_{\Delta T}$, $Ns_{\Delta P}$, and $Ns_{\Delta P}$ -to-*Ns* ratio varying with Reynolds number at different inlet temperature differences are shown in Figures 3.14 – 3.17, respectively.

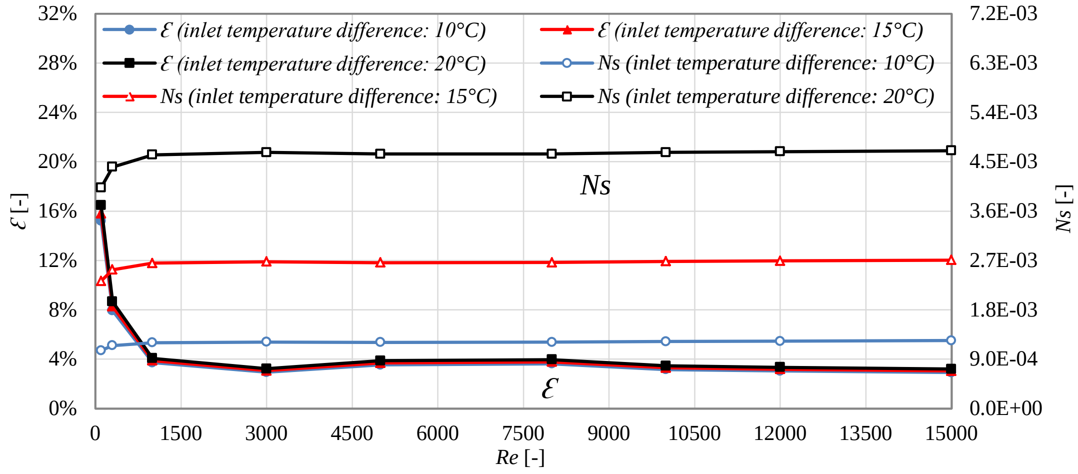

Figure 3.14 Variation trends of ε and *Ns* at three different inlet temperature differences

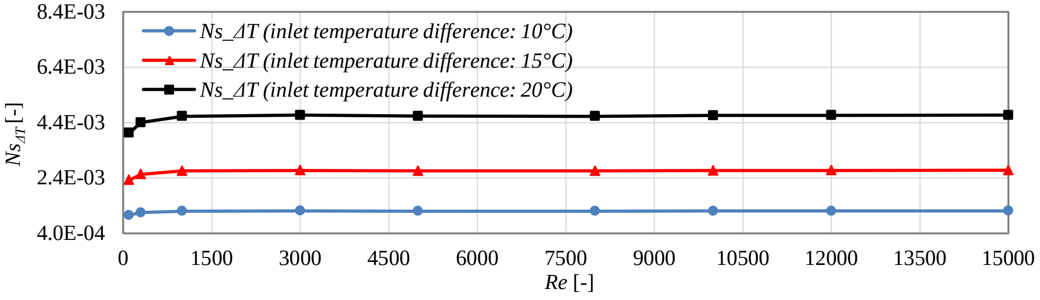

Figure 3.15 Variation trends of $Ns_{\Delta T}$ at three different inlet temperature differences

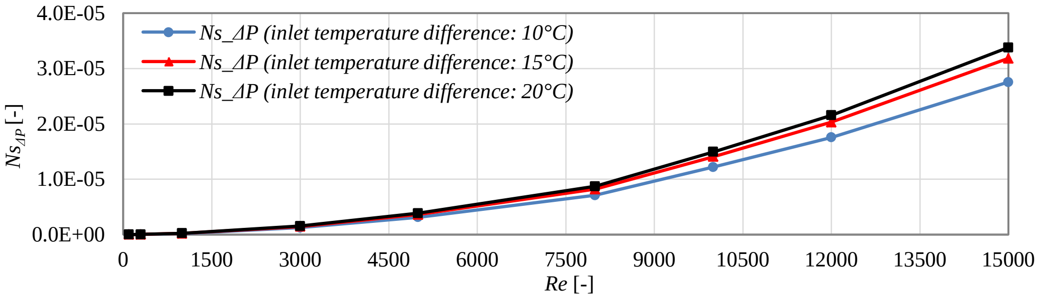

Figure 3. 16 Variation trends of $Ns_{\Delta P}$ at three different inlet temperature differences

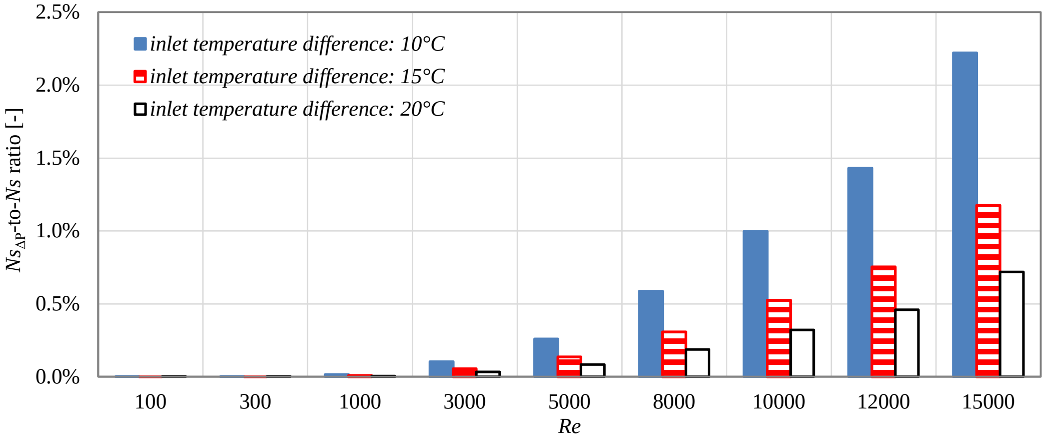

Figure 3.17 Variation trends of $Ns_{\Delta P}$-to-Ns ratio at different inlet temperature differences

It can be seen from Figure 3.14 that for water-to-water heat exchanger, Ns increase with the increase of inlet temperature difference at any Reynolds number but ε is not sensitive to the increase of inlet temperature difference. The variation trend of Ns is quite the same with that of $Ns_{\Delta T}$. The reason is also due to the low $Ns_{\Delta P}$ -to-Ns ratio at any Reynolds number as shown in Figures 3.17. In addition, just as that of air-to-air heat exchanger, $Ns_{\Delta P}$ is also not sensitive to the changer of inlet temperature difference, but increases slightly with the increase of inlet temperature difference at higher Reynolds number.

.

In regard to the $Ns_{\Delta P}$ -to-Ns ratio, as shown in Figures 3.17, at any Reynolds number, $Ns_{\Delta P}$ -to-Ns ratio also decreases with the increase of the inlet temperature difference, like Figure 3.9. But the falling range increases step by step with the increase of Reynolds number, which is just opposite to Figure 3.9. In addition, for any Reynolds number, the $Ns_{\Delta P}$ -to-Ns ratio is less than 2.5%.

3.3.3 Conclusion

For water-to-water heat exchanger defined in section 3.1, some conclusions can be obtained based on above analysis. Compared with air-to-air heat exchanger, the conclusions (1), (2), (4) expressed in section 3.2.3 are also applicable for water-to-water heat exchanger. For conclusion (3), the number of entropy production units due to pressure loss, $Ns_{\Delta P}$, is not sensitive to the increase of length-to-diameter and inlet temperature difference but increases slightly with the increase of inlet temperature difference at higher Reynolds number for water-to-water heat exchanger. For conclusions (5), the irreversible loss of water-to-water heat exchanger is mainly caused by heat transfer at any Reynolds number.

§ 3.4 Analysis of air-to-water heat exchanger

Air is assumed to be the high temperature working medium in this section.

3.4.1 Analysis of $Ns_{\Delta T}$ and $Ns_{\Delta P}$ in different length-to-diameter ratios

When the inlet temperature difference is fixed at 10°C, the trend of ε, Ns, $Ns_{\Delta T}$, $Ns_{\Delta P}$, and $Ns_{\Delta P}$ -to-Ns ratio varying with Reynolds number at different length-to-diameter ratios are shown in Figures 3.18 – 3.21, respectively.

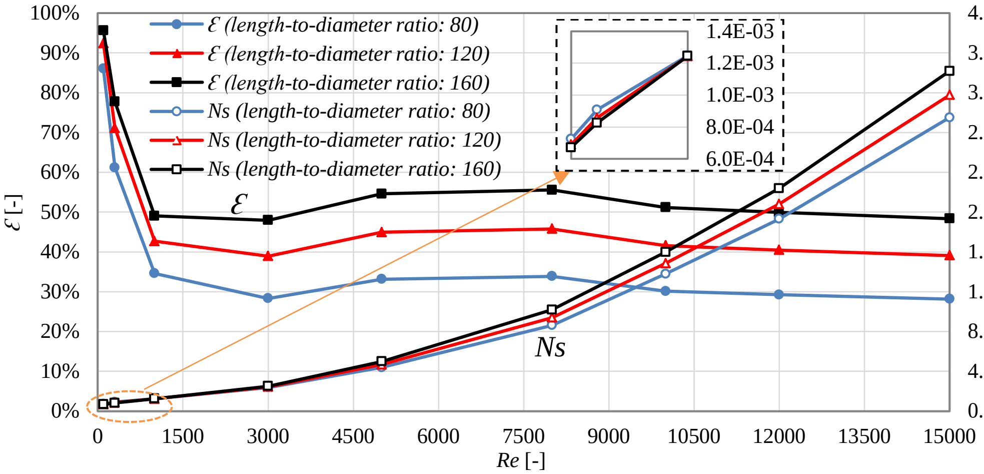

Figure 3.18 Variation trends of ε and Ns at three different length-to-diameter ratios

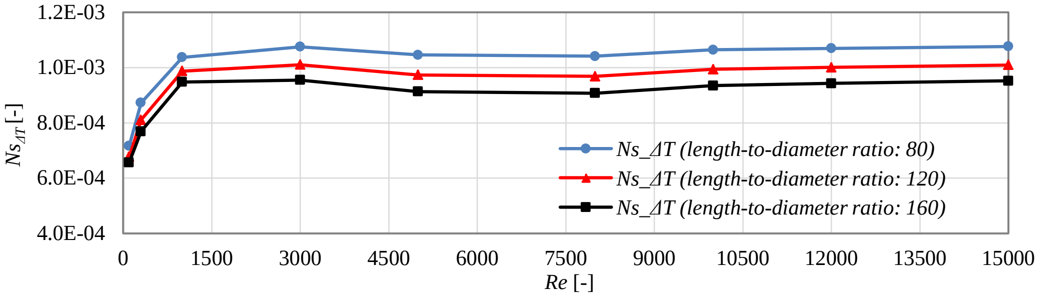

Figure 3.19 Variation trends of $Ns_{\Delta T}$ at three different length-to-diameter ratios

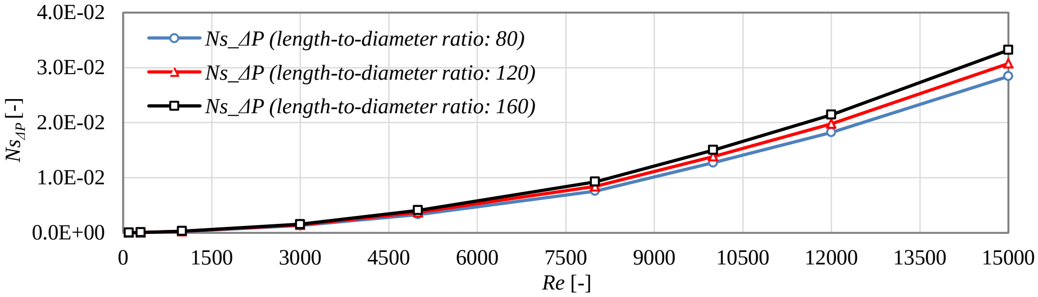

Figure 3.20 Variation trends of $Ns_{\Delta P}$ at three different length-to-diameter ratios

The variation trends of ε and *Ns* similar to those shown in Figure 3.2 can be seen from Figure 3.18. Due to the low $Ns_{\Delta P}$-to-*Ns* ratio at low Reynolds number, the variation trend of *Ns* with length-to-diameter ratio is identical with that of $Ns_{\Delta T}$ at low Reynolds number, and is identical with that of $Ns_{\Delta P}$ at higher Reynolds number, as shown in Figures 3.18 – 3.20.

In regard to the $Ns_{\Delta P}$ -to-*Ns* ratio, for any length-to-diameter ratio, the $Ns_{\Delta P}$ -to-*Ns* ratio is about 0% – 50% when the Reynolds number is 100 – 3000 and reach to high value rapidly when the Reynolds number is 5000 – 15000, as shown in Figure 3.21.

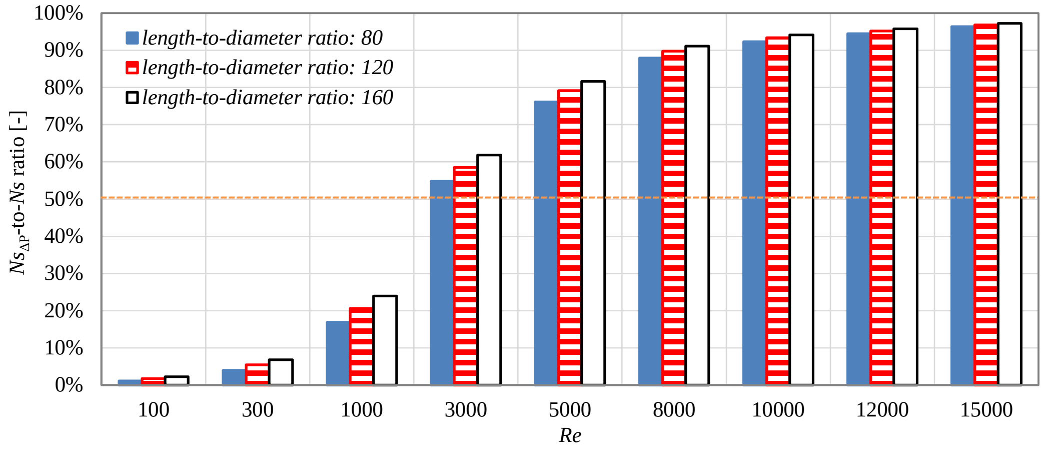

Figure 3.21 Variation trends of $Ns_{\Delta P}$-to-*Ns* ratio at different length-to-diameter ratios

3.4.2 Analysis of $Ns_{\Delta T}$ and $Ns_{\Delta P}$ at different inlet temperature differences

When the length-to-diameter ratio is fixed at 80, the trend of ε, *Ns*, $Ns_{\Delta T}$, $Ns_{\Delta P}$, and $Ns_{\Delta P}$ -to-*Ns* ratio varying with Reynolds number at different inlet temperature differences are shown in Figures 3.22 –

3.25, respectively.

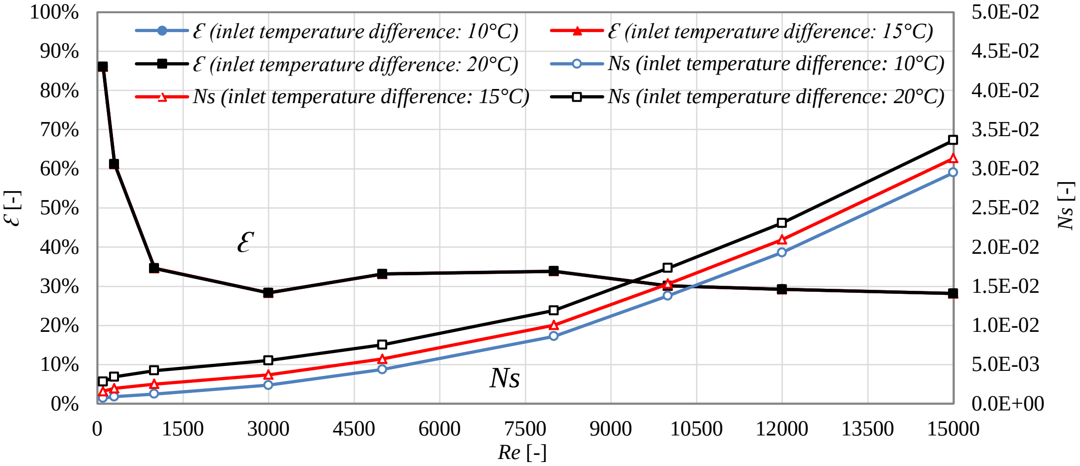

Figure 3.22 Variation trends of ε and Ns at three different inlet temperature differences

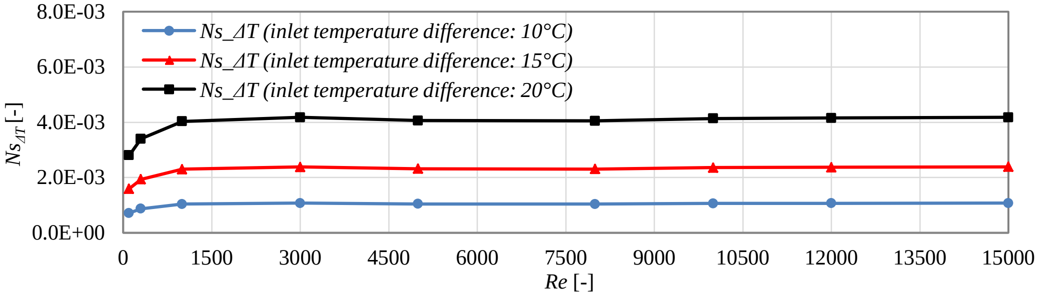

Figure 3.23 Variation trends of $Ns_{\Delta T}$ at three different inlet temperature differences

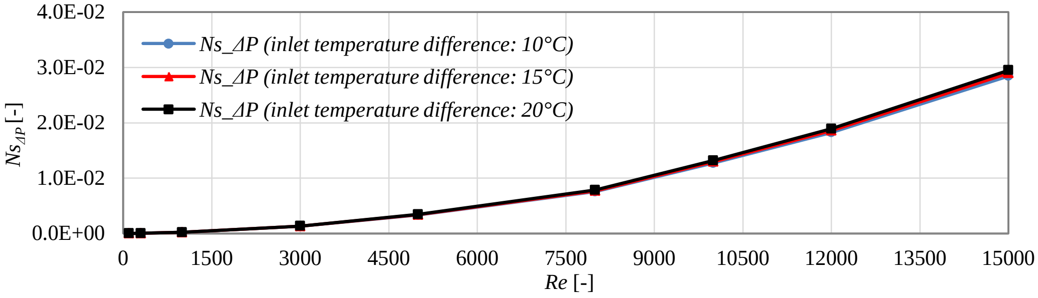

Figure 3.24 Variation trends of $Ns_{\Delta P}$ at three different inlet temperature differences

As shown in Figure 3.22, just like above-mentioned two kinds of heat exchangers, ε is not sensitive to the change of inlet temperature difference; *Ns* increases with the increase of inlet temperature. The variation trend of $Ns_{\Delta T}$ and $Ns_{\Delta P}$ are also the same with those of above-mentioned two kinds of heat exchangers. $Ns_{\Delta T}$ increases with the increase of inlet temperature and $Ns_{\Delta P}$ is not sensitive to the change of inlet temperature difference, as shown in Figures 3.23 and 3.24.

In regard to the $Ns_{\Delta P}$ -to-*Ns* ratio, as shown in Figure 3.25, for the inlet temperature difference of 10°C, the $Ns_{\Delta P}$ -to-*Ns* ratio is about 0% – 50% when the Reynolds number is 100 – 1000 and reach to 50% – 100% when the Reynolds number is 3000 – 15000; for the inlet temperature difference of 15°C, the $Ns_{\Delta P}$ -to-*Ns* ratio is about 0% – 50% when the Reynolds number is 100 – 3000 and greater than 50% when the Reynolds number is 5000 – 15000; for the inlet temperature difference of 20°C, the $Ns_{\Delta P}$ -to-*Ns* ratio is about 0% – 50% when the Reynolds number is 100 – 5000 and greater than 50% when the Reynolds number is 8000 – 15000.

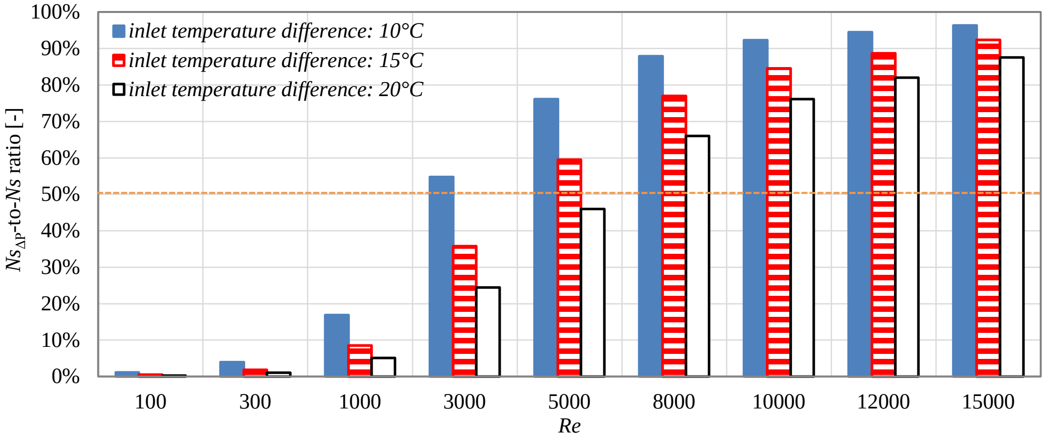

Figure 3.25 Variation trends of $Ns_{\Delta P}$-to-*Ns* ratio at different inlet temperature differences

3.4.3 Conclusion

For air (high temp.)-to-water (low temp.) heat exchanger defined in section 3.1, the conclusions expressed in section 3.2.3 are also applicable for air (high temp.)-to-water (low temp.) heat exchanger.

§ 3.5 Comparison of three kinds of heat exchangers

For convenience, the value of ε, *Ns*, $Ns_{\Delta T}$, $Ns_{\Delta P}$, and $Ns_{\Delta P}$ -to-*Ns* ratio of above-mentioned three kinds heat exchangers are compared when the length-to-diameter ratio and inlet temperature difference are fixed at 10°C and 80, respectively, as shown in Figures 3.26 – 3.30.

It can be seen from Figure 3.26 that under the same baseline, at any Reynolds number, the air-to-water heat exchanger achieves the highest effectiveness, the air-to-air heat exchanger is the second, and the water-to-water heat exchanger is the least. Therefore, a smaller heat capacity rate ratio helps to gain higher effectiveness of heat exchanger. In addition, for both air-to-air and water-to-water heat exchangers, the heat capacity rate is 1 under the setting conditions of this study, and then the effectiveness of heat exchanger is only the function of *NTU*, and is proportional to the value of *NTU*, as shown in Equation (2.14). Due to the smaller heat capacity of air, air-to-air heat exchanger will obtain the higher value of *NTU* from Equation (2.12). Therefore, the effectiveness of air-to-air heat exchanger is larger than that of water-to-water heat exchanger.

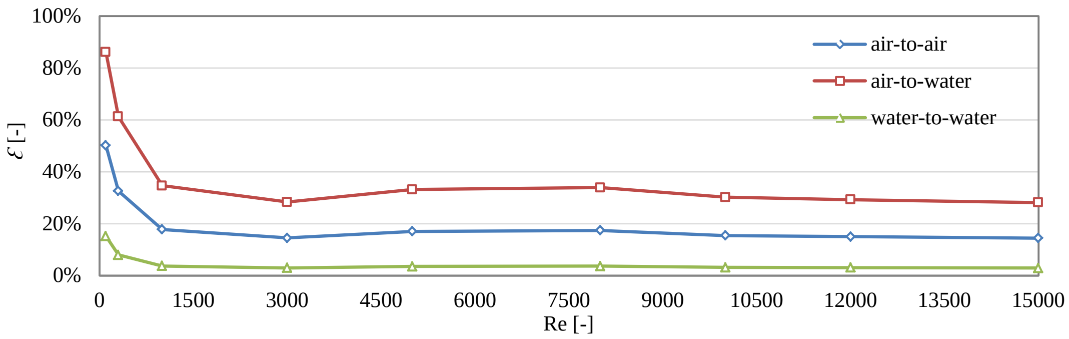

Figure 3 26 Variation trends of ε for three kinds of heat exchangers

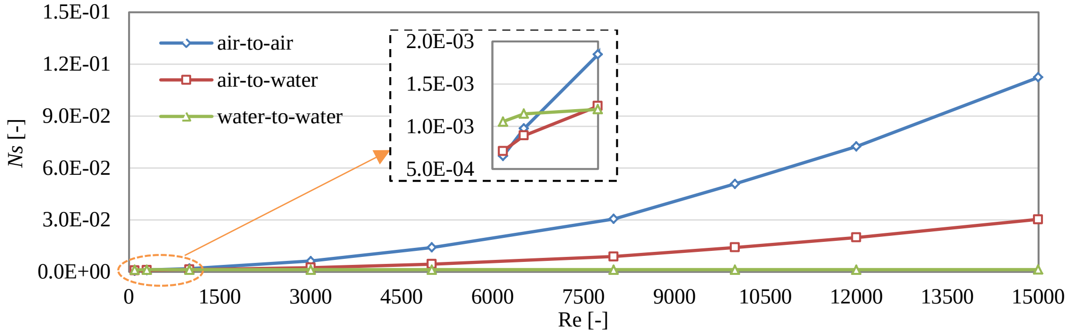

Figure 3.27 Variation trends of *Ns* for three kinds of heat exchangers

In addition, it can be seen from Figure 3.28 that the value of $Ns_{\Delta T}$ increases following the order of air-to-air, air-to-water, and water-to-water at any Reynolds number. But the value of $Ns_{\Delta P}$ increases following the opposite order as shown in Figure 3.29.

With respect to the comparison of *Ns* for three kinds of heat exchangers, as shown in Figures 3.27, when the Reynolds number is equal or greater than 1000, the ascending order of *Ns* for three kinds of heat exchangers is quite the same with that of $Ns_{\Delta P}$; when the Reynolds number is less than 1000, the ascending order of *Ns* for three kinds of heat exchangers mainly consistent with that of $Ns_{\Delta T}$.

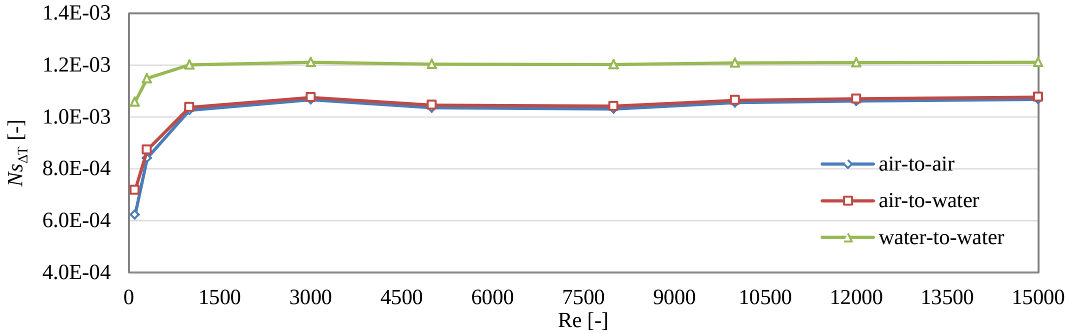

Figure 3.28 Variation trends of $Ns_{\Delta T}$ for three kinds of heat exchangers

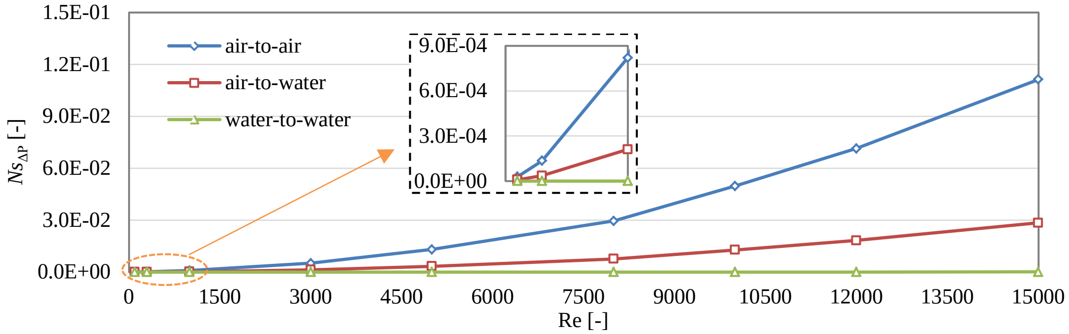

Figure 3.29 Variation trends of $Ns_{\Delta P}$ for three kinds of heat exchangers

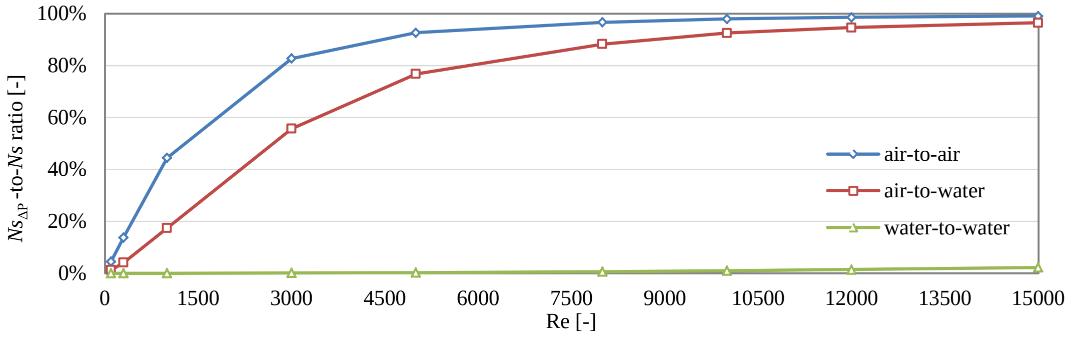

Figure 3.30 Variation trends of $Ns_{\Delta P}$ -to-*Ns* ratio for three kinds of heat exchangers

For the $Ns_{\Delta P}$-to-Ns ratio, the ascending order of $Ns_{\Delta P}$-to-Ns ratio for three kinds of heat exchangers is water-to-water, air-to-water, and air-to-air, as shown in Figure 3.30. For water-to-water heat exchanger, the irreversible loss is caused by heat transfer at any Reynolds number. For air-to-water and air-to-air heat exchangers, the irreversible loss is mainly caused by heat transfer at lower Reynolds number and by pressure loss at higher Reynolds number.

§ 3.6 Conclusions

In this Chapter, the values of $Ns_{\Delta T}$ and $Ns_{\Delta P}$ of three kinds of heat exchangers are compared under three kinds of inlet temperature differences, three kinds of length-to-diameter ratios, and nine kinds of inlet Reynolds numbers. Some conclusions are obtained as follows.

For air-to-air heat exchanger, the effectiveness of heat exchanger ε increases with the increase of length-to-diameter ratio but is not sensitive to the change of inlet temperature difference.; the number of entropy production units due to heat transfer, $Ns_{\Delta T}$, decreases with the increase of length-to-diameter ratio, and increases with the increase of inlet temperature difference; the number of entropy production units due to pressure loss, $Ns_{\Delta P}$, increases with the increase of length-to-diameter ratio, but is not sensitive to the change of inlet temperature difference; the $Ns_{\Delta P}$-to-Ns ratio increases with the increase of the length-to-diameter ratio, and decreases with the increase of the inlet temperature difference; the irreversible loss is mainly caused by heat transfer at lower Reynolds number and by pressure loss at higher Reynolds number.

For water-to-water heat exchanger, the number of entropy production units due to pressure loss, $Ns_{\Delta P}$, is not sensitive to the increase of length-to-diameter and inlet temperature difference but increases slightly with the increase of inlet temperature difference at higher Reynolds number for water-to-water heat exchanger. In addition, the irreversible loss of water-to-water heat exchanger is mainly caused by heat transfer at any Reynolds number. Other conclusions are same with those of air-to-air heat exchanger except for the above-mentioned two conclusions.

For air (high temp.)-to-water (low temp.) heat exchanger, conclusions are quite the same with those of air-to-air heat exchanger.

For the comparison of three kinds of heat exchangers, under the same baseline, at any Reynolds number, the air-to-water heat exchanger achieves the highest effectiveness, the air-to-air heat exchanger is the second, and the water-to-water heat exchanger is the least. The value of $Ns_{\Delta T}$ increases following the order of air-to-air, air-to-water, and water-to-water at any Reynolds number, but the value of $Ns_{\Delta P}$ increases following the opposite order. With respect to the comparison of *Ns* for three kinds of heat exchangers, when the Reynolds number is equal or greater than 1000, the ascending order of *Ns* for three kinds of heat exchangers is quite the same with that of $Ns_{\Delta P}$; when the Reynolds number is less than 1000, the ascending order of *Ns* for three kinds of heat exchangers mainly consistent with that of $Ns_{\Delta T}$. For the $Ns_{\Delta P}$ -to-*Ns* ratio, the ascending order of $Ns_{\Delta P}$ -to-*Ns* ratio for three kinds of heat exchangers is water-to-water, air-to-water, and air-to-air. For water-to-water heat exchanger, the irreversible loss is caused by heat transfer at any Reynolds number. For air-to-water and air-to-air heat exchangers, the irreversible loss is mainly caused by heat transfer at lower Reynolds number and by pressure loss at higher Reynolds number.

Chapter 4 Fin-shape optimization of plate-fin heat exchanger

Chapter 2 represents the expressions of the objective functions for thermodynamic optimization of three kinds of heat exchangers. By using those expressions, in Chapter 3, the sensitivity analysis is carried out based on an assumed theoretical heat exchanger for clarifying the main inducement of irreversible process in the heat exchanger for different working mediums. In this chapter, the thermodynamic fin-optimization of a specific type heat exchanger, namely plate-fin heat exchanger, is conducted by using above-mentioned objective functions.

§ 4.1 Introduction

Plate-fin heat exchangers are widely used in cryogenics and the aerospace industry because of their compactness and high thermal efficiency. As the secondary heat transfer surface, the fin is regarded as the most important heat transfer component in plate-fin heat exchangers, and its size is closely related to the heat transfer characteristics and pressure losses of the heat exchanger. Thus, optimizing the shape of plate-fin heat exchangers is important for their effectiveness and economy. In previous studies, the working media of plate-fin heat exchangers were often gas-to-gas or gas-to-liquid (Wen, 2007; Peng, 2008; Rao, 2013; Zhao, 2013). There are not many applications and studies of plate-fin heat exchangers in water systems for air-conditioning applications. Therefore, in this chapter, a water-to-water plate-fin heat exchanger applied to an air-conditioning system is studied. The fin height, fin pitch, fin thickness, and fin length are considered as four design parameters that need to be optimized. The genetic algorithm (GA), a widely used method for optimization, is adopted in this study.

As mentioned in the former Chapters, any heat transfer process is characterized by two types of losses, heat transfer through a finite temperature difference and a pressure drop in the heat transfer fluids (Singh, 2008), which correspond to Ns due to heat transfer ($Ns_{\Delta T}$) and Ns due to friction ($Ns_{\Delta P}$), respectively. To determine the proportion of $Ns_{\Delta T}$ and $Ns_{\Delta P}$ in a water-to-water plate-fin heat exchanger, in this Chapter, $Ns_{\Delta T}$, $Ns_{\Delta P}$, and Ns are considered as three single objective functions in the single objective optimization. Moreover, in order to avoid the possibility of significant increase in pump power, the multi-objective optimization is also conducted by taking $Ns_{\Delta T}$ and $Ns_{\Delta P}$ as the objective function respectively.

On the other hand, in design calculation of plate-fin heat exchangers, the comprehensive surface efficiency of the primary (plate) and secondary (fin) heat transfer surfaces is deduced assuming that the convective heat transfer coefficients of the plate and fin are the same (Kuppan, 2002; Kays, 1984; Wang, 1984). Actually, their values differ more or less according to the fin size (Wang, 2009). To obtain more precise results, the formula for calculating the comprehensive surface efficiency is modified by defining the convective heat transfer coefficients of the plate and fin as independent parameters.

Further, in the calculation of the convective heat transfer coefficients, the Colburn heat transfer factor *j* (Colburn factor for short) and Fanning friction factor *f* (Fanning factor for short) are generally adopted. In previous research, the Colburn and Fanning factors were often calculated using empirical equations (Mishra, 2009; Zarea, 2013; Pater, 2014; Sanaye, 2010). However, their values are generally greatly affected by the type of working media, the heat exchanger material, the fin size, and so on. According to the research of Hu and Herold (1995), for a liquid working medium, the value of the Colburn factor calculated using an empirical equation for air is approximately twice that calculated using experimental data for liquid at the same Reynolds number. Therefore, using empirical equations blindly might produce large errors in the calculation of the Colburn and Fanning factors. On the other hand, an experimental study might require time and money to obtain more precise results. Computational fluid dynamics (CFD), which has been used extensively in many fields of industry, can offer a simple high-precision method.

In light of the above, in this Chapter, a water-to-water plate-fin heat exchanger is taken as the research object. The convective heat transfer coefficients of the plate and fin are defined as independent parameters in the optimization, and their values are calculated by applying the multiple regression analysis equation to numerical simulation results. $Ns_{\Delta T}$, $Ns_{\Delta P}$, and Ns are considered as three single objective functions. Finally, according to the single objective optimization and multi-objective optimization, the optimal structural parameters of the heat exchanger are obtained using GA (Yin 2015).

§ 4.2 Thermal modelling of plate-fin heat exchanger

4.2.1 Basic components of plate-fin heat exchanger

According to the flow arrangement, there are three primary flow arrangements for a plate-fin heat exchanger: parallel flow, counter-flow, and cross flow. Thermodynamically, the counter-flow arrangement provides the highest heat (or cold) recovery, as mentioned in Chapter 2, therefore, only the counter-flow plate-fin heat exchanger is analyzed in this Chapter.

As shown in Figure 4.1, for plate-fin heat exchanger, corrugated metal fins are placed between flat plates.

The structure is joined together by brazing. The fins have the dual purpose of holding the plates get together, thus containing pressure, and of forming a secondary (fin) surface for heat transfer. With respect to the types of fin surface, there are mainly six kinds of fin surfaces, as shown in Figure 4.2. In this study, the most basic type, plain rectangular, is adopted for the calculation.

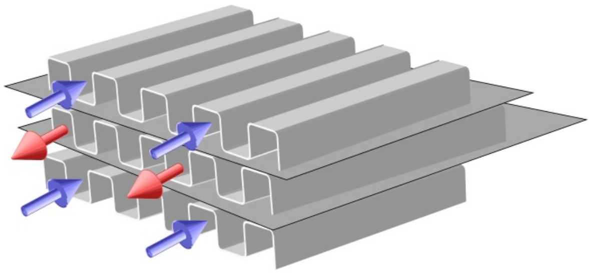

Figure 4.1 Counterflow plate-fin heat exchanger (http://thisisecs.com/blog/2008/11/04/heat-transfer/)

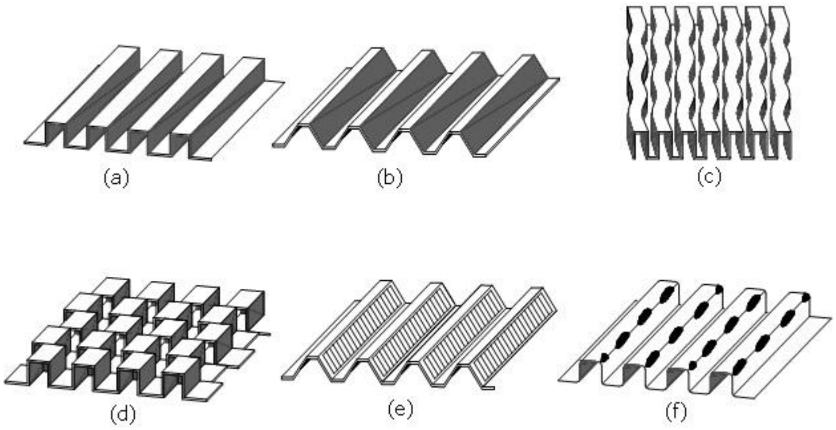

Figure 4.2 Types of plate fin surfaces: (a) Plain rectangular (b) Plain trapezoidal (c) Wavy (d) Serrated or offset strip fin (e) Louvered (f) Perforated (Alur, 2012)

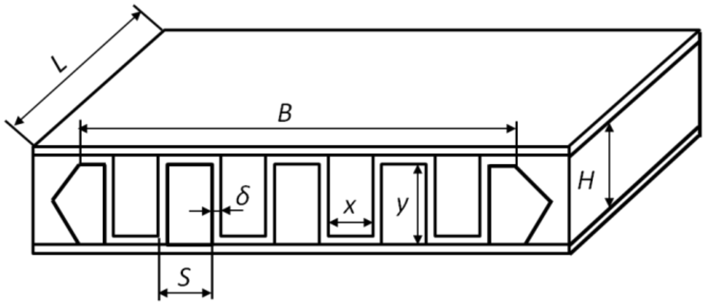

Figure 4.3 Basic components of a plate-fin heat exchanger

The basic components of a plate-fin heat exchanger are shown is Figure 4.3, where H [m], δ [m], S [m], L [m], B [m], x [m], y [m] are the fin height, fin thickness, fin pitch, fin length, effective width of fin, inner width and inner height of the fin, respectively.

4.2.2 Thermal modelling

Based on Figure 4.3, the total heat transfer surfaces F [m^2] for a hot or cold working medium of n layers is defined as

$$F = \frac{2(x+y)nBL}{S} \tag{4.1}$$

where x [m] and y [m] are the inner width and inner height of the fin, respectively:

$$x = S - \delta \tag{4.2}$$

$$y = H - \delta \tag{4.3}$$

The area of the primary (plate) and secondary (fin) heat transfer surfaces, F_1 [m^2] and F_2 [m^2], respectively, are defined as follows:

$$F_1 = \frac{x}{x+y} F \tag{4.4}$$

$$F_2 = \frac{y}{x+y} F \tag{4.5}$$

Therefore, the heat flux through the primary and secondary heat transfer surfaces, $\dot{Q}_1$[W] and $\dot{Q}_2$ [W], respectively, are obtained as follows:

$$\dot{Q}_1 = \alpha_w F_1 \left(T_w - T\right) \tag{4.6}$$

$$\dot{Q}_2 = \alpha_m F_2 \left(T_m - T\right) \tag{4.7}$$

where T_w [K], T_m [K], and T [K] are the surface temperature of the plate, surface temperature of the fin, and temperature of the working medium, respectively. Further, α_w [W/m^2·K] and α_m [W/m^2·K] are the convective heat transfer coefficients of the plate and fin, respectively, which can be obtained as follows

(Kuppan, 2002):

$$\alpha = \frac{j c_p G}{\mathrm{Pr}^{2/3}} \tag{4.8}$$

where c_p [J/kg·K], G [kg/m^2·s], and Pr [-] are the specific heat at constant pressure, mass flow rate, and Prandtl number, respectively. Further, j [-] is the Colburn factor, which is calculated by multiple regression analysis of the numerical simulation results in section 4.3 (Dong, 2002):

$$j = \frac{\alpha\, \mathrm{Pr}^{2/3}}{c_p G} = a\, \mathrm{Re}^d \left(L / D\right)^e \left(H / D\right)^i \left(\delta / D\right)^r \tag{4.9}$$

where a, d, e, i, and r are factors [-], and Re [-] and D [m] are the Reynolds number and equivalent diameter, respectively, of a single flow section. Re and D are defined as

$$\mathrm{Re} = \frac{G}{\rho} \cdot \frac{D}{\mu / \rho} \cdot 10^{-3} = \frac{GD}{\mu} \cdot 10^{-3} \tag{4.10}$$

$$D = \frac{4xy}{2\left(x + y\right)} = \frac{2xy}{x + y} \tag{4.11}$$

where ρ [kg/m^3] and μ [Pa·s] are the density and dynamic viscosity, respectively, of the working medium. Accordingly, the pressure loss of the heat exchanger, ΔP [Pa], and the corresponding Fanning factor f [-] can be obtained as follows (Kuppan, 2002; Dong, 2007):

$$\Delta P = \frac{4 f L G^2}{2 \rho D} \tag{4.12}$$

$$f = \frac{\rho D \Delta P}{2 L G^2} = a' \mathrm{Re}^{d'} \left(L / D\right)^{e'} \left(H / D\right)^{i'} \left(\delta / D\right)^{r'} \tag{4.13}$$

where a', d', e', i', and r' are factors [-]. The heat flux through the secondary heat transfer surfaces can generally be defined as follows, assuming that the convective heat transfer coefficients of the plate and fin are the same (Wang, 1984):

$$\dot{Q}_2 = \alpha_w F_2 \eta_f \left(T_w - T\right) \tag{4.14}$$

where η_f [%] is the fin efficiency, which is defined as

$$\eta_f = \frac{T_m - T}{T_w - T} \tag{4.15}$$

Then, according to Equations (4.4), (4.5), (4.6), and (4.14) and the total heat flux, defined as

$$\dot{Q} = \dot{Q}_1 + \dot{Q}_2 = \alpha_w F \eta_o \left(T_w - T\right) \tag{4.16}$$

the comprehensive surface efficiency of the primary and secondary heat transfer surfaces η_0 [%] is defined as (Kuppan, 2002; Kays, 1984; Wang, 1984)

$$\eta_\mathrm{o} = 1 - \frac{y}{x+y}\left(1 - \eta_f\right) \tag{4.17}$$

To obtain more precise results, Equation (4.14) is modified as follows by considering the convective heat transfer coefficients of the plate and fin as independent parameters:

$$\dot{Q}_2 = \alpha_w F_2 \eta_f \left(T_w - T\right) \cdot \frac{\alpha_m}{\alpha_w} \tag{4.18}$$

Therefore, from Equations (4.4), (4.5), (4.6), (4.16), and (4.18), the comprehensive surface efficiency of the primary and secondary heat transfer surfaces is modified as

$$\eta_\mathrm{o} = 1 - \frac{y}{x+y}\left(1 - \eta_f \cdot \frac{\alpha_m}{\alpha_w}\right) \tag{4.19}$$

where η_f is defined as follows (Wang, 1984) on the basis of Equation (4.15):

$$\eta_f = \frac{\tan(\omega b)}{\omega b} \tag{4.20}$$

Here b [m] is the size dimension of the secondary heat transfer surfaces, which is determined by the arrangement of high-/low-temperature channels. For a staggered arrangement, b is defined as

$$b = \frac{H}{2} \tag{4.21}$$

Further, ω is defined as

$$\omega = \sqrt{\frac{2\left[1/\left(1/\alpha_m + R\right)\right]}{\lambda\delta}} \tag{4.22}$$

where R [m^2·K/W] and λ [W/m·K] are the fouling resistance and thermal conductivity of the fin, respectively.

According to Equation (4.16), the heat flux of the high-/low-temperature working media are obtained as

$$\dot{Q}_h = \alpha_{wh} F_{oh} \eta_{oh} \left(T_h - T_w\right) \tag{4.23}$$

$$\dot{Q}_c = \alpha_{wc} F_{oc} \eta_{oc} \left(T_w - T_c\right) \tag{4.24}$$

where the subscripts h and c represent the high-/low-temperature working media, respectively. For steady-state heat transfer, $\dot{Q}_h = \dot{Q}_c = \dot{Q}$, the temperature difference between the high-/low-temperature working media can be defined as follows on the basis of Equations (4.23) and (4.24):

$$T_h - T_c = \dot{Q}\left(\frac{1}{\alpha_{wh} F_{oh} \eta_{oh}} + \frac{1}{\alpha_{wc} F_{oc} \eta_{oc}}\right) \tag{4.25}$$

Therefore, the total heat transfer coefficients corresponding to the high-/low-temperature channels are defined as follows:

$$K_h = \frac{1}{\dfrac{1}{\alpha_{wh}\eta_{oh}} + \dfrac{1}{\alpha_{wc}\eta_{oc}} \times \dfrac{F_{oh}}{F_{oc}}} \tag{4.26}$$

$$K_c = \frac{1}{\dfrac{1}{\alpha_{wc}\eta_{oc}} + \dfrac{1}{\alpha_{wh}\eta_{oh}} \times \dfrac{F_{oc}}{F_{oh}}} \tag{4.27}$$

where K_h [W/m^2·K] and K_c [W/m^2·K] are the total heat transfer coefficients for the high-/low-temperature channels, respectively. Then, based on Equation (2.12), the number of transfer units (NTU) of the plate-fin heat exchanger can be defined as (Kays, 1984)

$$NTU = \frac{K_h F_{oh}}{\left(c_p \dot{m}\right)_{\min}} = \frac{K_c F_{oc}}{\left(c_p \dot{m}\right)_{\min}} \tag{4.28}$$

Then, according to Equations (2.14), (2.34), (2.35), and (2.37), the objective functions of water-to-water plate-fin heat exchanger can be calculated.

§ 4.3 Numerical simulation

To determine the coefficients in the expressions of the Colburn factor and Fanning factor [Equations. (4.9) and (4.13), respectively], the corresponding necessary parameters are obtained by numerical simulation.

4.3.1 Reliability of CFD software

To ensure the reliability of the CFD software used in this analysis, a validation calculation is first performed for comparison with the experimental results (Kays, 1984). As shown in Figure 4.4, the calculation region is a small rectangular area of the low temperature channel (enclosed by the dotted line).

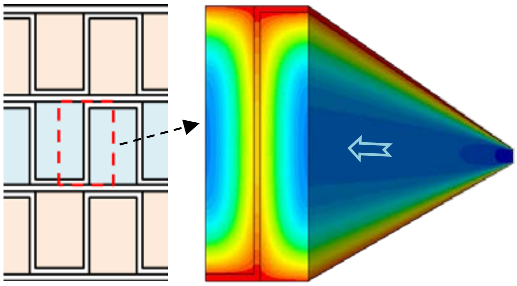

Figure 4.4 Calculation region

The length of the calculation region is set to 600 mm. The fin sizes are set to the same values as in the experiments (Kays, 1984): 10.3 mm (fin height), 0.254 mm (fin thickness), and 4.1 mm (fin pitch). The number of grids in the calculation region is 1,723,200. A steady simulation is adopted assuming laminar flow with flow rates of 128, 160, 192, 240, and 320 kg/(m^2·s). The temperature of the upper and lower boundaries and the inlet temperature of the working medium are set to 350 K and 283 K, respectively. The physical properties of the working medium are assumed to be invariant with temperature. The thermal conductivity of the plate and fin is set to 202 W/(m·K). The other calculation conditions are shown in Table 4.1.

Table 4.1 Calculation conditions

Inlet boundary	Constant flow rate
Outlet boundary	Constant pressure (0 Pa)
Lateral boundary	Symmetric
Fluid region	Water
Solid region	Aluminium
Density	997.561 [kg/m^3]
Dynamic viscosity	0.0008887 [Pa·s]
Specific heat	4181.72 [J/kg·K]
Thermal conductivity	0.620271 [W/m·K]

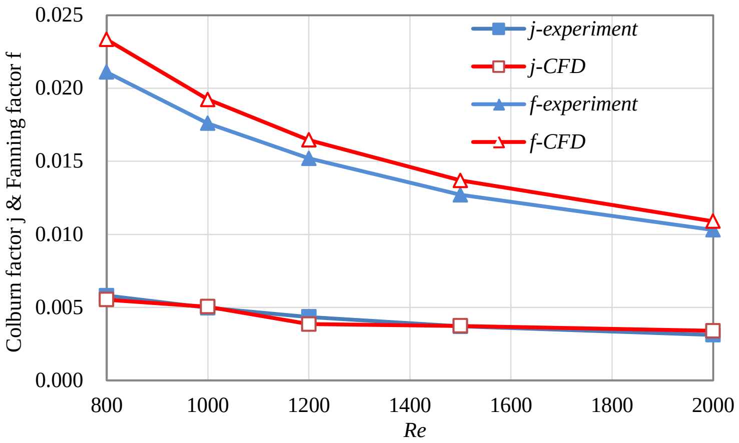

Figure 4.5 Comparison of numerical simulation results and experimental results

According to the convective heat transfer coefficient and pressure loss obtained by CFD, the Colburn factor *j* and Fanning factor *f* of the plate and fin can be calculated using Equations (4.9) and (4.13). For easy comparison with the experimental results, the average convective heat transfer coefficients of the plate and fin are adopted in the calculation. As shown in Figure 4.5, the numerical simulation results are in good agreement with the experimental results. The average errors of the Colburn and Fanning factors are 5% and 8%, respectively.

In addition, it can be seen that the difference between *f*-experiment and *f*-CFD becomes larger when the Reynolds number decreases in Figure 4.5. As for the reason of this trend, at first, factor *f* is the function of pressure loss. Meanwhile, pressure loss is also the function of coefficient of friction. In numerical simulation, the surfaces of plate and fin are assumed to be smooth. But as for the real plate-fin heat exchanger in the experiment, the surfaces of plate and fin have a certain amount of roughness. With regard to the smooth surface, the coefficient of friction is mainly affected by the Reynolds number. But for the rough surface, the coefficient of friction is also affected by the surface roughness. And the effect of surface roughness on the value of coefficient of friction will increase with the decrease of Reynolds number and decrease with the increase of Reynolds number. Therefore, that is why the difference between *f*-experiment and *f*-CFD becomes larger when the Reynolds number decreases.

4.3.2 Simulation object and conditions

In the plate-fin heat exchanger, the characteristic scales of the length and flow section are meter-scale and millimeter-scale, respectively. Therefore, it is very difficult to simulate the entire heat exchanger with the existing computing power. Only the region within the dotted line in Figure 4.6 is simulated.

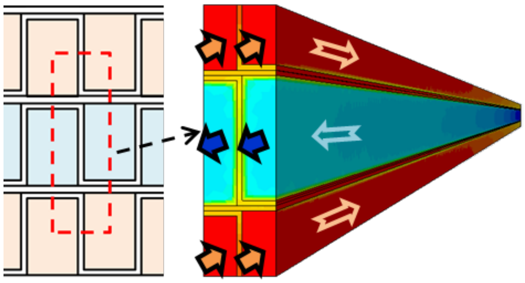

Figure 4.6 Simulation object

The upper and lower portions of the calculation region are high-temperature channels, and the middle portion is a low-temperature channel. The thickness of the plate is set to 0.6 mm. The fin size and flow rates of the high- and low-temperature channels are assumed to be the same. A steady simulation is adopted assuming laminar flow. The inlet temperature of the high-/low-temperature working media and the thermal conductivity of the plate and fin are set to 290 K, 283 K, and 237 W/(m·K), respectively. The physical properties of the working media are assumed to be invariant with temperature. The other calculation conditions are the same as in Table 4.1.

Table 4.2 Simulation conditions

Case	Height [mm]	Thickness [mm]	Pitch [mm]	Length [mm]	Mass flow rate [kg/m^2·s]
1	2.0	0.1	1.4	800	60, 160, 260, 360, 460
2	2.0	0.2	2.1	900	560, 660, 760, 860, 960
3	2.0	0.3	3.2	1000	60, 160, 260, 360, 460
4	2.5	0.1	1.4	1000	560, 660, 760, 860, 960
5	2.5	0.3	3.2	800	60, 160, 260, 360, 460
6	2.5	0.2	2.1	900	560, 660, 760, 860, 960
7	3.0	0.2	2.1	1000	60, 160, 260, 360, 460
8	3.0	0.1	1.4	900	560, 660, 760, 860, 960
9	3.0	0.3	3.2	800	60, 160, 260, 360, 460

Forty-five cases are simulated, as shown in Table 4.2, including three fin heights (2, 2.5, and 3 mm), three fin thicknesses (0.1, 0.2, and 0.3 mm), three fin pitches (1.4, 2.1, and 3.2 mm), three fin lengths (800, 900, and 1000 mm), and 10 mass flow rates. The inlet temperature of the low-temperature working medium (283 K) is adopted as the reference temperature for calculating the convective heat transfer coefficient. The inlet Reynolds number is 200–2300 according to Equation (4.10).

4.3.3 Grid independence test

To achieve perfect accuracy, each cross-sectional grid size is set to 0.1 mm. However, the characteristic scale along the length is meter-scale. The numerical simulation might be difficult, exhibiting variation with decreasing grid size under the existing computing power. To reduce the calculation load while maintaining the accuracy of the numerical simulation, a grid independence test of the grid size along the length is conducted for Case 1. The mass flow rate is set to 460 kg/(m^2·s). Figure 4.7 shows that after the grid size decreases to 1 mm, the convective heat transfer coefficient of the fin in the low-temperature channel is similarly constant. Therefore, 1 mm is set as the grid size along the length of the heat exchanger.

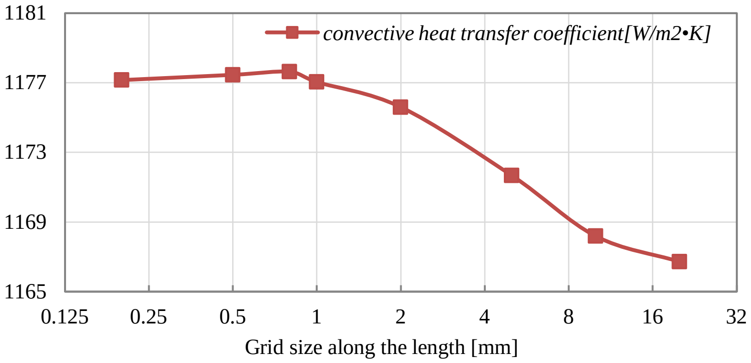

Figure 4.7 Grid independence test

4.3.4 Results and discussion

According to the research of Wang et al. (2009), when the average heat transfer coefficient is applied, the heat transfer rate of the primary heat transfer surface is overestimated, and that of the secondary heat transfer surface is underestimated.

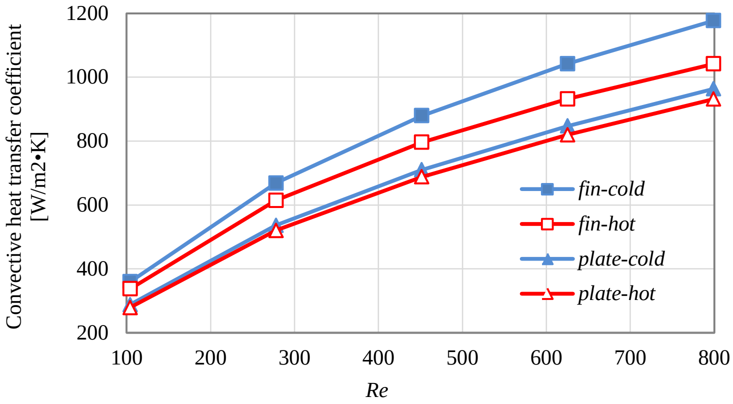

Figure 4.8 Convective heat transfer coefficient (Case 1)

In terms of this study, however, the heat transfer rate of the primary or secondary surface is closely related to the fin size. The values of the convective heat transfer coefficient for various Reynolds numbers in Cases 1 and 9 are shown in Figures 4.8 and 4.9, respectively. According to Equations.(4.4) and (4.5), the primary heat transfer surface area accounts for 40.6% and 51.8% of the total heat transfer surface areas in Cases 1 and 9, respectively. Further, the convective heat transfer coefficients of the plate in the high-/low-temperature channel are all smaller than that of the fin in Case 1. Case 9 is just the opposite. Therefore, the values of the convective heat transfer coefficients of the plate and fin depend on the proportions of the primary heat transfer surface area (plate) and secondary heat transfer surface area (fin).

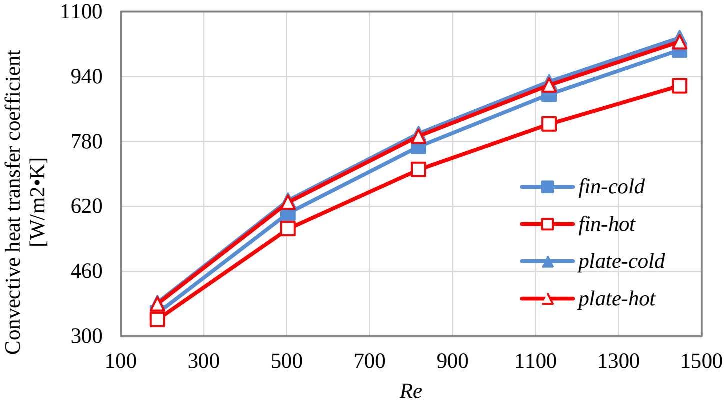

Figure 4.9 Convective heat transfer coefficient (Case 9)

On the basis of the convective heat transfer coefficient and pressure loss of the 45 cases obtained by numerical simulation, the expressions of six factors (Colburn factors of the fin in the high-/low-temperature channel j_{mh}, j_{mc}, Colburn factors of the plate in the high-/low-temperature channel j_{wh}, j_{wc}, and Fanning friction factors in the high-/low-temperature channel f_h, f_c, respectively) can be obtained as follows, as shown in Figures 4.10 – 4.15.

The scope of Equations (4.29) – (4.34) is: Re = 200–2300, H = 2–3 mm, δ = 0.1–0.3 mm, S = 1.4–3.2 mm, and L = 800–1000 mm.

$$j_{mh} = 0.7754\,\mathrm{Re}^{-0.4846}\left(L/D\right)^{-0.5264}\left(H/D\right)^{0.0023}\left(\delta/D\right)^{-0.1503} \quad R^2 = 0.9729 \tag{4.29}$$

$$j_{mc} = 0.7561\,\mathrm{Re}^{-0.4449}\left(L/D\right)^{-0.4959}\left(H/D\right)^{0.4977}\left(\delta/D\right)^{0.0183} \quad R^2 = 0.9725 \tag{4.30}$$

$$j_{wh} = 1.7324\,\mathrm{Re}^{-0.4847}\left(L/D\right)^{-0.5640}\left(H/D\right)^{-0.4837}\left(\delta/D\right)^{0.0437} \quad R^2 = 0.9878 \tag{4.31}$$

$$j_{wc} = 1.5484\,\mathrm{Re}^{-0.4817}\left(L/D\right)^{-0.5450}\left(H/D\right)^{-0.3789}\left(\delta/D\right)^{0.0504} \quad R^2 = 0.9890 \tag{4.32}$$

$$f_h = 3.9638\,\mathrm{Re}^{-0.9232}\left(L/D\right)^{0.1986}\left(H/D\right)^{-0.0390}\left(\delta/D\right)^{0.1340} \quad R^2 = 0.9859 \tag{4.33}$$

$$f_c = 3.9711\,\mathrm{Re}^{-0.9234}\left(L/D\right)^{0.1995}\left(H/D\right)^{-0.0364}\left(\delta/D\right)^{0.1369} \quad R^2 = 0.9859 \tag{4.34}$$

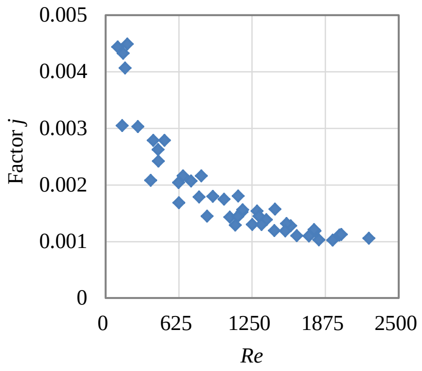

Figure 4.10 Relation between j_{mh} and *Re*

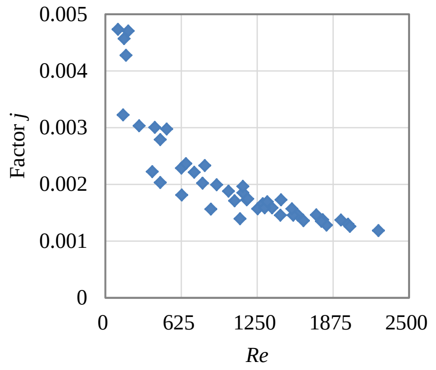

Figure 4.11 Relation between j_{mc} and *Re*

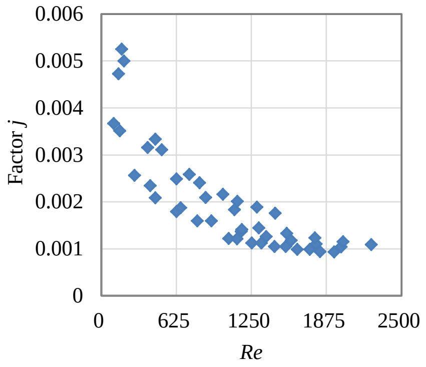

Figure 4.12 Relation between j_{wh} and *Re*

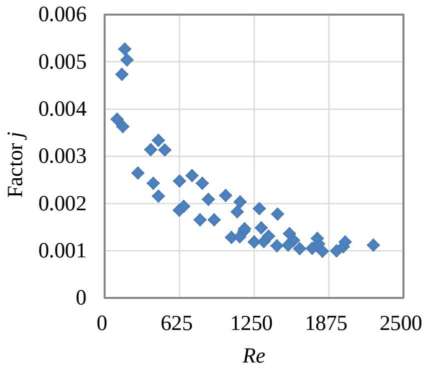

Figure 4.13 Relation between j_{wc} and *Re*

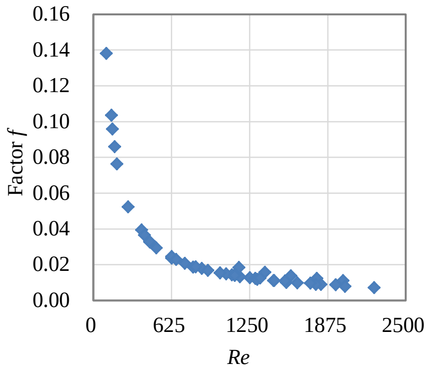

Figure 4.14 Relation between j_{wh} and *Re*

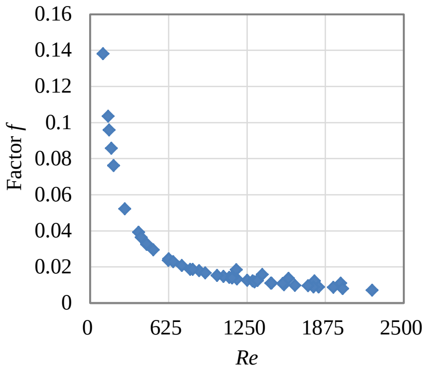

Figure 4. 15 Relation between j_{wc} and *Re*

It can be seen from Figure 4.10 – 4.15 that, for both Colburn factors and Fanning factors, the values of high temperature channels are same as those of low temperatures. The reason is as follows: For Colburn factors, since the inlet temperature difference is only 7°C in the case studies, the difference of temperature distribution for high-/low-temperature channels are not very obvious. Therefore, the difference of Colburn factors for high-/low-temperature channels are very small. For Fanning factors, since the arrangement of fin, fin type, and fin size are exactly the same for high-/low-temperature channels, the pressure distribution for high-/low-temperature channels are almost uniform. Then the value of Fanning factors are also very close. However, we would like to be able to provide a common method for any temperature level and any fin arrangement for high-/low-temperature channels. Therefore, in this study, we still adopt six equations to describe Colburn factors and Fanning factors, even the values of high-/low-temperature channels are very close in this case studies.

The results by CFD and empirical equations are also compared as shown in Figure 4.16. Using the fin size of Case 1, six kinds of factors based on CFD results are calculated by Equations (4.29) – (4.34); the conventional Colburn factors j and Fanning factor f based on empirical equations for plain fin are calculated by Equations (4.35) and (4.36), derived from the ALEX's specifications of the manufacturer of Kobe Steel (Chen, 1993).

$$\ln j = 0.103109(\ln \mathrm{Re})^2 - 1.9109(\ln \mathrm{Re}) + 3.211 \qquad \mathrm{Re} = 400 \sim 10000 \qquad (4.35)$$

$$\ln f = 0.106566(\ln \mathrm{Re})^2 - 2.12158(\ln \mathrm{Re}) + 5.82505 \qquad \mathrm{Re} = 400 \sim 10000 \qquad (4.36)$$

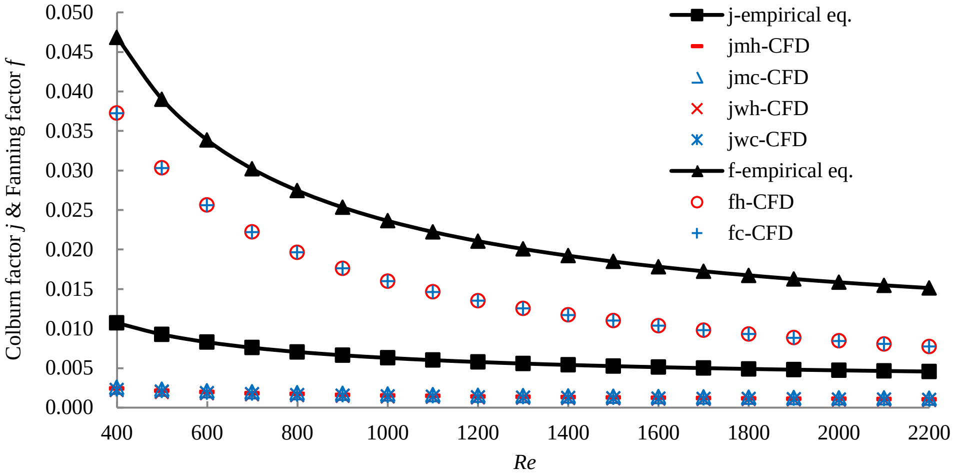

Figure 4.16 Comparison of results between CFD and empirical equations

When the Reynolds number is 400–2200, it can be seen that results by empirical equations are larger than CFD results at the same Reynolds number and the average relative differences of Colburn factor j

are larger than that of Fanning factor *f*. The main reasons for these trends are shown as follows: Firstly, the empirical equations only distinguish the type of fin, but not the size of fin for any type, which will result in remarkable errors. On the other hand, the surface roughness of fin is not considered in the CFD calculation. The calculation results by CFD will be slightly underestimated. Secondly, the empirical equations are obtained from the experimental date of gas, but not liquid. Using the empirical equations of gas for the prediction of liquid will overestimate the value of Colburn factor *j* and Fanning factor *f* due to the different physical property of working medium. But the effect of physical property on the Fanning factor *f* is relatively small, so the relative differences between the results of CFD and empirical equations for Fanning factor f are smaller. Since the difference of fin size and the type of fluid are not considered in the empirical equations, numerical simulation is more flexible and precise for the performance prediction on a certain heat exchanger.

§ 4.4 Case study

Based on the simulation results and the thermal modelling of plate-fin heat exchanger, firstly, in order to determine the validity of above-mentioned optimization method, a theoretical thermodynamic optimization is carried out to compare and analyze the value of $Ns_{\Delta P}$, $Ns_{\Delta T}$, and Ns, based on unfixed overall dimension of plate-fin heat exchanger. Then, combining with real optimization design of the heat exchanger, the thermodynamic optimization on an assumed plate-fin heat exchanger with fixed overall dimension are carried out by using constrained nonlinear optimization algorithms. The $Ns_{\Delta \mathrm{P}}$ -to-Ns ratio, the value of Ns, and the efficiency of heat exchanger ε, before and after the optimization, are compared.

4.4.1 Thermodynamic optimization with unfixed overall dimension

A water-to-water plate-fin heat exchanger with three high-temperature channels and three low-temperature channels is analysed. The effective width of the fin, coefficient of thermal expansion of water, and mass flow rate are set to 200 mm, 207×10^{-6} K^{-1}, and 673 $\mathrm{kg/m^2 \cdot s}$, respectively. The inlet temperatures of the high-/low-temperature channels are set to 290 K and 283 K, respectively. The fouling resistance is ignored. The other physical properties of the working media are the same as those in the former numerical simulation.

For single objective optimization by the GA, the population size, number of iterations, and crossover rate are set to 50, 1000, and 0.8, respectively. The mutation rate changes with the value of the fitness by adaptive mutation. The range of variables and optimal solutions are shown in Table 4.3. It can be seen that the optimal solutions for the objective function of $Ns_{\Delta P}$ and $Ns_{\Delta T}$ are in accordance with our daily engineering experience, which proves the feasibility of the optimization method to a certain extent.

Table 4.3 Range of variables and optimal solutions

	Fin height	Fin pitch	Fin thickness	Fin length
Range of variables	2–3 mm	1.4–3.2 mm	0.1–0.3 mm	800–1000 mm
Optimal solutions (Objective function: $Ns_{\Delta P}$)	3 mm	3.2 mm	0.1 mm	800 mm
Optimal solutions (Objective function: $Ns_{\Delta T}$)	2 mm	1.4 mm	0.3 mm	1000 mm
Optimal solutions (Objective function: Ns)	2 mm	1.4 mm	0.3 mm	1000 mm

As shown in Figures 4.17 – 4.19, the minimum values of the three objective functions ($Ns_{\Delta P}$, $Ns_{\Delta T}$, and Ns) are found to be constant at 7.172×10^{-7}, 3.835×10^{-4}, and 3.873×10^{-4}, respectively after about 180, 400, and 120 generations. The values and proportions of $Ns_{\Delta P}$ and $Ns_{\Delta T}$ are shown in Figure 4.20 when $Ns_{\Delta P}$, $Ns_{\Delta T}$, and Ns are minimized as objective functions. The optimal solutions in Table 4.3 and the values and proportions of $Ns_{\Delta P}$ and $Ns_{\Delta T}$ in Figure 4.20 are quite similar when $Ns_{\Delta T}$ and Ns are minimized because of the very small frictional irreversible loss. $Ns_{\Delta T}$ is about 100 times larger than $Ns_{\Delta P}$. When $Ns_{\Delta P}$ is minimized as the objective function, the $Ns_{\Delta T}$-to-$Ns_{\Delta P}$ ratio can reach 610, which is in accordance with the related results in Chapter 3.

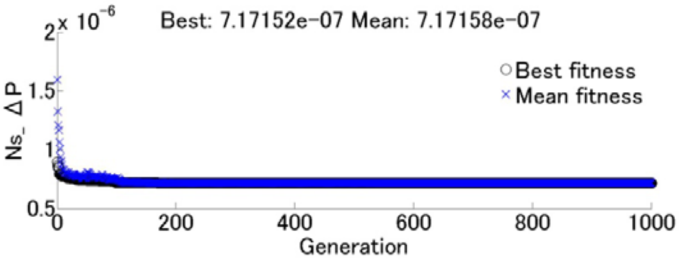

Figure 4.17 Iteration process for the minimisation of $Ns_{\Delta P}$

In addition, compared with the conditions in which $Ns_{\Delta T}$ and Ns are minimized as objective functions, when $Ns_{\Delta P}$ is minimized as the objective function, the ratio of $Ns_{\Delta P}$ between the two conditions is only 19%, but the ratio of $Ns_{\Delta T}$ and Ns between the two conditions can reach 124% and 123%, respectively, as shown in Figure 4.21.

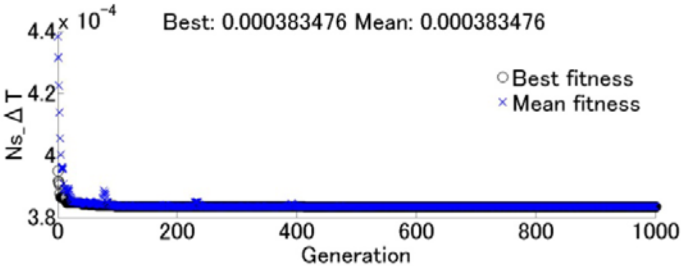

Figure 4.18 Iteration process for the minimisation of $Ns_{\Delta T}$

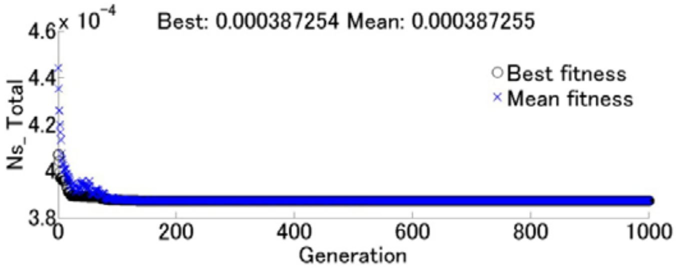

Figure 4.19 Iteration process for the minimisation of *Ns*

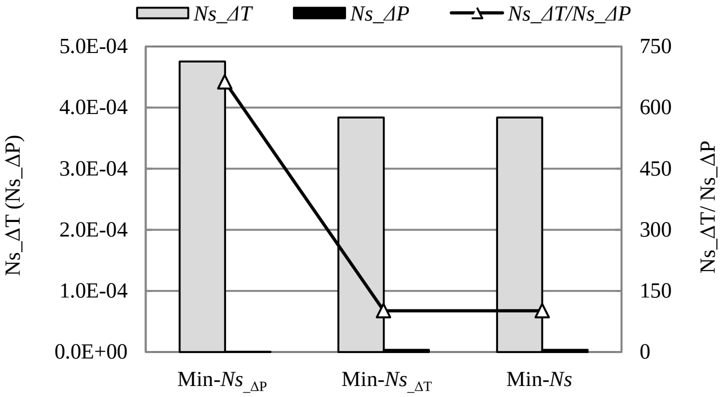

Figure 4.20 Values and proportions of $Ns_{\Delta P}$ and $Ns_{\Delta T}$ for each objective function

On the other hand, in order to avoid the possibility of significant increase in pump power when $Ns_{\Delta T}$ or *Ns* is taken as single objective function, the multi-objective optimization is also conducted by taking $Ns_{\Delta T}$ and $Ns_{\Delta P}$ as the objective function respectively (Guo 2010; Guo 2012), as shown in Figure 4.22. The population size, number of iterations, and crossover rate are set to 60, 5000, and 0.8, respectively. The mutation rate changes with the value of the fitness by adaptive mutation. From the Pareto front in Figure 4.22, the optimal shape of plate-fin heat exchanger can be determined according to the actual requirements.

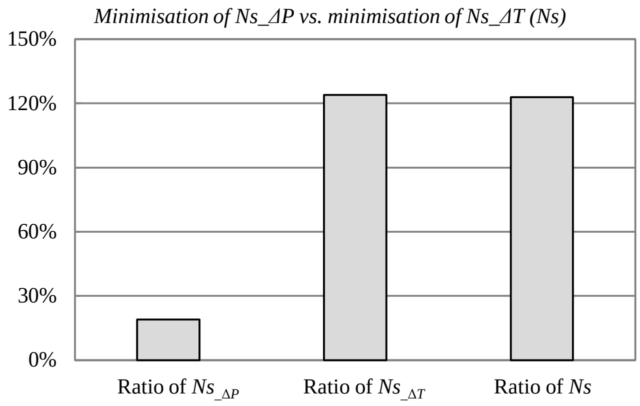

Figure 4.21 Ratio of $Ns_{\Delta P}$, $Ns_{\Delta T}$, and Ns between the minimizations of $Ns_{\Delta P}$ and $Ns_{\Delta T}$ (Ns)

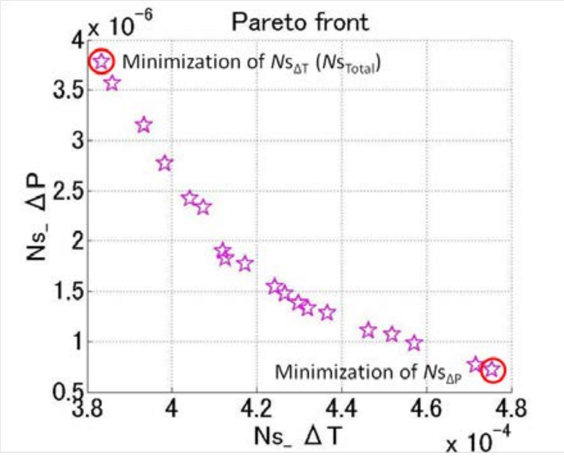

Figure 4.22 Pareto front of multi-objective optimization

4.4.2 Thermodynamic optimization with fixed overall dimension

In regard to the actual fin optimization of heat exchanger, the optimizations based on fixed overall dimension of heat exchanger are relatively common. Therefore, in this section, before and after the optimization, the effective width of the fin, the length and height of the heat exchanger, and the plate thickness are fixed as 800mm, 900mm, 180.6mm, and 0.6mm, respectively; the fin type is fixed as plain rectangular fin; the arrangement form of high-/low- temperature channels is fixed as stagger arrangement; the layer counts of high-/low-temperature channel are assumed to be always the same varying with the change of total layer counts; the working medium is fixed as water with the same physical property as shown in section 4.3; the inlet temperatures of high-/low-temperature channels are fixed as 290K and

283K, respectively; the mass flow rates for both high-/low-temperature working mediums are fixed as 3.826 kg/s (heat capacity: 16kW/K), as shown in Figure 4.23.

Before the optimization, the fin thickness, fin pitch, and fin height are assumed as 0.2mm, 3mm, and 2.4mm, respectively; the layer counts of high-/low-temperature channel are assumed as 30 and 30, respectively. The fin thickness, fin pitch, and fin height are considered as optimal variables; the layer counts will change with the change of fin height. For convenience, only *Ns* is taken as the objective function. The ranges of variables and optimal solutions are shown in Table 4.4.

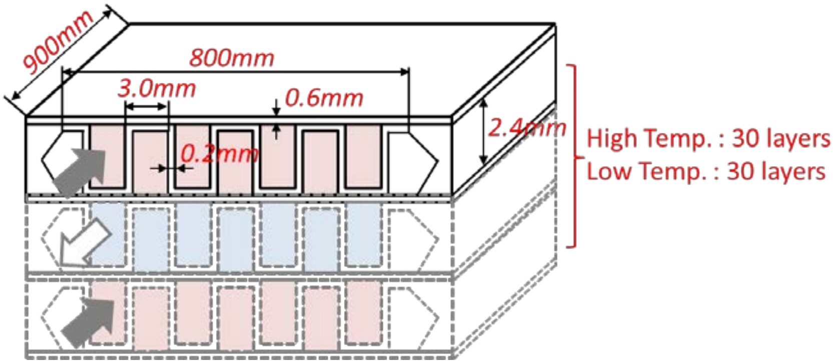

Figure 4.23 Optimization object before optimization

Table 4.4 Range of variables and optimal solutions

Objective function: *Ns*	Fin height	Fin pitch	Fin thickness	Layer counts for single fluid
Range of variables	2–3 mm	1.4–3.2 mm	0.1–0.3 mm	–
Before optimization	2.400 mm	3.000 mm	0.200 mm	30
After optimization	2.047 mm	2.534 mm	0.292 mm	34

It can be seen from Figure 4.24 that, after the optimization, the number of entropy production units, *Ns*, declines 5.7% from 3.34×10^{-6} to 3.16×10^{-6}. Accordingly, the efficiency of heat exchanger increases from 30.8% to 33.0%; the heat transfer amount also increases 7.1% from 49.3 kW to 52.8 kW. The results show that, by optimizing the fin size of plate-fin heat exchanger, the irreversible losses during the heat transfer process are reduced to some extent; the performance and amount of heat transfer all make a slight improvement.

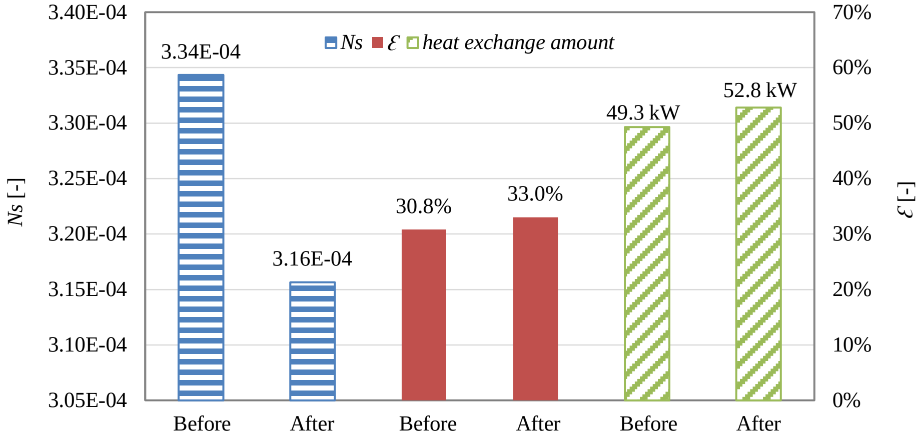

Figure 4.24 Value of Ns, ε, and heat exchange amount before and after the optimization

§ 4.5 Conclusions

In this Chapter, the optimal structural parameters of a water-to-water plate-fin heat exchanger are obtained by CFD. The main findings and innovations of this Chapter are listed below:

1) To obtain more precise results, the formula for calculating the comprehensive surface efficiency is modified by defining the convective heat transfer coefficients of the plate and fin as independent parameters.

2) The values of the Colburn factor and Fanning factor are calculated using the multiple regression analysis equation based on the numerical simulation results.

3) According to the numerical simulation results, the values of the convective heat transfer coefficients of the plate and fin depend on the proportions of the primary heat transfer surface area (plate) and secondary heat transfer surface area (fin).

4) $Ns_{\Delta T}$ is about 100 and 610 times $Ns_{\Delta P}$ when $Ns_{\Delta T}$ (Ns) and $Ns_{\Delta P}$, respectively, are minimized as objective functions in a case study with unfixed overall dimension of heat exchanger.

5) After the thermodynamic optimization on an assumed plate-fin heat exchanger with fixed overall dimension, the efficiency of heat exchanger increases from 30.8% to 33.0%; the heat transfer amount also increases 7.1% from 49.3 kW to 52.8 kW.

Chapter 5 Exergy analysis on an assumed chilled-water circuit

In previous three Chapters, the related research contents focused on the optimization of heat exchanger are presented. In an HVAC system of a building, in order to save energy and improve the system efficiency, in addition to improving the performance of related heat transfer units, reducing the power consumption of fluid-supply equipment, such as pump and fan, is also significant. In the following two Chapters, around the water pump in chilled water circuit, some ideal theoretical analysis of assumed chilled water circuit and some analysis of actual heat pump system based on the operating data are carried out from the viewpoint of exergy.

§ 5.1 Introduction

The energy use of an HVAC system accounts for a large proportion of a building’s total energy use (Westphalen 2001). Improving the efficiency of an HVAC system would therefore make a major contribution to energy saving within a building. In an HVAC system, in which the pumping system is one of the primary components, energy-use reduction by the pumping system is important. Maximum-load operation of an HVAC system accounts for only a small percentage of the overall operating time. Most water pumps are operated only under partial load (Matsushita 2011). Therefore, reducing the energy use of the pumping system when under only partial load will significantly improve the efficiency of the HVAC system.

In any investigation involving partial load, it is necessary to determine the degree of impact of the water temperature on the heat-transfer characteristics of the terminal units, such as the fan coil units (FCU). These are another primary component of an HVAC system, which transfer heat from the air to water through a coil in proportion to the log mean temperature difference (LMTD) (Crowther 2002). This is because the water temperature affects the LMTD and then the heat-transfer characteristics of the terminal unit, and thereby ultimately affects the indoor thermal environment, the cost of the terminal units, and the power of the pumps used in the chilled water circuit (TRANE 2002; Herbert 2011).

Previous studies regarding variable-flow control have mainly focused on comparing measured energy use before and after the adjustment of the control parameters or control methods (Izumiyama 2012) or the development and verification of new control methods (Matsushita et al. 2011). Regarding those previous studies into the effect of water temperature on heat transfer, the main research efforts have involved the analysis of the relationship between the water flow rate and the temperature difference between the supply and return water, based on data derived from the manufacturer's specifications (Kido et al. 2013).

All of the above-mentioned studies were carried out from the viewpoint of the amount of energy being consumed, but not the quality of that energy. In thermodynamics, energy can be divided into available and unavailable energy. Exergy is that energy that is available for use (Perrot 1998). Unlike a conventional energy analysis, an exergy analysis enables the direction of the exergy flow, as well as the value and location of the exergy consumption, to be clearly and easily determined (Shukuya 2013).

Therefore, a greater number of exergy analyses have been applied to the field of HVAC engineering in recent years. Wang et al. (2008) investigated the impact of the air-conditioning parameters on the exergy of the chilled water supplied to radiant panels and a cooling coil. Harrell and Mathias (2009) evaluated the central chilled-water system in a campus building using exergy-based cost accounting to quantify the magnitude and cost impact of internal losses with the goal of maximizing the chiller capacity utilization while minimizing the unit cost of the delivered chilled water. Taniguchi et al. (2014) developed an energy-saving air-separation unit based on an exergy analysis. However, as far as we know, there have been no exergy analyses of a chilled water circuit from the aspects of both the variable-flow control methods and the chilled water temperature. Therefore, in this Chapter, the effects of different variable-flow control methods and supply water temperatures on the exergy budget of an assumed chilled water circuit were analyzed theoretically (Yin 2015).

§ 5.2 Basic theory

Exergy is a property and is associated with the state of the system and the environment (Cengel 2014), which is the maximum amount of useful work that can be produced (or the minimum work that needs to be supplied) that brings the system into equilibrium with its environment (Martínez 2015). A system that is in equilibrium with its environment has zero exergy.

As shown in Figure 5.1, the classification of Exergy can be done in a way that is similar to the classification of energy (Gundersen 2011). But only thermo-mechanical exergy, which disregards any mixing and chemical reaction, will be discussed in this study. Combined with the research objects, the conception and corresponding calculation equations of two kinds of exergy are expressed as follows.

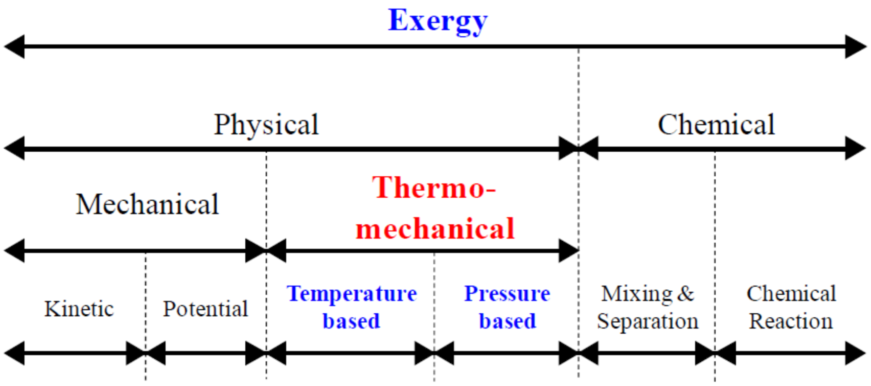

Figure 5.1 Classification of exergy

5.2.1 Exergy of heat transfer

Exergy can be transferred to or from a system by heat, work, and mass. For the heat transfer equipments in HVAC system, heat transfer is always accompanied by exergy transfer. If the environment temperature is T_0, a thermal reservoir at temperature T has certain amount of exergy both when T is higher than T_0 and when T is lower than T_0. The exergy contained by the thermal reservoir at a temperature higher than its environment is an ability of thermal energy contained by the thermal reservoir to disperse into the environment. On the other hand, the exergy contained at a temperature lower than its environment is an ability of the thermal reservoir, in which there is a lack of thermal energy compared to the environment, to let the thermal energy in the environment flow into it. We call the former "warm" exergy and the latter "cool" exergy (Shukuya 1996).

For the calculation of worm exergy and cool exergy, Figure 5.2 is helpful for understanding the meaning of calculation process. Figure 5.2(a) and 5.2(b) represent the sketch map of Carnot cycle and reverse Carnot cycle. T_h and T_c are the temperature of high-temperature and low-temperature thermal reservoir, respectively. Q_h is the heat released from high-temperature thermal reservoir in Carnot cycle or the heat absorbed by high-temperature thermal reservoir in reverse Carnot cycle. Similarly, Q_c is the heat absorbed by low-temperature thermal reservoir in Carnot cycle or the heat released from low-temperature thermal reservoir in reverse Carnot cycle. W is the maximum work output to the environment in Carnot cycle or the minimum work input from the environment in reverse Carnot cycle. Due to the definition of exergy (maximum produced work or minimum supplied work), W is just the exergy of the system in Carnot cycle or reverse Carnot cycle.

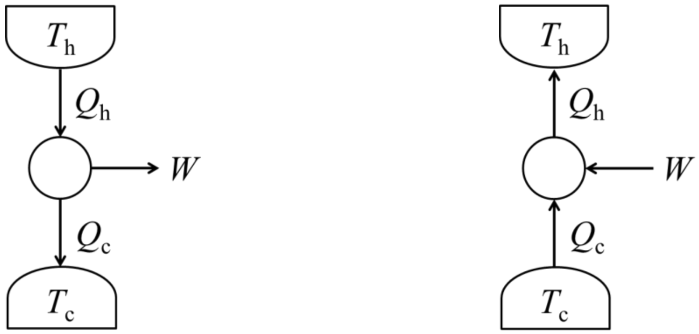

(a) Carnot cycle (b) Reverse Carnot cycle

Figure 5.2 Carnot cycle and reverse Carnot cycle between two thermal reservoirs

According to Figure 5.2, when the temperature of thermal reservoir is higher than the temperature of environment, the warm exergy is the maximum work output extracted from the thermal reservoir to the environment when heat is released from system or the minimum work input supplied by the environment to the thermal reservoir when heat is absorbed by thermal reservoir. Similarly, when the temperature of system is lower than the temperature of thermal reservoir, the cool exergy is the maximum work output extracted from the thermal reservoir to the environment when heat is absorbed by thermal reservoir or the minimum work input supplied by the environment to the thermal reservoir when heat is released from thermal reservoir. Therefore, the flow direction of heat for a thermal reservoir is identical with that of warm exergy and is opposite of that of cool exergy.

Based on the corresponding calculation equations of Carnot cycle and reverse Carnot cycle, the rate of exergy by heat, namely the rate of warm exergy or cool exergy, can be expressed as (Gundersen 2011)

$$\dot{X}_{heat} = \pm\dot{Q}\left(1-\frac{T_0}{T}\right) \tag{5.1}$$

where $\dot{X}_{heat}$ [kW] is the rate of exergy by heat, $\dot{Q}$ [kW] is the rate of heat flow transferred from or to the thermal reservoir, "+" and "-" mean heat release and heat absorption, respectively, T_0 [K] is the temperature of environment, T [K] is the temperature of thermal reservoir.

5.2.2 Exergy of flow processes

In HAVC system, the analysis on the moving air and water is necessary. To clarify the calculation method of the corresponding exergy generated in the flow processes will contribute to the exergy analysis on the HAVC system. For the working fluid flow, assuming steady state and neglecting the changes in kinetic and potential energy for the process, the exergy generated in the flow processes is the technical work which can be exported by the working mediums.

According to the first law of thermodynamics, the micro change of technical work $\dot{W}_t$ [kW] can be expressed as (Kestin 1979)

$$d\dot{W}_t = \dot{m}\delta q - \dot{m}dh \tag{5.2}$$

If the working medium is brought into equilibrium with its environment from the temperature of T to T_0 reversibly, according to the Equations (2.21) and (5.2), the exergy of flow processes can be expressed as

$$\dot{X}_{flow} = \dot{m}\int_{s}^{s_0} T_0 ds - \dot{m}\int_{h}^{h_0} dh = \dot{m}\int_{T}^{T_0} T_0 \frac{c_p dT}{T} - \dot{m}\int_{T}^{T_0} c_p dT = c_p\dot{m}\left(T - T_0\right) - c_p\dot{m}T_0 \, ln\frac{T}{T_0} \tag{5.3}$$

where c_p [kJ/(kg·K)], $\dot{m}$ [kg/s] are the specific heat capacity at constant pressure and mass flow rate, respectively.

§ 5.3 Assumed system and its corresponding exergy budget

The assumed system is shown in Figure 5.3. For simplicity, it was assumed that there is only one FCU on the demand side and one pump for supplying the chilled water. The system consists of three subsystems: the air channel inside the FCU, the tube wall between air and water inside the FCU, and the chilled water channel inside the tube. The flow of exergy through the three subsystems is shown in Figure 5.4. It can be seen that the main flow direction of exergy is from chilled water to the air in FCU. The calculations of corresponding exergy are shown in Equations (5.4) – (5.22).

In equations (5.4) – (5.22), the mean air temperature $T_{a,ave}$ [K] in the FCU is approximated by the mean value of supply and return air temperature, $T_{a,sup}$ [K] and $T_{a,re}$ [K], respectively; the mean chilled water temperature $T_{w,ave}$ [K] is approximated by the mean value of inlet and outlet temperature of chilled water circuit, $T_{w,in}$ [K] and $T_{w,out}$ [K], respectively; c_a [kJ/(kg·K)], ρ_a [kg/m^3], $\dot{F}_a$ [m^3/h], c_w [kJ/(kg·K)], ρ_w [kg/m^3], and $\dot{F}_w$ [m^3/h] are the specific heat capacity at constant pressure, the density, and flow rate of the air and chilled water, respectively; $\dot{Q}$ [kW] is the thermal-energy transfer rate in the FCU; $\dot{S}_{\mathrm{g,a}}$ [kW/K], $\dot{S}_{\mathrm{g,HE}}$ [kW/K] and $\dot{S}_{\mathrm{g,w}}$ [kW/K] are the entropy generation rate generated in the air within the FCU, in the tube wall between air and water, and in the water within the chilled water circuit, respectively.

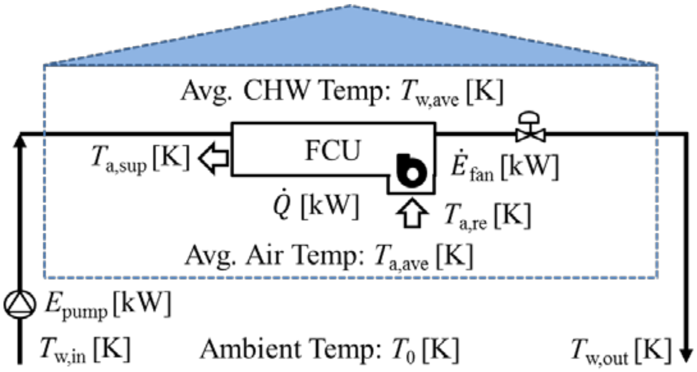
Avg. CHW Temp: $T_{\mathrm{w,ave}}$ [K]
$T_{\mathrm{a,sup}}$ [K]
FCU
$\dot{E}_{\mathrm{fan}}$ [kW]
$\dot{Q}$ [kW]
$T_{\mathrm{a,re}}$ [K]
Avg. Air Temp: $T_{\mathrm{a,ave}}$ [K]
E_{pump} [kW]
$T_{\mathrm{w,in}}$ [K]
Ambient Temp: T_0 [K]
$T_{\mathrm{w,out}}$ [K]

Figure 5.3 Assumed chilled water circuit

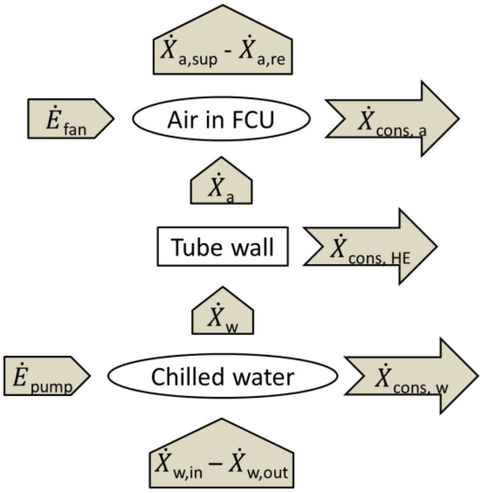
$\dot{X}_{\mathrm{a,sup}} - \dot{X}_{\mathrm{a,re}}$
$\dot{E}_{\mathrm{fan}}$
Air in FCU
$\dot{X}_{\mathrm{cons,\ a}}$
$\dot{X}_{\mathrm{a}}$
Tube wall
$\dot{X}_{\mathrm{cons,\ HE}}$
$\dot{X}_{\mathrm{w}}$
$\dot{E}_{\mathrm{pump}}$
Chilled water
$\dot{X}_{\mathrm{cons,\ w}}$
$\dot{X}_{\mathrm{w,in}} - \dot{X}_{\mathrm{w,out}}$

Figure 5.4 The flow of exergy through the system

Equations (5.4) and (5.5) show the energy budget and entropy budget of the air subsystem. By combining these two equations together with the ambient temperature, T_0 [K], the exergy-budget equation can be developed, as shown in Equation (5.6) (Li 2014).

$$\dot{E}_{fan} + c_a \rho_a \dot{F}_a \left(T_{a,re} - T_0\right)\big/3600 = c_a \rho_a \dot{F}_a \left(T_{a,\sup} - T_0\right)\big/3600 + \dot{Q} \tag{5.4}$$

$$c_a \rho_a \dot{F}_a \cdot \ln\left(T_{a,re} / T_0\right) / 3600 + \dot{S}_{g,a} = c_a \rho_a \dot{F}_a \cdot \ln\left(T_{a,\mathrm{sup}} / T_0\right) / 3600 + \dot{Q} / T_{a,ave} \tag{5.5}$$

$$\dot{E}_{fan} + \dot{X}_a - \dot{X}_{cons,a} = \dot{X}_{a,\mathrm{sup}} - \dot{X}_{a,re} \tag{5.6}$$

In the same way, the exergy budget of the tube-wall subsystem are given by Equation (5.9) using Equations (5.7) and (5.8) together with T_0; the chilled-water subsystem are given by Equation (5.12) using Equations (5.10) and (5.11) together with T_0, respectively.

$$\dot{Q} = \dot{Q} \tag{5.7}$$

$$\dot{Q} / T_{a,ave} + \dot{S}_{g,HE} = \dot{Q} / T_{w,ave} \tag{5.8}$$

$$\dot{X}_w - \dot{X}_{cons,HE} = \dot{X}_a \tag{5.9}$$

$$\dot{E}_{pump} + c_w \rho_w \dot{F}_{\mathrm{w}} \left(T_{\mathrm{w,in}} - T_0\right) / 3600 + \dot{Q} = c_w \rho_w \dot{F}_w \left(T_{w,out} - T_0\right) / 3600 \tag{5.10}$$

$$c_w \rho_w \dot{F}_{\mathrm{w}} \cdot \ln\left(T_{w,in} / T_0\right) / 3600 + \dot{Q} / T_{w,ave} + \dot{S}_{g,w} = c_w \rho_w \dot{F}_w \cdot \ln\left(T_{w,out} / T_0\right) / 3600 \tag{5.11}$$

$$\dot{E}_{pump} + \dot{X}_{w,in} - \dot{X}_{cons,w} = \dot{X}_w + \dot{X}_{w,out} \tag{5.12}$$

By combining Equations (5.6), (5.9) and (5.12), the exergy-budget equation for the entire system can be deduced, as given by Equation (5.13).

$$\left(\left(\dot{E}_{fan} + \dot{E}_{pump}\right) + \left(\dot{X}_{w,in} - \dot{X}_{w,out}\right)\right) - \left(\dot{X}_{cons,a} + \dot{X}_{cons,HE} + \dot{X}_{cons,w}\right) = \dot{X}_{a,\mathrm{sup}} - \dot{X}_{a,re} \tag{5.13}$$

The overall exergy input rate is the sum of the fan power $\dot{E}_{\mathrm{fan}}$ [kW], pump power $\dot{E}_{\mathrm{pump}}$ [kW], and the net exergy input rate from the chiller to the chilled water circuit, expressed as the difference between $\dot{X}_{\mathrm{w,in}}$ [kW] and $\dot{X}_{\mathrm{w,out}}$ [kW]. $\dot{X}_{\mathrm{w,in}}$ is the rate of exergy carried by the supply water leaving the chiller and $\dot{X}_{\mathrm{w,out}}$ is that carried by the return water coming from the FCU and going towards the chiller, respectively, as shown in Equations (5.14) and (5.15).

$$\dot{X}_{w,in} = \left(c_w \rho_w \dot{F}_{\mathrm{w}} \left(T_{w,in} - T_0\right) - c_w \rho_w \dot{F}_w T_0 \cdot \ln\left(T_{w,in} / T_0\right)\right) / 3600 \tag{5.14}$$

$$\dot{X}_{\mathrm{w,out}} = \left(c_w \rho_w \dot{F}_{\mathrm{w}} \left(T_{w,out} - T_0\right) - c_w \rho_w \dot{F}_w T_0 \cdot \ln\left(T_{w,out} / T_o\right)\right) / 3600 \tag{5.15}$$

The overall exergy consumption rate is the sum of $\dot{X}_{\mathrm{cons,a}}$ [kW], $\dot{X}_{\mathrm{cons,HE}}$ [kW], and $\dot{X}_{\mathrm{cons,w}}$ [kW], that are the rate of exergy consumed in the air within the FCU, in the tube wall between air and water, and in the water within the chilled water circuit, respectively, as shown in Equations (5.16), (5.17), and (5.18).

$$\dot{X}_{cons,\mathrm{a}} = \dot{S}_{g,a} T_0 \tag{5.16}$$

$$\dot{X}_{cons,\mathrm{HE}} = \dot{S}_{g,HE} T_0 \tag{5.17}$$

$$\dot{X}_{cons,w} = \dot{S}_{g,w} T_0 \tag{5.18}$$

The exergy output rate is the net exergy output rate from the FCU to the indoor space, expressed as the difference between $\dot{X}_{\mathrm{a,sup}}$ [kW] and $\dot{X}_{\mathrm{a,re}}$ [kW]. $\dot{X}_{\mathrm{a,sup}}$ is the rate of exergy carried by supply air leaving the FCU and $\dot{X}_{\mathrm{a,re}}$ is that of the exergy carried by the return air coming into the FCU, respectively, as shown in Equations (5.19) and (5.20).

$$\dot{X}_{a,\mathrm{sup}} = \left(c_a \rho_a \dot{F}_a \left(T_{a,\mathrm{sup}} - T_0 \right) - c_a \rho_a \dot{F}_a T_0 \cdot \ln\left(T_{a,\mathrm{sup}} / T_0 \right) \right) \Big/ 3600 \tag{5.19}$$

$$\dot{X}_{a,re} = \left(c_a \rho_a \dot{F}_a \left(T_{a,re} - T_0 \right) - c_a \rho_a \dot{F}_a T_0 \cdot \ln\left(T_{a,re} / T_0 \right) \right) \Big/ 3600 \tag{5.20}$$

$\dot{X}_{\mathrm{a}}$ [kW] and $\dot{X}_{\mathrm{w}}$ [kW] in Equations (5.6), (5.9) and (5.12) are the rate of exergy absorbed by air due to heat release and that discharging from chilled water due to heat absorption, respectively, as shown in Equations (5.21) and (5.22).

$$\dot{X}_a = \left(1 - T_0 / T_{a,ave} \right) \left(-\dot{Q} \right) \tag{5.21}$$

$$\dot{X}_w = \left(1 - T_0 / T_{w,ave} \right) \left(-\dot{Q} \right) \tag{5.22}$$

§ 5.4 Pump power and heat-transfer characteristics of FCU

5.4.1 Four variable-flow control modes

Four methods of variable-flow control for the chilled water circuit were assumed, as shown in Figures 5.5 – 5.8. In each figure, the left-hand side shows the control mode while the right-hand side shows the corresponding operating point of the pump. The system curve and pump performance curve are represented by a dotted line and solid line, respectively. The intersection of the two curves is the operating point of the pump at any instant. Point A is the rated operating point, without any adjustment, under full load. If the flow rate is reduced from 100% to X%, the operating point of the pump moves from point A to point B according to the variable-flow control method being applied.

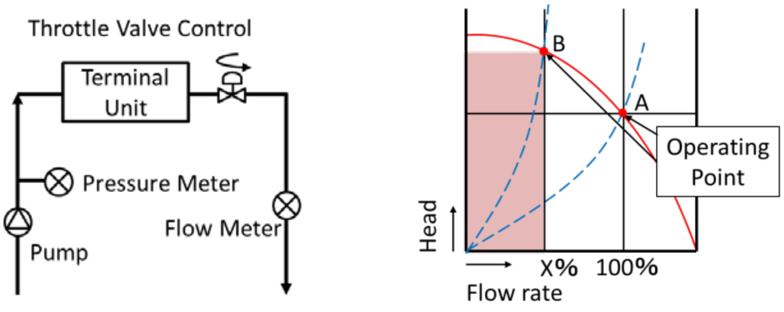
Throttle Valve Control
Terminal Unit
Pressure Meter
Flow Meter
Pump
B
A
Operating Point
Head
X%
100%
Flow rate

(a) (b)

Figure 5.5 Throttle-valve (TV) control

As shown in Figure 5.5, in the case of throttle-valve control (TV control), the water flow rate is adjusted only by the throttle valve with no change in the pump frequency. The other three methods apply variable-frequency control.

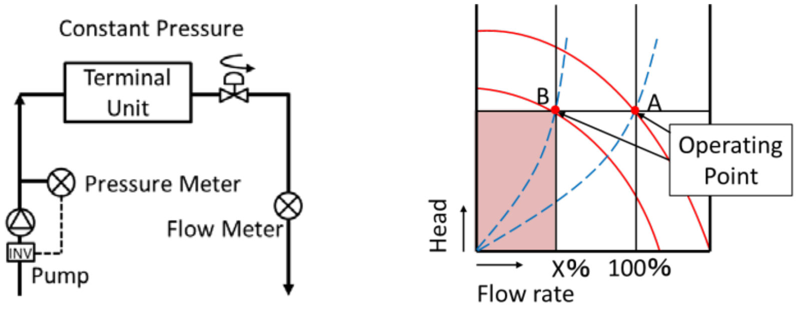
Constant Pressure
Terminal Unit
Pressure Meter
Flow Meter
INV
Pump
B
A
Operating Point
Head
X%
100%
Flow rate

(a) (b)

Figure 5.6 Constant-pressure (CP) control

For constant-pressure control (CP control), the pump maintains a constant discharge pressure to the chilled-water circuit by automatically adjusting motor speeds to meet. For constant-differential-pressure control (CDP control), the pump maintains a constant pressure difference at a specific interval for the chilled water system. In usual, the constant value is the pressure difference across the most significant distant load in the index circuit. As shown in Figure 5.7, the value is the sum of the pressure drop of terminal unit, piping, and two-way control valve under design flow conditions. Predictive system curve control (PSC control) is a new advanced control method by which further energy saving can be achieved. As its name suggests, the discharge pressure of the pump will be determined by a predictive system curve which describes the relationship between the pump discharge pressure and the water flow rate demand of chilled water circuit. The predictive system curve must be obtained by a precise commissioning process during the installation of control system.

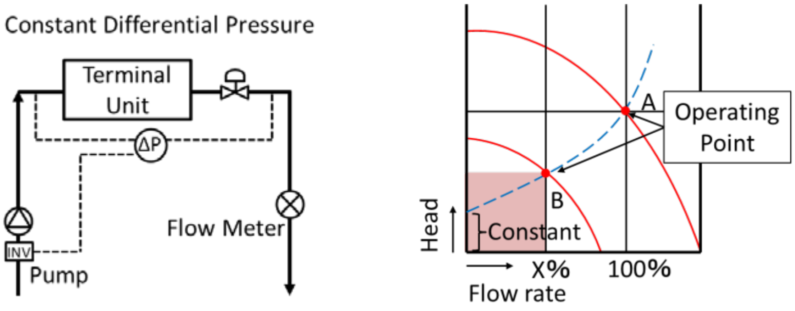
Constant Differential Pressure
Terminal Unit
ΔP
Flow Meter
INV
Pump
A
Operating Point
B
Constant
Head
X%
100%
Flow rate

(a) (b)

Figure 5.7 Constant-differential-pressure (CDP) control

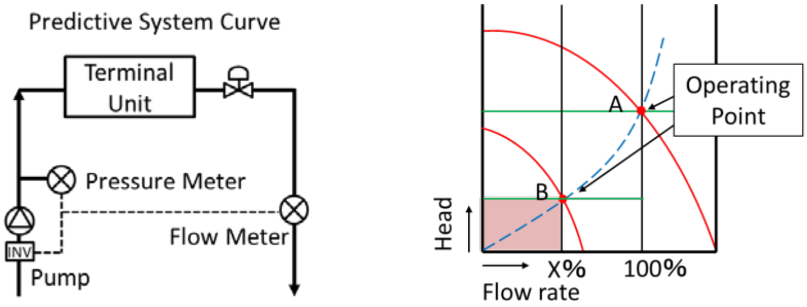
Predictive System Curve
Terminal Unit
Pressure Meter
Flow Meter
INV
Pump
Operating Point
A
B
Head
X%
100%
Flow rate

(a) (b)

Figure 5.8 Predictive-system-curve (PSC) control

5.4.2 Calculation of pump power

The system curve and pump performance curve both approximate to a quadratic curve. When the flow rate changes from a rate of $\dot{F}_A$ [m^3/h] to $\dot{F}_B$ [m^3/h], the pump power in each of the variable-flow control modes is calculated according to the following procedures.

For TV control, when the flow rate is zero, the pumping head is assumed to be n times the value of the rated pumping head (H_A [m]). Subsequently, according to the value of point ($0, n \cdot H_A$) and the rated point ($\dot{F}_A$, H_A), the quadratic equation of the pump performance curve can be expressed by Equation (5.23). By substituting the flow rate of point B ($\dot{F}_B$) into Equation (5.23), the pumping head for point B (H_B [m])

can be calculated. The hydraulic power at point B ($\dot{P}_{\mathrm{B}}$ [kW]) can then be calculated using Equation (5.24), in which γ [N/m^3] represents the specific weight of water. Using $\dot{P}_{\mathrm{B}}$ and the pump efficiency at point B (η_{B} [%]), the shaft power at point B ($\dot{E}_{\mathrm{B}}$ [kW]) can then be calculated from Equation (5.25).

$$H = nH_A - \left[(n-1) H_A / \dot{F}_A^2 \right] \cdot \dot{F}^2 \tag{5.23}$$

$$\dot{P}_B = \gamma \dot{F}_B H_B / 3{,}600{,}000 \tag{5.24}$$

$$\dot{E}_B = \dot{P}_B / \eta_B \tag{5.25}$$

For CP control, the shaft power $\dot{E}_{\mathrm{B}}$ is proportional to the flow rate $\dot{F}_{\mathrm{B}}$ due to the constant pumping head at each operating point, as given by Equation (5.26). For CDP control, the pumping head H_{B} can be calculated from the system curve, as given by Equation (5.27), in which k [-] and h [m] represent the friction coefficient and the corresponding pumping head, respectively, based on a constant pressure difference. Then, using Equations (5.24) and (5.25), the shaft power $\dot{E}_{\mathrm{B}}$ can be obtained.

$$\dot{E}_B = \left(\dot{F}_B / \dot{F}_A \right) \cdot \dot{P}_A / \eta_B \tag{5.26}$$

$$H_{\mathrm{B}} = k\dot{F}_B^{\ 2} + h \tag{5.27}$$

For PSC control, the relationship between the flow rate and the pumping head satisfies the pump affinity laws, so that the shaft power $\dot{E}_{\mathrm{B}}$ can be calculated using Equation (5.28) (Volk 2013).

$$\dot{E}_B = \left(\dot{F}_B / \dot{F}_{\ A} \right)^3 \cdot \dot{P}_A / \eta_B \tag{5.28}$$

5.4.3 Heat-transfer characteristics of FCU

Dehumidification was not taken into account in this study. The heat-transfer characteristic of the dry coil in the FCU can be represented by a semi-empirical formula with respect to the relationship between the relative heat-transfer rate $\dot{Q}/\dot{Q}^*$ and the relative water flow rate $\dot{F}/\dot{F}^*$, as given by Equation (5.29) (Shi 1986).

$$\frac{Q}{Q^*} = \frac{1}{1+\alpha\left(\frac{1}{F/F^*}-1\right)} \tag{5.29}$$

The characteristic coefficient of FCU α [-] is defined by Equation (5.30), in which $T^*_{\mathrm{w,in}}$ [K], $T^*_{\mathrm{w,out}}$[K], and $T^*_{\mathrm{a,re}}$ [K] represent the inlet and outlet temperatures of the chilled water circuit and the return air temperature for the design condition, respectively.

$$\alpha = 0.6\frac{T^*_{w,in} - T^*_{w,out}}{T^*_{w,in} - T^*_{a,re}} \tag{5.30}$$

The establishment conditions of Equation (5.29) are as follows:

(1) The flow rate of air side is constant along with the change of water flow rate.

(2) The inlet temperature of water side is constant.

(3) The inlet temperature of air side is constant.

(4) The heat transfer type is counter flow.

(5) The temperature difference of high-/low-temperature working mediums at the left end of heat exchanger is relatively close to that at the right end of heat exchanger, so that the log mean temperature difference can be replaced by arithmetic mean temperature difference.

§ 5.5 Calculation parameters

The full-load condition and partial load condition of FCU are analyzed. For each condition, four kinds of variable-flow control modes are discussed and compared.

5.5.1 Settings of supply water temperature

The temperature settings of full-load condition and partial-load condition are shown in Figures 5.9 and 5.10. For both full-load condition and partial load condition, the ambient temperature is fixed at 32°C. In addition, based on the establishment conditions of Equation (5.29), the return air temperature are fixed at 27°C; the supply water temperature of Cases 1 and 2 are fixed at 7°C and 12°C, respectively.

With respect to other temperature settings, under full-load condition, the supply air temperature in Cases 1 and 2 is set to a point 10°C and 5°C lower than return air temperature, respectively; the return water temperature in Cases 1 and 2 is set to a point 5°C higher than the supply water temperature under full-load, respectively. But under partial-load condition, both supply air temperature and return water temperature will vary with the heat transfer rate in the FCU and with the variable-flow control mode.

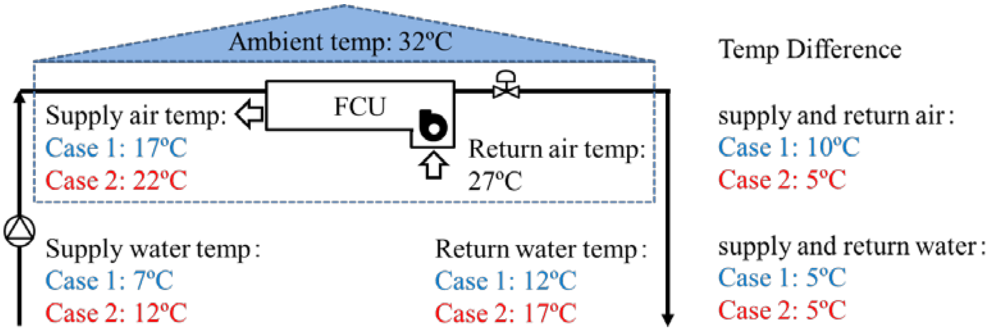
Ambient temp: 32ºC
FCU
Supply air temp:
Case 1: 17ºC
Case 2: 22ºC
Return air temp:
27ºC
Supply water temp:
Case 1: 7ºC
Case 2: 12ºC
Return water temp:
Case 1: 12ºC
Case 2: 17ºC
Temp Difference
supply and return air:
Case 1: 10ºC
Case 2: 5ºC
supply and return water:
Case 1: 5ºC
Case 2: 5ºC

Figure 5.9 Temperature setting under full-load condition

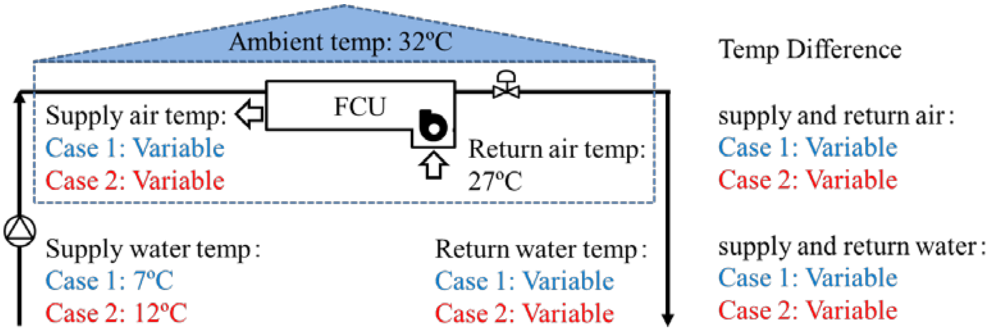
Ambient temp: 32ºC
FCU
Supply air temp:
Case 1: Variable
Case 2: Variable
Return air temp:
27ºC
Supply water temp:
Case 1: 7ºC
Case 2: 12ºC
Return water temp:
Case 1: Variable
Case 2: Variable
Temp Difference
supply and return air:
Case 1: Variable
Case 2: Variable
supply and return water:
Case 1: Variable
Case 2: Variable

Figure 5.10 Temperature setting under partial-load condition

5.5.2 Settings of pumping head

The pumping head consists of three parts, as shown in Figure 5.11: the head loss caused by the on-way resistance, the local resistance, and the resistance of the equipment. In the chilled water circuit, the length of straight pipe, the equivalent diameter, the equivalent roughness, and the water velocity are set to 40 m, 40 mm, 0.15 mm, and 0.59 m/s, respectively. So the corresponding head loss caused by the on-way resistance is 7.6 m. The head loss of the two-way valve is set to 5 m; the other local resistance is assumed to be 150% of that of the on-way resistance. Then, the head loss of total local resistance can be obtained as 16.4 m. The head loss of both the FCU and the chiller are set to 10 m, so that the head loss resulting from the resistance in the equipment is 20 m. Therefore, the total head loss is 44 m.

If the corresponding pumping head *h*, based on a constant pressure difference in Equation (5.27) is assumed to be 15 m, the coefficient *k* will be 4.08, given the parameter values mentioned above. The coefficient *n* in Equation (5.23), used to calculate the pumping head in throttle-valve-control mode is assumed to be 1.4.

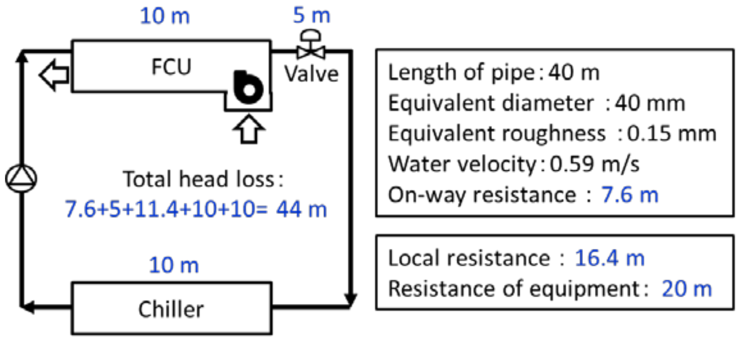
10 m
5 m
FCU
Valve
Total head loss:
7.6+5+11.4+10+10= 44 m
10 m
Chiller
Length of pipe: 40 m
Equivalent diameter : 40 mm
Equivalent roughness : 0.15 mm
Water velocity: 0.59 m/s
On-way resistance : 7.6 m
Local resistance : 16.4 m
Resistance of equipment: 20 m

Figure 5.11 Pumping head settings

5.5.3 Settings of power and flow rate of pump and fan

The pump efficiency is assumed to be constant at 60%. According to the parameters related to the piping, water velocity, and pumping head described above, the flow rate and pumping power under full-load are 2.7 m^3/h and 0.53 kW, respectively. Under partial-load, the pump power decreases depending on the variable-flow control mode. The design heat-transfer rate is assumed to be 15 kW.

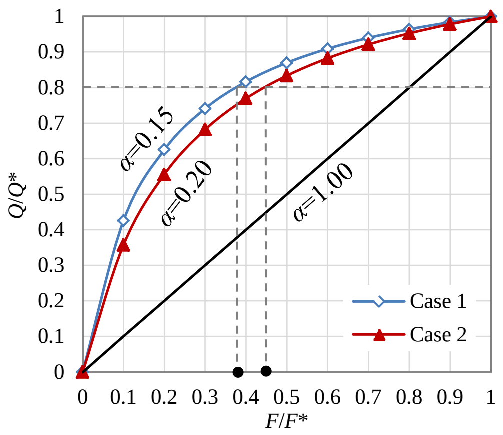

Figure 5.12 Relative heat-transfer rate versus relative water flow rate

By substituting the temperature values given above into Equations (5.29) and (5.30), when the heat-transfer rate falls to 80% of the design value (12 kW), the relative flow rates in Cases 1 and 2 change to 37.4% and 44.5% of the design value, respectively, as shown in Figure 5.12.

Since the primary focus of this study is not the fan but rather the pump, the fan power in Cases 1 and 2 under full-load is simply assumed to be 0.2 kW and 0.4 kW, respectively, based on the assumed design heat-transfer rate by reference to the manufacturer's specifications. According to the heat-transfer rate of the FCU, the fan power, and the related temperature settings, the flow rate of the fan under full-load is 4108 m^3/h and 8106 m^3/h for Cases 1 and 2, respectively. Under partial-load, due to the establishment conditions of Equation (5.29), the flow rate and power of the fan for Cases 1 and 2 remain the same.

§ 5.6 Calculation Results

5.6.1 Pumping head and pumping power

The pumping head and pumping power of Cases 1 and 2 under four kinds of control modes are shown in Figures 5.13 and 5.14, respectively. In these figures, the vertical bars, from left to right, represent rated mode, and the throttle-valve control mode, constant-pressure control mode, constant-differential-pressure control mode, and predictive-system-curve control mode.

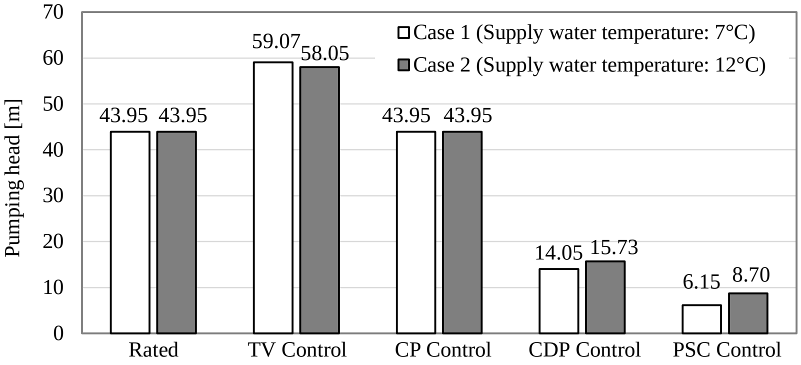

Figure 5.13 Comparison of pumping head

Under partial-load conditions, it can be seen from Figure 5.13 as follows. The pumping heads of TV control are the highest, which are about 1.3 times of those under full-load, since the water flow rates are adjusted only by the throttle valve with no change in the pump frequency. For the CP control, just as the name suggest, the pumping heads remain the same. With respect to the CDP control and PSC control, the pumping heads are reduced significantly compared with the former two control modes. Especially for the PSC control, the pumping head of Cases 1 and 2 are reduced by 90% and 85%, respectively, compared with that under full-load. For any control mode under partial-load, due to the slightly different relative flow rates in Cases 1 and 2, as shown in Figure 5.12, the pumping heads of Cases 1 and 2 for certain control mode are slightly different except of the CP control.

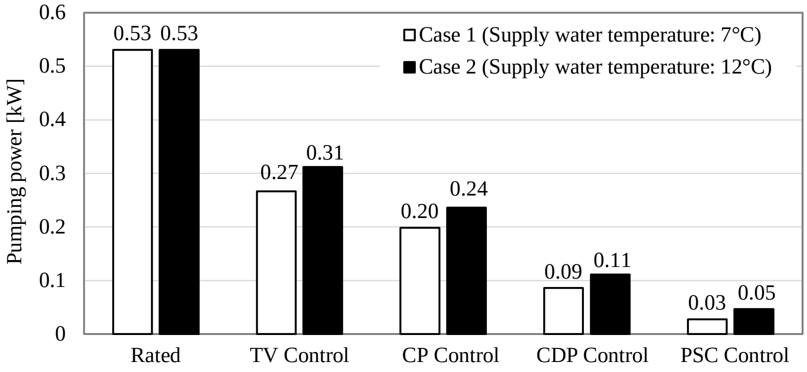

Figure 5.14 Comparison of pumping power

The pumping power under partial-load is smaller than that under full-load, as shown in Figure 5.14. In addition, the pumping power under any variable-frequency control mode is smaller than that under throttle-valve control. In variable-frequency control mode, the pumping power decrease in the following order: constant-pressure control, constant-differential-pressure control, and predictive-system-curve control. Especially for the Case 1 under PSC control, the pumping power is reduced by 94% compared with that under full-load. Moreover, for the comparison of Cases 1 and 2 for a certain control mode, since the relative flow rate of Case 1 is slightly smaller than that of Case 2, the pumping power of Case 1 is also slightly smaller than that of Case 2.

5.6.2 Exergy budget of the system

The rates of exergy input and output under full-load (15 kW) and partial-load (12 kW) conditions for Cases 1 and 2 are shown in Figures 5.15 and 5.16, respectively. The differences between the rates of exergy input and output in the two cases are the rate of exergy consumptions, as shown in Figure 5.17. In these figures, the vertical bars, from left to right, represent rated mode, and the TV, CP, CDP, and PSC control modes. The exergy consumption patterns for the two cases are shown in Figure 5.18.

For the improvement of a certain thermodynamic system, under the condition of a fixed value of exergy requirements, that is the exergy demand, we should think about how we can reduce the exergy input to the whole system as much as possible. Since the total amount of energy resources is limited on the earth, "energy saving" means that we should reduce the exergy input for running a variety of systems including air-conditioning systems in buildings. In this study, the thermal energy requirement of demand side was assumed to be constant at 15 kW under full-load condition and at 12 kW under partial-load condition, thereby the difference in the rate of exergy input are mainly investigated for these demand values.

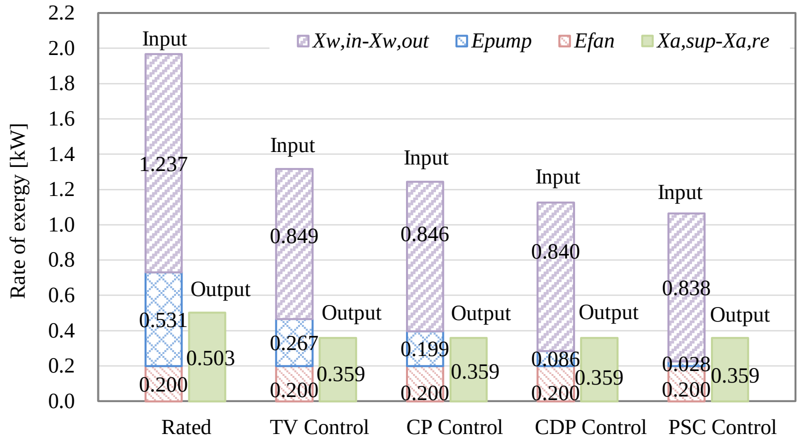

Figure 5.15 The rates of exergy input and output (Case 1)

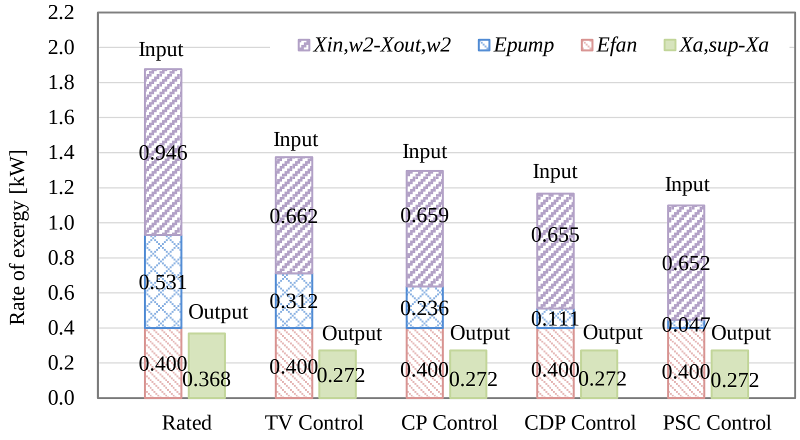

Figure 5.16 The rates of exergy input and output (Case 2)

It can be seen from Figures 5.15 and 5.16 that for both Cases 1 and 2, the rates of exergy input under any partial-load condition are smaller than those under full-load condition and those under any variable-frequency control mode are smaller than those under throttle-valve control mode. In variable-frequency control mode, the rates of exergy input decrease in the following order: constant-pressure control, constant-differential-pressure control, and predictive-system-curve control. Regarding the effect of the supply water temperature, the rate of exergy inputs are smaller at 12°C (Case 2) than at 7°C (Case 1).

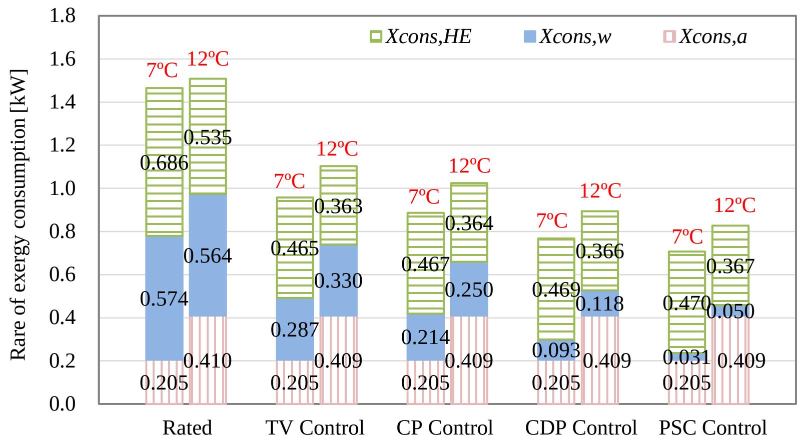

Figure 5.17 The rates of exergy consumption of two Cases

As shown in Figure 5.17, the rates of exergy consumed in the water within the chilled water circuit are also decease in the following order: rated mode, constant-pressure control mode, constant-differential-pressure control mode, and predictive-system-curve control mode. But it is noted that the rates of overall exergy consumption at the supply water temperature of 12°C are larger than those at 7°C, which may sound a little different from conventional engineering-practice knowledge that higher chilled water temperature would improve the efficiency of chiller and result in smaller exergy consumption. The reason for this is that the boundary of the system analyzed in this Chapter is the chilled water circuit alone except the chiller, as shown in Figure 5.3, in order to confine our analysis in this study to the variable-flow control modes. How the rate of exergy consumption consumed in the refrigeration cycle affects the whole amount of exergy consumption would be to be investigated in next Chapter based on the analysis on the actual operating data.

Combining Figures 5.15 – 5.17, the exergy consumption patterns of Cases 1 and 2 are shown in Figure 5.18. It can be seen that for each case the flow direction of exergy is from the input (net input from the chiller) to the output (output to the indoor environment) of the system by passing through the chilled water circuit, tube wall between chilled water and air in FCU, and the air channel in FCU. Along with the flow direction of exergy, the rate of exergy input for each case is consumed gradually. The rate of exergy consumption at each subsystem can also be obtained clearly.

Above points are the greatest merits of exergy analysis compared with the traditional energy analysis. Since the energy analysis is based on the first law of thermodynamics, energy is never destroyed during a process, therefore, the value and direction of the reduction in the available energy cannot be clearly and easily determined.

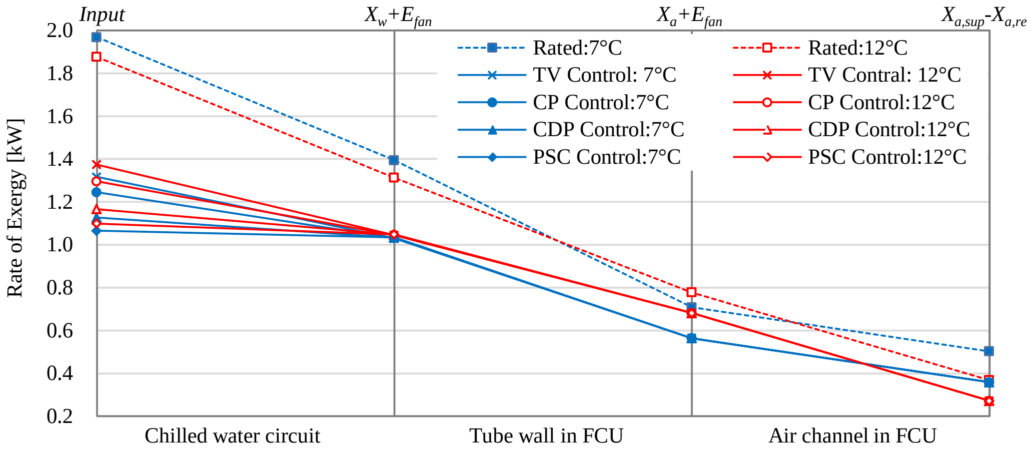

Figure 5.18 Exergy consumption patterns of two Cases

§ 5.7 Conclusions

In this Chapter, the exergy analysis on an assumed chilled-water circuit system under four variable-flow control modes and two supply water temperatures are carried out, the major findings are summarized as follows.

(1) The rates of exergy input and exergy consumption under any partial-load condition are significantly smaller than those under full-load condition.

(2) The rates of exergy input and exergy consumption under any variable-frequency control mode are smaller than those under throttle-valve control mode.

(3) In variable-frequency control mode, the rate of exergy inputs decrease in the following order: constant-pressure control, constant-differential-pressure control, and predictive-system-curve control.

(4) Regarding the effect of the supply water temperature, the rate of exergy inputs are smaller at 12°C than at 7°C.

(5) The use of the variable-frequency control mode and a higher chilled water temperature will effectively reduce the exergy input to the system.

Chapter 6 Performance analysis on a heat pump system of an actual building

In the previous Chapter, the exergy analysis on an assumed chilled-water circuit is carried out. In this Chapter, the performance of an actual heat pump system at each step of the system renovation and modification are compared and analysed. Meanwhile, in order to clarify the effect of chilled water temperature, operation mode of compressor and pumps, and the type of heat exchanger on the system performance, the exergy analysis based on the actual operating date of heat pump system are carried out.

§ 6.1 Introduction

As one of the new systems using renewable energy sources, the heat pump system has attracted more and more attention in recent years for energy saving. However, even the inner property of certain system is energy-efficient, without the right design and reasonable operation, energy saving is impossible. In this study, the actual measurements of performance verification on a heat pump system of an actual building are carried out. While grasping the performance of system, some corresponding renovations and modification are conducted on the system. The operation results before and after the renovations and modification are also analysed and verified.

Among them, the energy-saving performance after the variable-frequency transformation of compressor and water pumps, after the temperature adjustment of child water, and after the replacement of heat exchanger from stainless steel plate heat exchanger to aluminium plate-fin heat exchanger are mainly focused on in the following.

§ 6.2 System summary

The heat pump system applied to the 21KOMCEE (21 Komaba Center for Educational Excellence) in the Komaba II campus of the University of Tokyo is the research object in this study. 21KOMCEE has five floors and one underground level floor. The total floor area of the building is 4,477m^2. It includes several studios and convention rooms such as halls and meeting rooms (Ooka 2013). The appearance of the 21KOMCEE is shown in Figure 6.1.

Both ground heat and ground water are utilized as heat source in the heat pump system as shown in Figure 6.2. For the ground heat source, 10 boreholes with 100m depth are drilled. For each borehole, a single type of U tube made of cross-linked poly-ethylene is installed. The total capacity of the ground heat source is roughly estimated to 50 kW. For the ground water source, two pairs of wells are installed:

one for lifting water and the other for injection. The water is lifted at a rate of about 100 l/min, which can be translated to a roughly estimated heat rate extracted from this ground water system as 70 kW, with the assumption of a temperature difference of 5ºC. Chilled water for cooling and heated water for heating from all heat pumps are usually stored in the heat storage tank which is installed under the basement, with the capacity of 300 ton (Ooka 2013).

Figure 6.1 The appearance 21KOMCEE

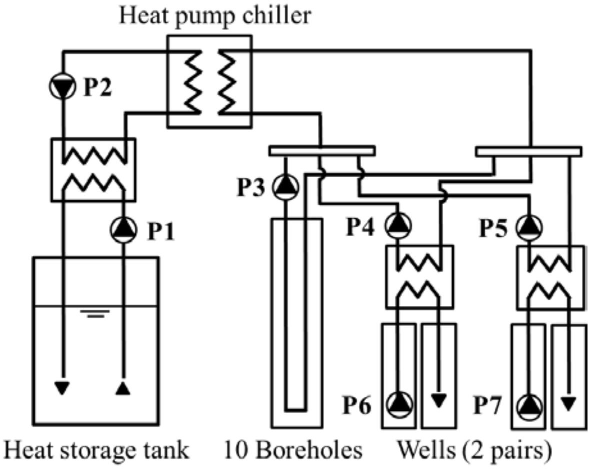
Heat pump chiller
P2
P3
P1
P4
P5
P6
P7
Heat storage tank
10 Boreholes
Wells (2 pairs)

Figure 6.2 Heat pump systems

§ 6.3 Investigation on COP improvement of the modified system

The property of the heat pump system before and after the system renovation and modification is described in Table 6.1. The performances of cooling mode are mainly focused on in this study.

Table 6.1 Properties of heat pumps before and after the system renovation and modification

Cooling Mode	Initial 13/07/23	Step 1 13/10/11	Step 2 14/06/04	Step 3 13/07/23	Step 2 14/08/26	Step 5 14/10/03
Power of heat pump chiller [kW] Rated value: 20.1/30.3 (cooling/heating)	19.7	16.2	27.8	14.0	20.0	14.9
Pumping power of cooling-water side [kW] Rated value: 11.9	12.8	10.9	10.7	8.8	10.7	10.6
Pumping power of chilled-water side [kW] Rated value: 3.7	5.7	6.1	4.8	3.6	3.9	3.8
System power consumption [kW] Rated value: 35.7	38.3	33.3	43.3	26.3	34.5	29.3
Cooling/Heating ability [kW] Rated value: 101.1/121.2 (cooling/heating)	82.3	86.5	132.2	68.8	100.3	95.5
COP of heat pump chiller Rated value: 5.0/4.0 (cooling/heating)	4.2	5.3	4.7	4.9	5.0	6.4
System COP	2.2	2.6	3.0	2.6	2.9	3.2

The operating data of each stage are shown as follows.

(1) Initial condition

The operating data of the heat pump system before the renovation are shown in Figure 6.3. The average refrigerating capacity is 82.3 kW. The average COP of the heat pump chiller is 4.2, which is slightly lower than the rated value (5.0). The reason is that the average outlet chilled water temperature of the heat pump chiller is only 5.8ºC, compared with the rated value of 7.0ºC. In addition, the average system COP is just 2.2, which is about only half of the average COP of heat pump chiller. It means that the pumping power in the system is almost the same with the power of heat pump chiller. Therefore, the pumping power of the system should be reduced while improving the COP of heat pump chiller.

(2) Step 1 of renovation and modification

The operating data after the step 1 of renovation and modification are shown in Figure 6.4. The variable-frequency transformation is added to the compressor of the heat pump chiller. Moreover, the average outlet chilled water temperature of the heat pump chiller is increased to 7.7ºC. Then the average COP of the heat pump chiller is also increased by 26% from 4.2 to 5.3. But the average COP is 2.6, the reduction of pumping power is still an important topic.

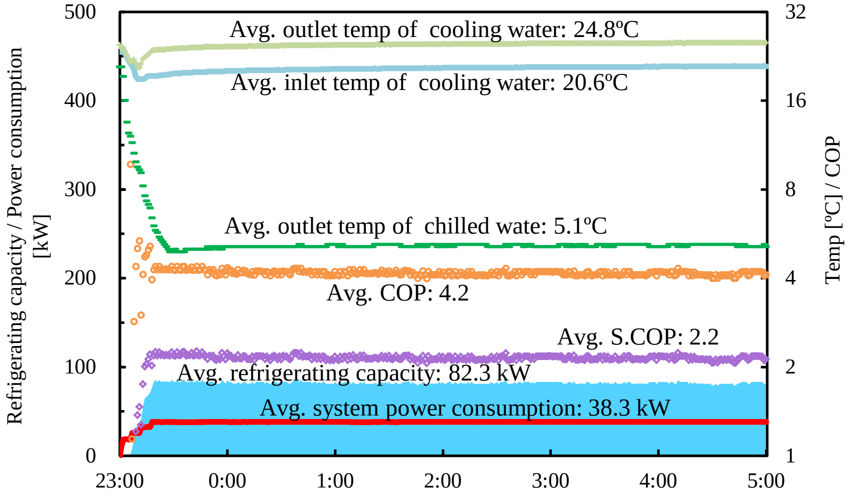

Figure 6.3 Operating data during the night of 2013/07/23

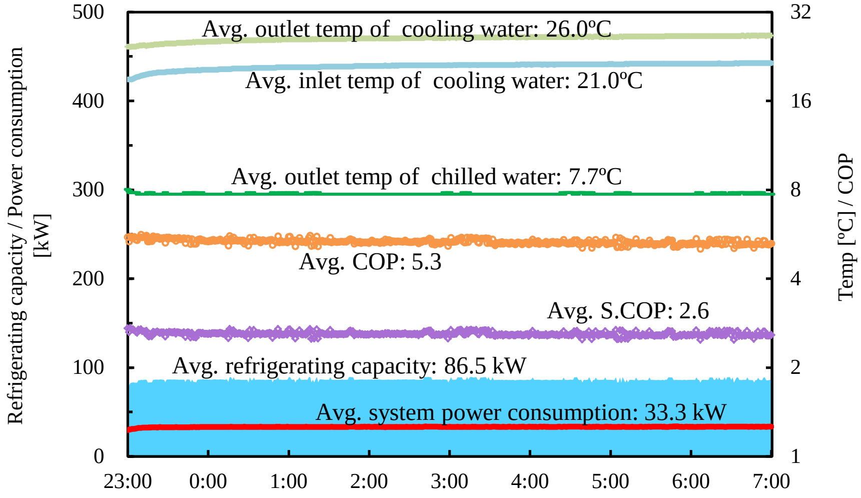

Figure 6.4 Operating data during the night of 2013/10/11

(3) Step 2 of renovation and modification

The operating data after the step 2 of renovation and modification are shown in Figure 6.5. In order to reduce the pumping power of the system, in this step, the variable-frequency transformations are added to the water pumps numbered as P2, P3, P4, and P5, as shown in Figure 6.2. The average COP of the heat pump chiller decreases from 5.3 to 4.7, compared with step 1 of renovation and modification, but the average refrigerating capacity of the heat pump chiller increases from 86.5 kW to 132.2 kW, with the reduction of average pumping power from 17.0 kW to 15.5 kW. It means that the average pumping power per unit average refrigerating capacity decreases from 0.197 to 0.117. Therefore, the average system COP increases from 2.6 to 3.0. The reason for the decrease of the average COP of heat pump chiller might be the overlarge average refrigerating capacity, compared with the rated value (101.1 kW), which will lead to the efficiency drop of compressor in the heat pump chiller.

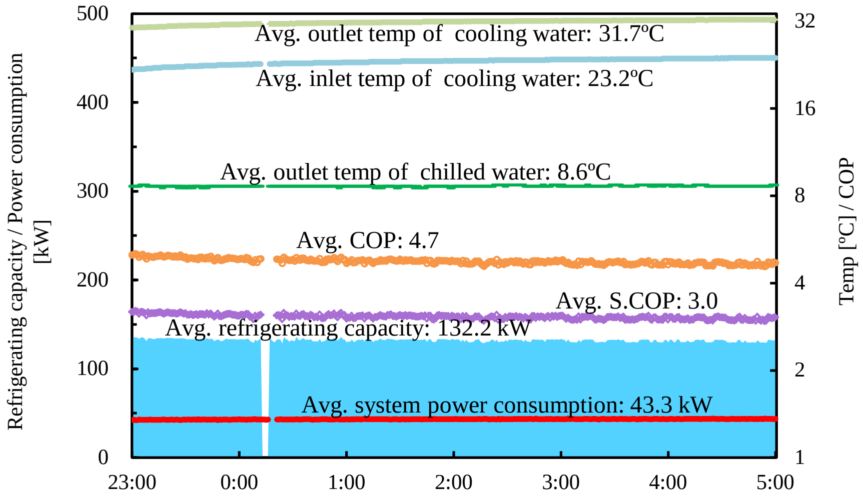

Figure 6.5 Operating data during the night of 2014/06/04

(4) Step 3 of renovation and modification

The operating data after the step 3 of renovation and modification are shown in Figure 6.6. According to the problem of overlarge average refrigerating capacity in step 2, the upper limit of rotating speed of compressor is confined, so that the average refrigerating capacity decreases from 132.2 kW to 68.8 kW. The average COP of heat pump chiller also increases slightly from 4.7 to 4.9. In addition, though the average pumping power decrease from 15.5 kW to 12.4 kW, the average pumping power per unit average refrigerating capacity increases from 0.117 to 0.180. Therefore, the average system COP decreases from 3.0 to 2.6, compared with that after step 2.

(5) Step 4 of renovation and modification

The operating data after the step 4 of renovation and modification are shown in Figure 6.7. In step 4, in order to increase the lower refrigerating capacity, the upper limit of rotating speed of compressor is extended, so that the average refrigerating capacity increases from 68.8 kW to 100.3 kW. Then the average COP of heat pump chiller also increases slightly from 4.9 to 5.0. Along with the increase of average refrigerating capacity, the water flow rate in the water circuit also increases. Therefore, the average pumping power increases from 12.4 kW to 14.6 kW. But by combining the effect of both refrigerating capacity and pumping power, the average pumping power per unit average refrigerating capacity decreases from 0.180 to 0.145. Meanwhile, the average system COP increases from 2.6 to 2.9, compared with that after step 3.

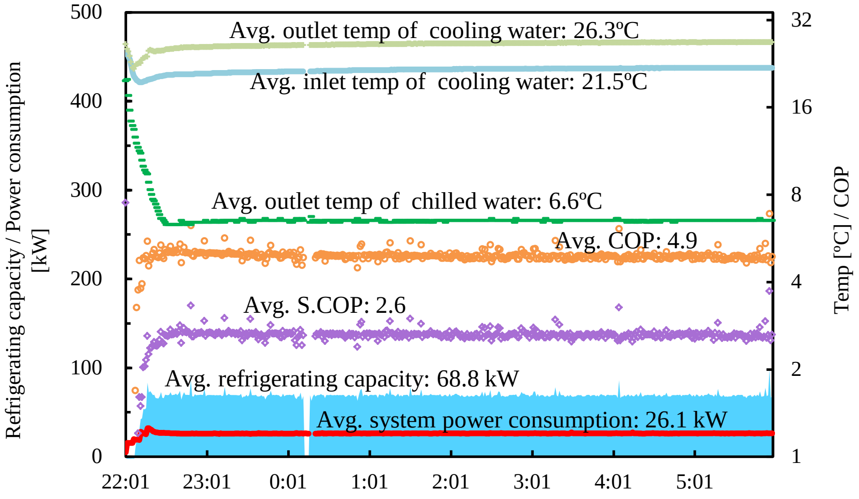

Figure 6.6 Operating data during the night of 2014/08/26

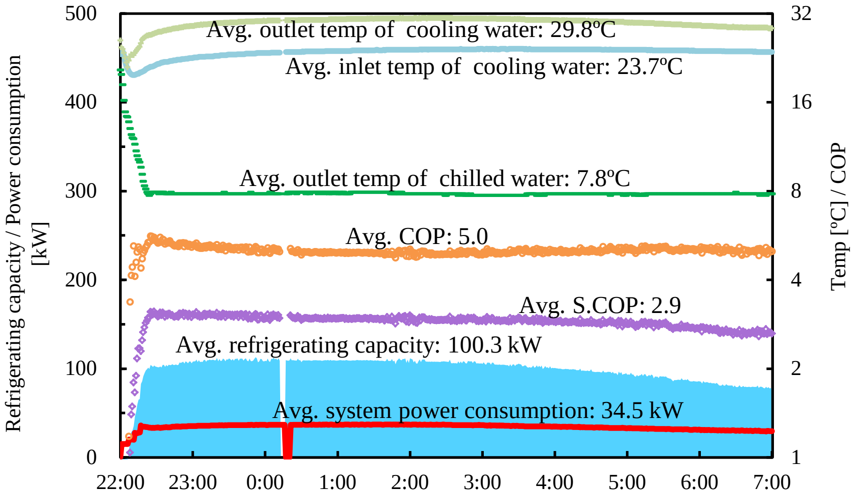

Figure 6.7 Operating data during the night of 2014/10/03

(6) Step 5 of renovation and modification

The operating data after the step 5 of renovation and modification are shown in Figure 6.8. In step 5, the corresponding heat exchangers demonstrated in Figure 6.2 are replaced from stainless steel plate heat exchanger to aluminium plate-fin heat exchanger. After the replacement, the heat transfer performance of heat exchangers is improved significantly, so the temperature difference between heat source side and demand side is decreased. Therefore, the average COP of heat pump chiller increases significantly from 5.0 to 6.4, which lead to the improvement of the average system COP from 2.9 to 3.2.

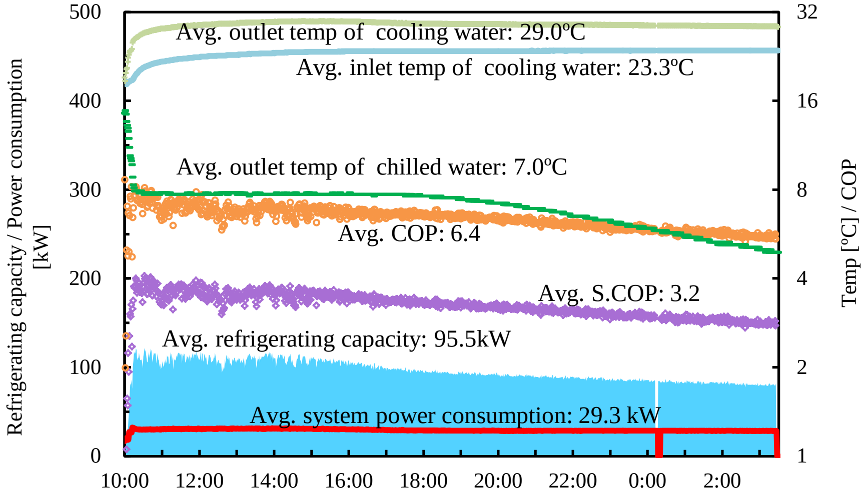

Figure 6.8 Operating data during the daytime of 2014/11/11

§ 6.4 Exergy analysis on the heat pump system

In order to further clarify the effect of corresponding system renovation and modification on the system performance, the exergy analysis on the heat pump system is carried out. Due to the complexity of the actual system, only part of the system is chosen as the research object, as shown in Figure 6.9. The corresponding flow of exergy through the system is shown in Figure 6.10. It can be seen than the main flow direction of the exergy is from the cooling water circuit to the chilled water circuit by passing through the refrigeration cycle.

The analysis object in this Chapter can be divided into four subsystems, which will be expressed in the following. Moreover, in order to combine with actual situation, unlike the ideal theoretical analysis in Chapter 5, both the heat loss from the system to the surrounding and the heat invasion from the surrounding to the system are considered during the exergy analysis.

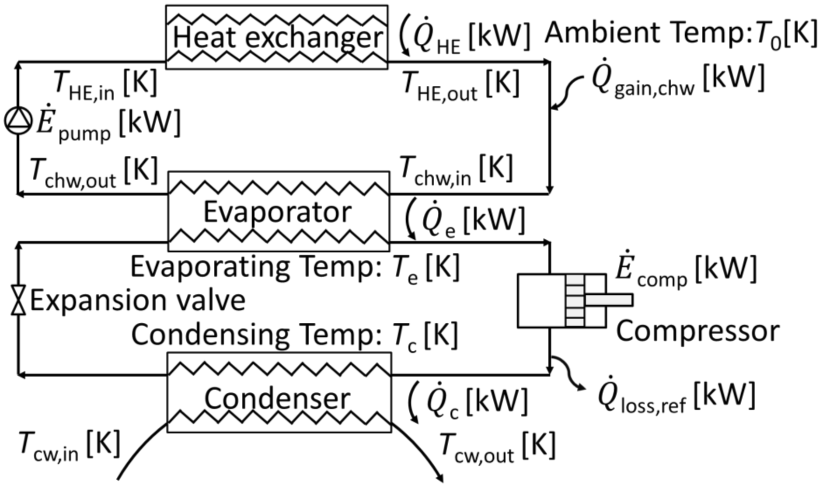
Heat exchanger
$\dot{Q}_{\mathrm{HE}}$ [kW]
Ambient Temp: T_0 [K]
$T_{\mathrm{HE,in}}$ [K]
$T_{\mathrm{HE,out}}$ [K]
$\dot{Q}_{\mathrm{gain,chw}}$ [kW]
$\dot{E}_{\mathrm{pump}}$ [kW]
$T_{\mathrm{chw,out}}$ [K]
$T_{\mathrm{chw,in}}$ [K]
Evaporator
$\dot{Q}_{\mathrm{e}}$ [kW]
Evaporating Temp: T_{e} [K]
$\dot{E}_{\mathrm{comp}}$ [kW]
Expansion valve
Compressor
Condensing Temp: T_{c} [K]
Condenser
$\dot{Q}_{\mathrm{c}}$ [kW]
$\dot{Q}_{\mathrm{loss,ref}}$ [kW]
$T_{\mathrm{cw,in}}$ [K]
$T_{\mathrm{cw,out}}$ [K]

Figure 6.9 Analysis object in the heat pump system

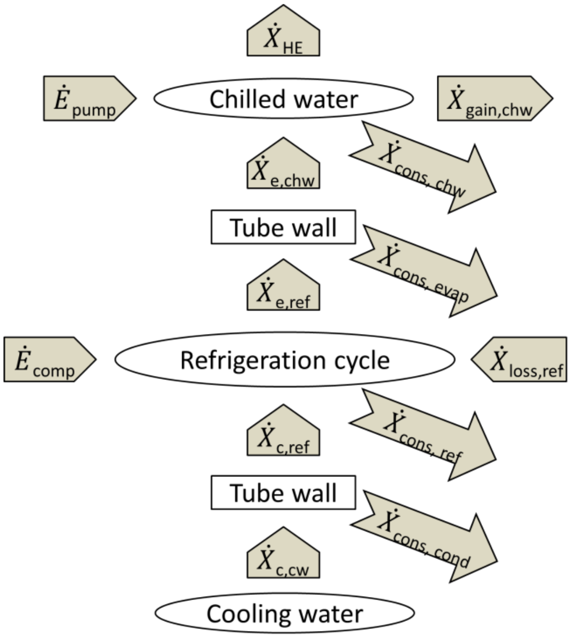
$\dot{X}_{\mathrm{HE}}$
$\dot{E}_{\mathrm{pump}}$
Chilled water
$\dot{X}_{\mathrm{gain,chw}}$
$\dot{X}_{\mathrm{e,chw}}$
$\dot{X}_{\mathrm{cons,\ chw}}$
Tube wall
$\dot{X}_{\mathrm{cons,\ evap}}$
$\dot{X}_{\mathrm{e,ref}}$
$\dot{E}_{\mathrm{comp}}$
Refrigeration cycle
$\dot{X}_{\mathrm{loss,ref}}$
$\dot{X}_{\mathrm{cons,\ ref}}$
$\dot{X}_{\mathrm{c,ref}}$
Tube wall
$\dot{X}_{\mathrm{cons,\ cond}}$
$\dot{X}_{\mathrm{c,cw}}$
Cooling water

Figure 6.10 Direction of exergy flow

6.4.1 Exergy budget of the system

As mentioned before, the analysis object is divided into four subsystems: the tube wall between cooling water and refrigerant in condenser, the refrigeration cycle, the tube wall between refrigerant and chilled water in evaporator, and the chilled water circuit.

In the following equations, the mean cooling water temperature $T_{\mathrm{cw,ave}}$ [K] is approximated by the mean value of inlet temperature $T_{\mathrm{cw,in}}$ [K] and outlet temperature $T_{\mathrm{cw,out}}$ [K] of cooling water; The mean refrigerant temperature $T_{\mathrm{ref,ave}}$ [K] is approximated by the mean value of evaporating temperature T_{e} [K] and condensing temperature T_{c} [K]; The mean chilled temperature $T_{\mathrm{chw,ave}}$ [K] in the evaporator is approximated by the mean value of inlet temperature $T_{\mathrm{chw,in}}$ [K] and outlet temperature $T_{\mathrm{chw,out}}$ [K] of chilled water in the evaporator; The mean chilled water temperature $T_{\mathrm{HE,ave}}$ [K] in the heat exchanger is approximated by the mean value of inlet temperature $T_{\mathrm{HE,in}}$ [K] and outlet temperature $T_{\mathrm{HE,out}}$ [K] of chilled water in the heat exchanger. $\dot{S}_{\mathrm{g,cond}}$ [kW/K], $\dot{S}_{\mathrm{g,ref}}$ [kW/K], $\dot{S}_{\mathrm{g,evap}}$ [kW/K], and $\dot{S}_{\mathrm{g,chw}}$ [kW/K] are the rate of entropy generated in the tube wall between cooling water and refrigerant, in the refrigeration cycle, in the tube wall between refrigerant and chilled water, and in the chilled water circuit, respectively. $\dot{Q}_{HE}$ [kW], $\dot{Q}_{gain,chw}$ [kW], $\dot{Q}_{e}$ [kW], $\dot{Q}_{loss,ref}$ [kW], $\dot{Q}_{c}$ [kW] are the heat transfer rate in the heat exchanger, the heat invasion rate from surrounding to the chilled water circuit, the heat transfer rate in the evaporator, the heat loss rate from refrigeration cycle to the surrounding, and the heat transfer rate in the condenser, respectively. $\dot{E}_{pump}$ [kW] and $\dot{E}_{comp}$ [kW] are the powers of pump and compressor, respectively.

(1) The tube wall between cooling water and refrigerant in condenser

The first subsystem is shown in Figure 6.11. The energy budget and entropy budget of the subsystem are shown in Equations (6.1) and (6.2), respectively. By combining these two equations together with the ambient temperature, T_0 [K], the exergy-budget equation can be developed, as shown in Equation (6.3).

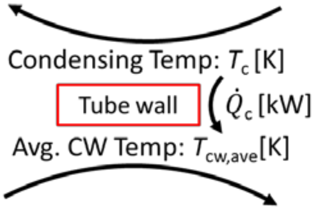
Condensing Temp: T_c [K]
Tube wall
$\dot{Q}_c$ [kW]
Avg. CW Temp: $T_{\mathrm{cw,ave}}$[K]

Figure 6.11 Subsystem 1

$$\dot{Q}_c = \dot{Q}_c \tag{6.1}$$

$$\dot{Q}_c / T_c + \dot{S}_{g,cond} = \dot{Q}_c / T_{cw,ave} \tag{6.2}$$

$$\dot{X}_{c,cw} - \dot{X}_{cons,cond} = \dot{X}_{c,ref} \tag{6.3}$$

$\dot{X}_{c,cw}$ [kW], $\dot{X}_{cons,cond}$ [kW], and $\dot{X}_{c,ref}$ [kW] in Equation (6.3) are the rate of exergy discharging from cooling water due to heat absorption $\dot{Q}_c$ in the condenser, the rate of exergy consumed in the tube wall between cooling water and refrigerant, and the rate of exergy absorbed by refrigerant due to heat release $\dot{Q}_c$ in condenser, respectively, which are expressed in Equations (6.4) – (6.6).

$$\dot{X}_{c,cw} = \left(1 - T_0 / T_{cw,ave}\right)\left(-\dot{Q}_c\right) \tag{6.4}$$

$$\dot{X}_{cons,cond} = \dot{S}_{g,cond} T_0 \tag{6.5}$$

$$\dot{X}_{c,ref} = \left(1 - T_0 / T_c\right)\left(-\dot{Q}_c\right) \tag{6.6}$$

(2) The refrigeration cycle

The second subsystem is shown in Figure 6.12. The energy budget, entropy budget, and exergy budget of the subsystem are shown in Equations (6.7) – (6.9), respectively.

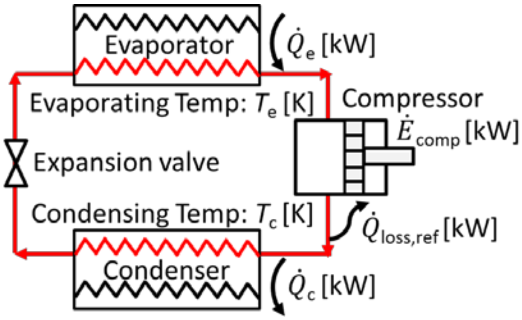

Figure 6.12 Subsystem 2

$$\dot{Q}_e + \dot{E}_{comp} = \dot{Q}_c + \dot{Q}_{loss,ref} \tag{6.7}$$

$$\dot{Q}_e / T_e + \dot{S}_{g,ref} = \dot{Q}_c / T_c + \dot{Q}_{loss,ref} / T_{ref,ave} \tag{6.8}$$

$$\dot{E}_{comp} + \dot{X}_{c,ref} + \dot{X}_{loss,ref} - \dot{X}_{cons,ref} = \dot{X}_{e,ref} \tag{6.9}$$

$\dot{X}_{loss,ref}$ [kW], $\dot{X}_{cons,ref}$ [kW], and $\dot{X}_{e,ref}$ [kW] in Equation (6.9) are the rate of exergy absorbed by refrigerant due to net heat loss $\dot{Q}_{loss,ref}$ from the refrigeration cycle to the surrounding, the rate of exergy consumed in the refrigeration cycle, and rate of exergy discharging from refrigerant due to heat absorption $\dot{Q}_e$ in the evaporator, respectively, which are expressed in Equations (6.10) – (6.12).

$$\dot{X}_{loss,ref} = \left(1 - T_0 / T_{ref,ave}\right)\left(-\dot{Q}_{loss,ref}\right) \tag{6.10}$$

$$\dot{X}_{cons,ref} = \dot{S}_{g,ref} T_0 \tag{6.11}$$

$$\dot{X}_{e,ref} = \left(1 - T_0 / T_e\right)\left(-\dot{Q}_e\right) \tag{6.12}$$

(3) The tube wall between refrigerant and chilled water in evaporator

The third subsystem is shown in Figure 6.13. The energy budget, entropy budget, and exergy budget of the subsystem are shown in Equations (6.13) – (6.15), respectively.

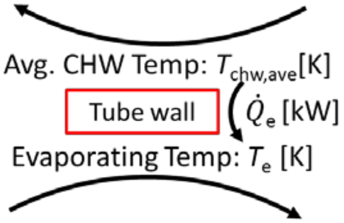

Figure 6.13 Subsystem 3

$$\dot{Q}_e = \dot{Q}_e \tag{6.13}$$

$$\dot{Q}_e / T_{chw,ave} + \dot{S}_{g,evap} = \dot{Q}_e / T_e \tag{6.14}$$

$$\dot{X}_{e,ref} - \dot{X}_{cons,evap} = \dot{X}_{e,chw} \tag{6.15}$$

$\dot{X}_{cons,evap}$ [kW] and $\dot{X}_{e,chw}$ [kW] in Equation (6.15) are the rate of exergy consumed in the tube wall between refrigerant and chilled water and the rate of exergy absorbed by chilled water due to heat release $\dot{Q}_e$ in the evaporator, respectively, which are expressed in Equations (6.16) – (6.17).

$$\dot{X}_{cons,evap} = \dot{S}_{g,evap} T_0 \tag{6.16}$$

$$\dot{X}_{e,chw} = \left(1 - T_0 / T_{chw,ave}\right)\left(-\dot{Q}_e\right) \tag{6.17}$$

(4) The chilled water circuit

The fourth subsystem is shown in Figure 6.14. The energy budget, entropy budget, and exergy budget of the subsystem are shown in Equations (6.18) – (6.20), respectively.

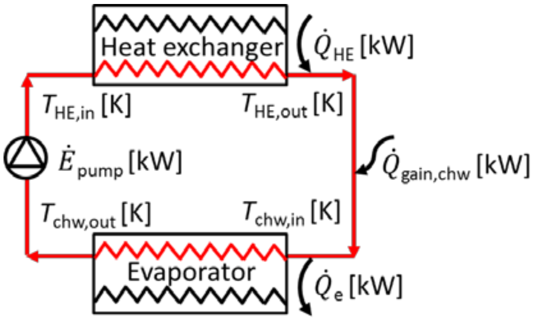
Heat exchanger
$\dot{Q}_{\mathrm{HE}}$ [kW]
$T_{\mathrm{HE,in}}$ [K]
$T_{\mathrm{HE,out}}$ [K]
$\dot{E}_{\mathrm{pump}}$ [kW]
$\dot{Q}_{\mathrm{gain,chw}}$ [kW]
$T_{\mathrm{chw,out}}$ [K]
$T_{\mathrm{chw,in}}$ [K]
Evaporator
$\dot{Q}_{\mathrm{e}}$ [kW]

Figure 6.14 Subsystem 4

$$\dot{Q}_{HE} + \dot{E}_{pump} + \dot{Q}_{gain,chw} = \dot{Q}_e \tag{6.18}$$

$$\dot{Q}_{HE} \big/ T_{HE,ave} + \dot{Q}_{gain,chw} \big/ T_{chw,ave} + \dot{S}_{g,chw} = \dot{Q}_e \big/ T_{evap,ave} \tag{6.19}$$

$$\dot{E}_{pump} + \dot{X}_{e,chw} - \dot{X}_{cons,chw} = \dot{X}_{HE} + \dot{X}_{gain,chw} \tag{6.20}$$

$\dot{X}_{cons,chw}$ [kW], $\dot{X}_{HE}$ [kW] and $\dot{X}_{gain,chw}$ [kW] in Equation (6.20) are the rate of exergy consumed in the chilled water circuit, the rate of exergy discharging from chilled water due to heat absorption $\dot{Q}_{HE}$ in the heat exchanger, and the rate of exergy discharging from chilled water due to heat invasion $\dot{Q}_{gain,chw}$ from surrounding to the chilled water circuit, respectively, which are expressed in Equations (6.21) – (6.22).

$$\dot{X}_{cons,chw} = \dot{S}_{g,chw} T_0 \tag{6.21}$$

$$\dot{X}_{HE} = \left(1 - T_0 \big/ T_{HE,ave}\right)\left(-\dot{Q}_{HE}\right) \tag{6.22}$$

$$\dot{X}_{gain,chw} = \left(1 - T_0 \big/ T_{chw,ave}\right)\left(-\dot{Q}_{gain,chw}\right) \tag{6.23}$$

(5) Exergy budget of the system

By combining Equations (6.3), (6.9), (6.15) and (6.20), the exergy-budget equation for the entire system can be deduced, as given by Equation (6.24). The overall exergy input rate is the sum of the compressor power $\dot{E}_{comp}$, pump power $\dot{E}_{pump}$, and the rate of exergy discharging from cooling water due to heat absorption $\dot{Q}_c$ in the condenser, $\dot{X}_{c,cw}$. The overall exergy consumption rates are the sum of the exergy consumption rates in the four subsystems and the rate of net exergy discharging from system to the environment ($\dot{X}_{gain,chw} - \dot{X}_{loss,ref}$). The exergy output rate is the rate of exergy discharging from chilled water due to heat absorption $\dot{Q}_{HE}$ in the heat exchanger, $\dot{X}_{HE}$.

$$\left(\dot{E}_{comp}+\dot{E}_{pump}+\dot{X}_{c,cw}\right)-\left(\dot{X}_{cons,cond}+\dot{X}_{cons,ref}+\dot{X}_{cons,evap}+\dot{X}_{cons,chw}+\dot{X}_{gain,chw}-\dot{X}_{loss,ref}\right)=\dot{X}_{HE} \quad (6.24)$$

The exergy efficiency β [-], the net power consumption rate per unit exergy output rate η_1 [-], the rate of exergy consumed in the tube wall between cooling water and refrigerant in condenser per unit exergy output rate η_2 [-], the rate of exergy consumed in the refrigeration cycle per unit exergy output rate η_3 [-], the rate of exergy consumed in the tube wall between refrigerant and chilled water in evaporator per unit exergy output rate η_4 [-], and the rate of exergy consumed in the chilled water circuit per unit exergy output rate η_5 [-] are expressed in Equations (6.25) – (6.30).

$$\beta=\dot{X}_{HE}\Big/\left(\dot{E}_{comp}+\dot{E}_{pump}+\dot{X}_{c,cw}\right) \quad (6.25)$$

$$\eta_1=\left(\dot{E}_{comp}+\dot{E}_{pump}-\dot{X}_{HE}\right)\Big/\dot{X}_{HE} \quad (6.26)$$

$$\eta_2=\dot{X}_{cons,cond}\Big/\dot{X}_{HE} \quad (6.27)$$

$$\eta_3=\dot{X}_{cons,ref}\Big/\dot{X}_{HE} \quad (6.28)$$

$$\eta_4=\dot{X}_{cons,evap}\Big/\dot{X}_{HE} \quad (6.29)$$

$$\eta_5=\dot{X}_{cons,chw}\Big/\dot{X}_{HE} \quad (6.30)$$

6.4.2 Calculation results and discussion

In order to clarify the effect of system renovation and modification on the system performance, three sets of representative operating data are chosen as the comparison of objects, that is the initial operating data, the operating data after steps 4 and 5 of the of system renovation and modification, respectively. The operating data after steps 4 represent the final system performance after the variable-frequency transformation of compressor and water pumps and the temperature adjustment of child water. The operating data after steps 5 represent the system performance after the replacement of heat exchanger from stainless steel plate heat exchanger to aluminum plate-fin heat exchanger.

The corresponding time averaged operating data needed in the exergy analysis are shown in Figure 6.15. Since all the operating data are in the cooling mode, the environment temperature adopted in the calculation is fixed at 32ºC uniformly. Moreover, due to the difficulty in detecting the evaporating temperature and condensing temperature, in this study, the evaporating temperature is assumed to be 2ºC lower than the outlet chilled water temperature of evaporator; the condensing temperature is assumed to be 2ºC higher than the outlet cooling water temperature of condenser.

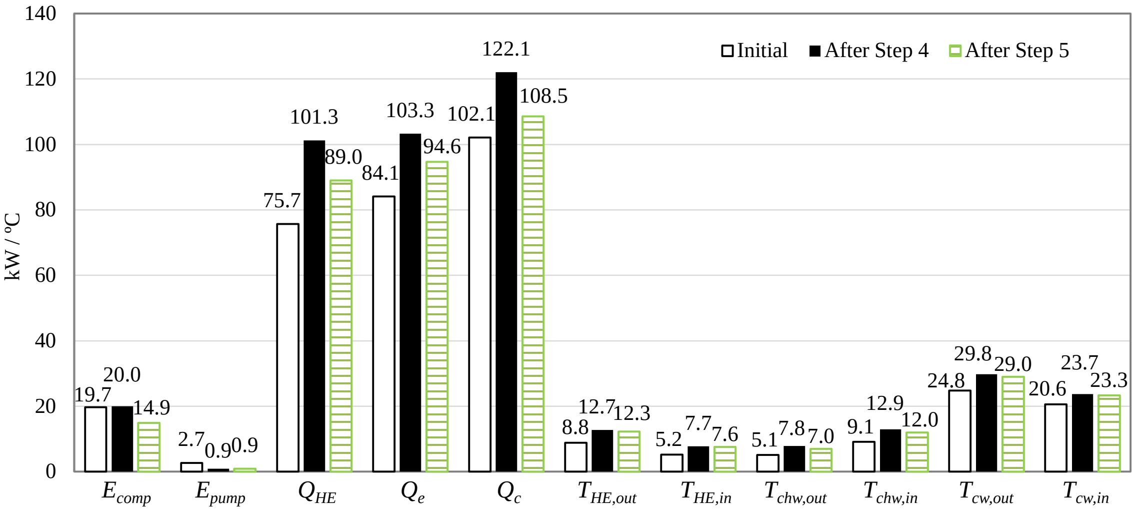

Figure 6.15 Operating date before and after the system renovation and modification

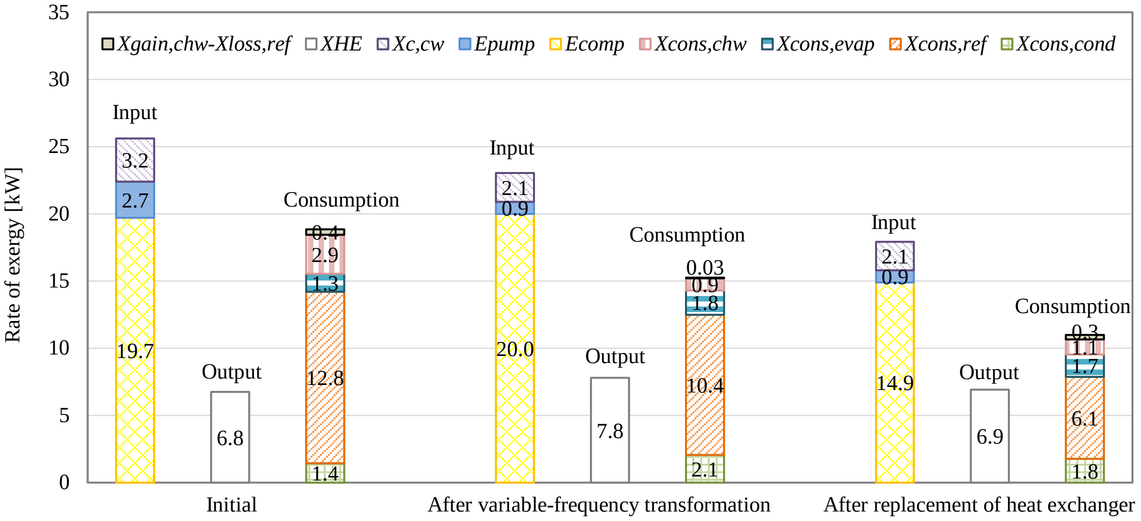

Figure 6.16 Exergy budget before and after the system renovation and modification

The input exergy rate, output exergy rate, and exergy consumption rate of the three stages are shown in Figure 6.16. For achieving the energy saving, or rather the exergy saving, to reduce the exergy consumption rate is significant. It can be seen that in the initial stage, the rates of exergy consumed in the refrigeration cycle ($\dot{X}_{cons,ref}$) and chiller water circuit ($\dot{X}_{cons,chw}$) contribute the most to the total rate exergy consumption rate, at 69.6% and 15.8%, respectively. Reduction of the exergy consumption rate of the two parts will benefit the system performance.

Due to the different refrigerating capacity for each stages, in order to compare each stage on the same basis, the exergy efficiency β, the net power consumption rate per unit exergy output rate η_1, the rate of exergy consumed in the tube wall between cooling water and refrigerant in condenser per unit exergy output rate η_2, the rate of exergy consumed in the refrigeration cycle per unit exergy output rate η_3, the rate of exergy consumed in the tube wall between refrigerant and chilled water in evaporator per unit exergy output rate η_4, and the rate of exergy consumed in the chilled water circuit per unit exergy output rate η_5 of each stage are compared, as shown in Figure 6.17.

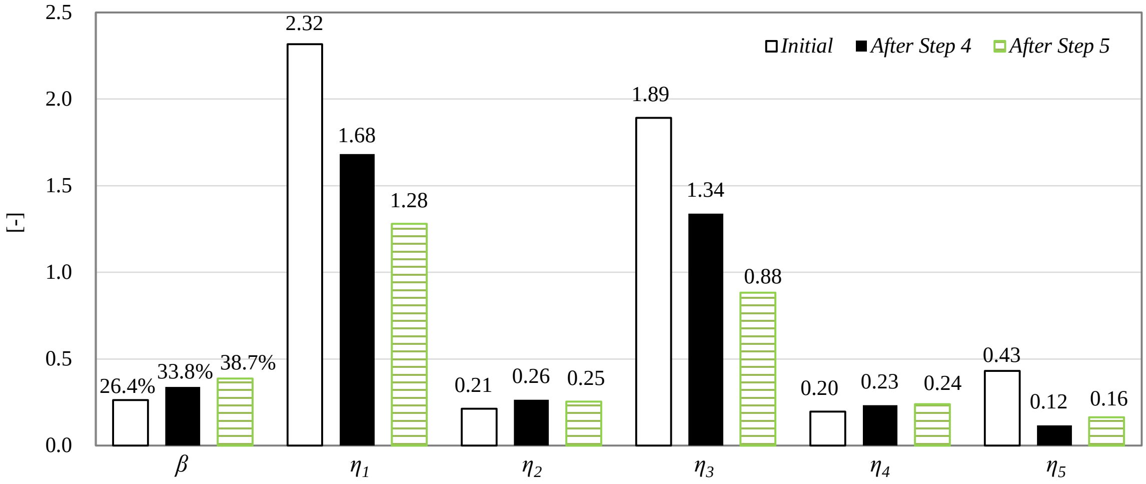

Figure 6.17 Exergy efficiency and dimensionless exergy consumption rates

It can be seen that the exergy efficiency β increases from 26.4% to 33.8% after the variable-frequency transformation of compressor and water pumps, and the temperature rise of outlet chilled water from 5.1ºC to 7.8ºC; then further increases from 33.8% to 38.7% after the replacement of heat exchanger from stainless steel plate heat exchanger to aluminum plate-fin heat exchanger. Generally speaking, a good result has been obtained after the corresponding system renovations and modification.

For the system performance after the step 4 of renovations and modification, due to the variable-frequency transformation of compressor and the temperature rise of outlet chilled water, the performance of the heat pump chiller is improved significantly, the rate of exergy consumed in the refrigeration cycle per unit exergy output rate η_3 decreases 29.1% from 1.89 to 1.34. Moreover, due to the variable-frequency transformation of chilled water pump, the rate of exergy consumed in the chilled water circuit per unit exergy output rate η_5 decreases 72.1% from 0.43 to 0.12, accompany with the reduction of pumping power from 2.7 kW to 0.9 kW. Therefore, since the dimensionless value of the two parts accounting for the largest amounts of exergy consumption rate, as mentioned before, have been reduced obviously, the net power consumption rate per unit exergy output rate η_1 also decreases 27.6% from 2.32 to 1.68. In addition, though both the rate of exergy consumed in the tube wall between cooling water and refrigerant in condenser per unit exergy output rate η_2, and the rate of exergy consumed in the tube wall between refrigerant and chilled water in evaporator per unit exergy output rate η_4 increase slightly, compared with the initial stage, the corresponding effect on the exergy efficiency is limited due to the smaller proportion in the total exergy consumption rate.

For the system performance after the step 5 of renovations and modification, due to the improvement of heat transfer performance after the replacement of heat exchanger from stainless steel plate heat exchanger to aluminum plate-fin heat exchanger, the rate of exergy consumed in the refrigeration cycle per unit exergy output rate η_3 further decreases from 1.34 to 0.88, the decreasing ranges of which are 34.3% compared with the value after step 4, and 53.4% compared with the initial stage, respectively. The pumping power is same with that after step 4 as 0.9 kW, but the rate of exergy consumed in the chilled water circuit per unit exergy output rate η_5 increases slightly, since the output exergy rate decreases from 7.8 kW to 6.9 kW, as shown in Figure 6.16. But the decreasing range of η_3 is larger than the increasing range of η_5, then the net power consumption rate per unit exergy output rate η_1 further decreases from 1.68 to 1.28, the decreasing ranges of which are 23.8% compared with the value after step 4, and 44.8% compared with the initial stage, respectively. In addition, the variations of η_2 and η_4 are very small; therefore, the corresponding effect on the exergy efficiency is limited, like the stage after step 4.

§ 6.5 Conclusions

In this chapter, the performance of a heat pump system in an actual building before and after the system renovations and modification are compared and analysed. Then the exergy analysis based on the operating data of three representative stages are carried out. Some conclusions can be obtained as follows.

(1) The COP of heat pump chiller will decrease when the refrigerating capacity is overlarge or too small.

(2) Varying with the decrease of the refrigerating capacity, the pumping power per unit refrigerating capacity decreases.

(3) After the corresponding system renovations and modification, the system COP and system exergy efficiency increase.

(4) Varying with the increase of the outlet temperature of chilled water, the COP of heat pump chiller increases; the rate of exergy consumed in the refrigeration cycle per unit exergy output rate decreases.

(5) After the variable-frequency transformation of compressor, the COP of heat pump chiller increases; the rate of exergy consumed in the refrigeration cycle per unit exergy output rate decreases; the net power consumption rate per unit exergy output rate decreases.

(6) After the variable-frequency transformation of water pump, the pumping power decreases; the rate of exergy consumed in the chilled water circuit per unit exergy output rate decreases.

(7) After the replacement of heat exchanger from stainless steel plate heat exchanger to aluminium plate-fin heat exchanger, the rate of exergy consumed in the refrigeration cycle per unit exergy output rate decreases; the net power consumption rate per unit exergy output rate decreases.

Chapter 7 Conclusions and recommendations

In this study, from the point of view of energy saving on HVAC system, the improvement of heat transfer performance of related heat transfer equipment and the reduction of pumping power and compressor power in HVAC system are mainly focused on for improving the performance of the whole HVAC system. At first, based on an assumed simple counter-flow indirect contact type heat exchanger unit, the values of $Ns_{\Delta T}$ and $Ns_{\Delta P}$ of three kinds of heat exchangers are compared under three kinds of inlet temperature differences, three kinds of length-to-diameter ratios, and nine kinds of inlet Reynolds numbers. Then, the thermodynamic fin-optimization of a water-to-water plate-fin heat exchanger is carried out by using CFD and optimization algorithms. Next, around the water pump in chilled water circuit, the exergy analysis on an assumed chilled-water circuit under four variable-flow control strategies and two supply water temperatures are conducted. At last, the performance analysis and exergy analysis on a heat pump system of an actual building before and after the system renovation and modification are carried out to clarify the effect of chilled water temperature, operation mode of compressor and pumps, and the type of heat exchanger on the system performance. Some useful conclusions are achieved as follows.

§ 7.1 Conclusions

For the main inducement of irreversible process in the heat exchanger for different working mediums, the corresponding conclusions are as follows.

For air-to-air heat exchanger, the effectiveness of heat exchanger ε increases with the increase of length-to-diameter ratio but is not sensitive to the change of inlet temperature difference.; the number of entropy production units due to heat transfer, $Ns_{\Delta T}$, decreases with the increase of length-to-diameter ratio, and increases with the increase of inlet temperature difference; the number of entropy production units due to pressure loss, $Ns_{\Delta P}$, increases with the increase of length-to-diameter ratio, but is not sensitive to the change of inlet temperature difference; the $Ns_{\Delta P}$ -to-Ns ratio increases with the increase of the length-to-diameter ratio, and decreases with the increase of the inlet temperature difference; the irreversible loss is mainly caused by heat transfer at lower Reynolds number and by pressure loss at higher Reynolds number.

For water-to-water heat exchanger, the number of entropy production units due to pressure loss, $Ns_{\Delta P}$, is not sensitive to the increase of length-to-diameter and inlet temperature difference but increases slightly with the increase of inlet temperature difference at higher Reynolds number for water-to-water heat exchanger. In addition, the irreversible loss of water-to-water heat exchanger is mainly caused by heat transfer at any Reynolds number. Other conclusions are same with those of air-to-air heat exchanger except for the above-mentioned two conclusions.

For air (high temp.)-to-water (low temp.) heat exchanger, conclusions are quite the same with those of air-to-air heat exchanger.

For the comparison of three kinds of heat exchangers, under the same baseline, at any Reynolds number, the air-to-water heat exchanger achieves the highest effectiveness, the air-to-air heat exchanger is the second, and the water-to-water heat exchanger is the least. The value of $Ns_{\Delta T}$ increases following the order of air-to-air, air-to-water, and water-to-water at any Reynolds number, but the value of $Ns_{\Delta P}$ increases following the opposite order. With respect to the comparison of Ns for three kinds of heat exchangers, when the Reynolds number is equal or greater than 1000, the ascending order of Ns for three kinds of heat exchangers is quite the same with that of $Ns_{\Delta P}$; when the Reynolds number is less than 1000, the ascending order of Ns for three kinds of heat exchangers mainly consistent with that of $Ns_{\Delta T}$. For the $Ns_{\Delta P}$ -to-Ns ratio, the ascending order of $Ns_{\Delta P}$ -to-Ns ratio for three kinds of heat exchangers is water-to-water, air-to-water, and air-to-air. For water-to-water heat exchanger, the irreversible loss is caused by heat transfer at any Reynolds number. For air-to-water and air-to-air heat exchangers, the irreversible loss is mainly caused by heat transfer at lower Reynolds number and by pressure loss at higher Reynolds number.

For the fin-shape optimization of plate-fin heat exchanger, to obtain more precise results, the formula for calculating the comprehensive surface efficiency is modified by defining the convective heat transfer coefficients of the plate and fin as independent parameters in this study. The values of the Colburn factor and Fanning factor are calculated using the multiple regression analysis equation based on the numerical simulation results. In addition, according to the numerical simulation results, the values of the convective heat transfer coefficients of the plate and fin depend on the proportions of the primary heat transfer surface area (plate) and secondary heat transfer surface area (fin). For the comparison of $Ns_{\Delta T}$ and $Ns_{\Delta P}$, $Ns_{\Delta T}$ is about 100 and 610 times $Ns_{\Delta P}$ when $Ns_{\Delta T}$ (Ns) and $Ns_{\Delta P}$, respectively, are minimized as objective functions in a case study with unfixed overall dimension of heat exchanger. After the thermodynamic optimization on an assumed plate-fin heat exchanger with fixed overall dimension, the efficiency of heat exchanger increases from 30.8% to 33.0%; the heat transfer amount also increases 7.1% from 49.3 kW to 52.8 kW.

With respect to the exergy analysis on an assumed chilled-water circuit system under four variable-flow control modes and two supply water temperatures, it can be found that the rates of exergy input and exergy consumption under any partial-load condition are significantly smaller than those under full-load condition; the rates of exergy input and exergy consumption under any variable-frequency control mode are smaller than those under throttle-valve control mode; in variable-frequency control mode, the rate of exergy inputs decrease in the following order: constant-pressure control, constant-differential-pressure control, and predictive-system-curve control. Moreover, regarding the effect of the supply water temperature, the rate of exergy inputs are smaller at 12°C than at 7°C. Therefore, the use of the variable-frequency control mode and a higher chilled water temperature will effectively reduce the exergy input to the system.

After the performance analysis and exergy analysis on an actual heat pump system, it can be found that the COP of heat pump chiller will decrease when the refrigerating capacity is overlarge or too small; varying with the decrease of the refrigerating capacity, the pumping power per unit refrigerating capacity decreases. In regard to the system renovations and modification, after the corresponding system renovations and modification, the system COP and system exergy efficiency increase. Varying with the increase of the outlet temperature of chilled water, the COP of heat pump chiller increases; the rate of exergy consumed in the refrigeration cycle per unit exergy output rate decreases. After the variable-frequency transformation of compressor, the COP of heat pump chiller increases; the rate of exergy consumed in the refrigeration cycle per unit exergy output rate decreases; the net power consumption rate per unit exergy output rate decreases. After the variable-frequency transformation of water pump, the pumping power decreases; the rate of exergy consumed in the chilled water circuit per unit exergy output rate decreases. After the replacement of heat exchanger from stainless steel plate heat exchanger to aluminium plate-fin heat exchanger, the rate of exergy consumed in the refrigeration cycle per unit exergy output rate decreases; the net power consumption rate per unit exergy output rate decreases.

§ 7.2 Recommendations for future studies

(1) In the optimization of plate-fin heat exchanger, the fin type is the basic type, plain rectangular, the heat exchanger with other complicated fin type can be optimized in the future study.

(2) The related research on the CFD study of water-refrigerant heat exchanger and air-refrigerant heat exchanger are not so much right now. The CFD simulation of heat exchanger with refrigerant can be

paid more attrition in future.

(3) The inlet temperatures of high-/low- temperature channels are fixed at constant value in the CFD simulation of heat exchanger. To enrich database of Colburn heat transfer factor *j* and Fanning friction factor *f*, the CFD simulation based on different temperature conditions can be carried out in future.

(4) In the exergy analysis on an assumed chilled-water circuit system, only the variable-flow control modes of water pumps are focused on, the effect of variable-flow control modes of fans on the performance of HVAC system can be studied in future.

(5) The boundary of the analysis object in the exergy analysis on an actual heat pump system is limited; the exergy analysis with larger boundary can be conducted in future for further clarifying the system performance.

(6) In the exergy analysis based on actual operating data, only the time-averaged data are adopted in the calculation. For clarifying the dynamic performance of the system, the dynamic exergy analysis can be carried out in future.

(7) The exergy analysis can be also applied to the optimization of heat exchanger.

Reference

A

Ahmadi P., et al., 2011: Cost and entropy generation minimization of a cross-flow plate fin heat exchanger using multi-objective genetic algorithm, Journal of Heat Transfer, 133, pp. 021801.1–021801.10.

Alur S, 2012: Experimental Studies on Plate Fin Heat Exchangers, PhD dissertation, National Institute of Technology Rourkela

Asadi M., 2013: Entropy minimization in plate-fin heat exchanger using cuckoo algorithm, Wyno Journal of Engineering & Technology Research, 1, pp. 21–29.

B

Bagdade S.D., ASM, 2002: ASM Ready Reference: Thermal Properties of Metals (Materials Data Series), ASM International, USA

Bejan A. et al., 1976: Thermal Design and Optimization, John Wiley & Sons, Inc., New York

Bejan A. et al., 1977: The concept of irreversibility in heat exchanger design: Counterflow heat exchangers for gas-to-gas applications, J. Heat Transfer, 99, pp. 374-380

Bejan A., 1982: Entropy Generation through Heat and Fluid Flow, 1st edition, Wiley, New York

C

Cengel Y., Boles M., 2014: Thermodynamics: An Engineering Approach, 8th edition, McGraw-Hill, Boston

Chen C., Shen Y., 1993: Cryogenic Heat Exchanger. Beijing: China Machine Press, Beijing (in Chinese)

Chen L., 2012: Fluid Mechanics and Thermotechnical Basis, 2nd edition, Tsinghua University Press, Beijing (in Chinese)

Crowther H., 2002: Why change the chilled water temperature range, Engineering System Solutions, 14th edition, MCQUAY

D

Dong J. et al., 2007: Flow and heat transfer on compact smooth fin surfaces, Transactions of the Chinese Society for Agricultural Machinery, 38, pp. 53-56 (in Chinese)

G

Gundersen T., 2011: An introduction to the concept of exergy and energy quality, Energy and Process

Engineering, pp. 1-26

Guo J., et al., 2010: Multi-Objective Optimization of Heat Exchanger Design by Entropy Generation Minimization, Journal of Heat Transfer, 132, 081801

Guo J., Xu M., 2012: The application of entransy dissipation theory in optimization design of heat exchanger, Applied Thermal Engineering, 36, pp. 227-235

H

Harrell J.M., Mathias, J.A., 2009: Improving efficiency in a campus central chilled water system using exergy analysis, ASHRAE Transactions, 115, pp. 507–522

Herbert W. Stanford III, 2011: HVAC Water Chillers and Cooling Towers: Fundamentals, Application, and Operation, 2nd edition, CRC

Hu S., Herold K.E., 1995: Prandtl number effect on offset fin heat exchanger performance: experimental results, International Journal of Heat and Mass Transfer, 38, pp. 1053-1061

I

Izumiyama H., et al., 2012: Control parameter setting for secondary water circuit on an actual project, Transactions of the Society of Heating, Air Conditioning and Sanitary Engineers of Japan, 2, pp. 1239–1242 (in Japanese)

K

Kays W.M., London A.L., 1984: Compact Heat Exchanger, 3rd edition, McGraw-Hill, New York

Kestin J., 1979: A Course In Thermodynamics, CRC Press, USA

Klein S., Nellis G., 2011: Thermodynamics, 1st edition, Cambridge University Press, New York

Kido T., et al., 2013: Control logic that maintains a difference in water temperature between fan coil unit inflow and outflow while keeping living areas comfortable, Azbil Technical Review, 54, pp. 74–81 (in Japanese)

Kuppan T., 2002: Heat Exchanger Design Handbook, Marcel Dekker, New York

L

Li R. et al. 2014: Theoretical analysis on ground source heat pump and air source heat pump systems by the concepts of cool and warm exergy, Energy and Buildings, 75, pp. 447-455

M

Martin H, 2010: M5 Heat Transfer in Fluidized Beds, VDI Heat Atlas, 2nd edition, Springer-Verlag Berlin Heidelberg, pp. 1301-1310.

Martínez I., 2015: Isidoro Martínez' lectures on Thermodynamics, http://webserver.dmt.upm.es/~isidoro/bk3/

Massoud M., 2005: Engineering Thermofluids: Thermodynamics, Fluid Mechanics, and Heat Transfer, Springer-Verlag Berlin Heidelberg, Germany

Matsushita N., et al., 2011: Development and verification of the control method using surplus pressure of the primary pump in heating and cooling plant system for building air-conditioning. Transactions of the Society of Heating, Air Conditioning and Sanitary Engineers of Japan, 166, pp.19–26

McClintock F.A., 1951: The design of heat exchangers for minimum irreversibility, 1951 ASME Annual Meeting, Paper No. 51-A-108.

Mishra M. et al., 2009: Second law based optimisation of crossflow plate-fin heat exchanger design using genetic algorithm, Applied Thermal Engineering, 29, pp. 2983–2989

Moran M.J. et al., 2010: Fundamentals of Engineering Thermodynamics, 7th edition, John Wiley & Sons, Inc., New York

N

Nag, 2010: Basic And Applied Thermodynamics 2/E, 2nd edition, McGraw Hill Education Private Limited, New Delhi

O

Ooka R., et al., 2013: Zero energy building project in the University of Tokyo, the REHVA Congress CLIMA 2013, ID:298

P

Patel V., Savsani V., 2014: Optimization of a plate-fin heat exchanger design through an improved multi-objective teaching-learning based optimization (MO-ITLBO) algorithm, Chemical Engineering Research and Design, 92, pp. 2371-2382

Peng H., Ling X., 2008: Optimal design approach for the plate-fin heat exchangers using neural networks cooperated with genetic algorithms, Applied Thermal Engineering, 28, pp. 642-650

Perrot P., 1998: A to Z of Thermodynamics, Oxford University Press

R

Rao R.V., Patel V., 2013: Multi-objective optimization of heat exchangers using a modified teaching-learning-based optimization algorithm, Applied Mathematical Modelling, 37, pp. 1147-1162

S

Sanaye S., Hajabdollahi H., 2010: Thermal-economic multi-objective optimization of plate fin heat exchanger using genetic algorithm, Applied Energy, 87, pp. 1893-1902

Serth R.W., Lestin T.G., 2014: Process Heat Transfer: Principles, Applications and Rules of Thumb, 2ed edition, 2014 Elsevier Inc., USA

Shah, R. K., 2002: Fundamentals of Heat Exchanger Design, John Wiley & Sons, Inc., New Jersey

Shi J., 1986: Choice of Control Valve, 1st edition, China Building Industry Press (in Chinese)

Shukuya M., 1996: Warm exergy and cool exergy, Proceedings of Annual Meeting, Building Science Section, Architectural Institute of Japan, pp. 453–454 (in Japanese)

Shukuya M., 2013: Exergy: Theory and Applications in the Built Environment, Springer-Verlag, London

Singh,V. et al., 2008: Usefulness of entropy generation minimization through a heat exchanger modeling tool, International Refrigeration and Air Conditioning Conference, Paper 958

T

Taniguchi M., et al., 2014: Energy saving air separation plant based on exergy analysis, Research and development, Kobe Steel Engineering Reports, 64, pp. 45–48

Thirumaleshwa M., 2009: Fundamentals of Heat and Mass Transfer, 2nd edition, Dorling Kindersley (India) Pvt. Ltd, Delhi

TRANE, 2002: Cooling-coil heat transfer, Engineers Newsletter 31-1, TRANE

V

Volk M., 2013: Pump Characteristics and Applications, 3rd edition, CRC

W

Wang S., 1984: Plate-fin Heat Exchanger, 1st ed., Chemical Industry Press, Beijing

Wang S., et al., 2008: Evaluating the low exergy of chilled water in a radiant cooling system. Energy and Buildings, 40, pp. 1856–1865

Wang Y.Q., 2009: Numerical study on plate-fin heat exchangers with plain fins and serrated fins at low Reynolds number, Chemical Engineering & Technology, 32, pp. 1219-1226

Wen J. et al., 2007: Experimental investigation of header configuration improvement in plate–fin heat exchanger, Applied Thermal Engineering, 27, pp. 1761-1770

Westphalen, D., Koszalinski, S. 2001: Energy Consumption Characteristics of Commercial Building HVAC Systems, Volume I: Chillers, Refrigerant Compressors, and Heating Systems. Arthur D. Little

X

Xu Z. M., 1996: A modified entropy generation number for heat exchangers, Journal of Thermal Science, 5, pp. 257-263

Y

Yin H., et al., 2015: Exergy analysis on chilled-water circuit system with four variable-flow control strategies and two supply water temperatures, Journal of Environmental Engineering, AIJ, 80, pp. 425-432

Yin H., Ooka R., 2015: Shape optimization of water-to-water plate-fin heat exchanger using computational fluid dynamics and genetic algorithm, Applied Thermal Engineering, 80, pp. 310-318

Z

Zarea H., et al., 2013: Optimal design of plate-fin heat exchangers by a Bees Algorithm, Applied Thermal Engineering, 69, pp. 267-277

Zhao M., Li Y., 2013: An effective layer pattern optimization model for multi-stream plate-fin heat exchanger using genetic algorithm, International Journal of Heat and Mass Transfer,60, pp. 480-489

Appendix

Publication list

１．査読付き論文（筆頭著者）

1) 尹航, 大岡龍三, 宿谷昌則, 四種類の変流量制御方式及び二種類の送水温度条件下での配管系のエクセルギー解析, 日本建築学会環境系論文集, 80 巻, 711 号, 425-432, 2015 年 5 月

2) Hang Yin, Ryozo Ooka, Multi-Variable Shape optimization of water-to-water plate-fin heat exchanger using computational fluid dynamics and genetic algorithm, Applied Thermal Engineering, 80, pp. 310-318, 2015

3) Hang Yin, Ryozo Ooka, Masanori Shukuya, Exergy analysis of chilled water circuit under different variable-flow control methods and supply water temperatures, 2015 ASHRAE Annual Conference. Atlanta, GA, June 27-July 1, 2015 (accepted)

２．査読付き論文（筆頭著者以外）

なし

３．査読無し論文（国際会議発表論文含む）（筆頭著者）

4) 尹航、大岡龍三、「プレートフィン型熱交換器の伝熱性能に関するＣＦＤ解析」、日本建築学会大会学術講演梗概集、札幌、2013.8

5) 尹航、大岡龍三、「プレートフィン型熱交換器の熱力学最適化設計に関する研究–数値解析及び遺伝的アルゴリズムを用いた熱交換器形状最適化」、空気調和・衛生工学会大会、長野、2013.9

6) 尹航、大岡龍三、宿谷昌則、李栄玲、「二次側配管系の冷房時における三種類の変流量制御方式に関するエクセルギー解析」、日本建築学会大会学術講演梗概集、近畿、2014.9

7) Hang Yin, Ryozo Ooka, Masanori Shukuya, Application of exergy analysis to chilled water circuit and heat pump system, 6th International Building Physics Conference. Turin, Italy, June 14-17, 2015 (accepted)

8) 尹航、大岡龍三、宿谷昌則、「実建築に導入された地中熱ヒートポンプシステムの性能に関する研究　その２：ヒートポンプシステム改修前後のエクセルギー解析」、日本建築学会大会学術講演梗概集、関東、2015.9（採用）

４．査読無し論文（国際会議発表論文含む）（筆頭著者以外）

9) 大岡龍三、尹航、宿谷昌則、「実建築に導入された地中熱ヒートポンプシステムの性能に関する研究　その１：実測に基づく、ヒートポンプシステム改修の COP 向上の検討」、日本建築学会大会学術講演梗概集、関東、2015.9（採用）

５．その他（研究活動を示すもの）

1) アジアシンポジウム（日中韓交流会）
   - 東京（東京大学）、研究発表 2013.11
   - 北京（清華大学）、研究発表 2014.10
2) 慶応大学伊香賀研究室との研究交流会、年間４回
   - 研究発表　2013.10
   - 研究発表　2015.05
3) IIS PhD Student Life 研究発表　2014.7
4) 温熱環境実測
   - 神奈川県横浜市緑区十日市場町　2012.05
   - 西武ドーム　2015.05

Acknowledgments

I would like to express my gratitude to all those who helped me during my three years PhD life.

My deepest gratitude goes first and foremost to Professor Ryozo Ooka, my supervisor, for his constant encouragement and guidance. He gave me bunches of advice and helped me conquer many difficulties in both my study and my life. Moreover, he has walked me through all the stages of the writing of this thesis. Without his consistent and illuminating instruction, this thesis could not have reached its present form. I also would like to express my heartfelt gratitude to my secondary advisor, Professor Shinsuke Kato. I do appreciate his patience, encouragement, and professional instructions during my PhD life.

I am also greatly indebted to the Professor Masanori Shukuya, who taught me a lot about the knowledge of exergy and gave me many suggestions on my research papers.

In addition, I would like to express my gratitude to other members of my doctoral dissertation supervisory committees, Professor Naoki Shikazono and Professor Yasunori Akashi, for their brilliant comments and suggestions.

I also owe my sincere gratitude to all my lab colleagues as follows, who gave me their help and time in listening to me and helping me work out my problems during the difficult course of my PhD life. (The present lab colleagues: Professor Tosiuki Hino, Mr. Takeo Takahashi, Dr. Hideki Kikumoto, Dr. Jongyeon Lim. The former graduate students: Rongling Li, Shi Chen, Xuan Cheng and so on. The present graduate students: Minsik Kim, Wonjun Choi, Hyokeum Hwang, Kan Lin, Daisuke Kawahara, Yusuke Arima, Keigo Nakajima, Li Wang, Sintaro Ikeda, Naoko Sugisaki, Qiuyue Wang, Tatuhiro Yamamoto, Sintaro Kobayasi, Misaki Tanimoto, Yan Xu, Mingzhe Liu and so on. The lab secretaries: Ms. Yumiko Yamada, Ms. Miyuki Mori, Ms. Ai Takeuti and Ms. Keiko Higuchi.

Last my thanks would go to my beloved family and friends for their loving considerations and great confidence in me all through these years.

May 16, 2015

Hang YIN